

**PHOSPHODIESTERASE 1 (PDE1) AT THE CROSSROADS OF CALCIUM AND
CYCLIC NUCLEOTIDE SIGNALING IN DIABETIC NEPHROPATHY**

by

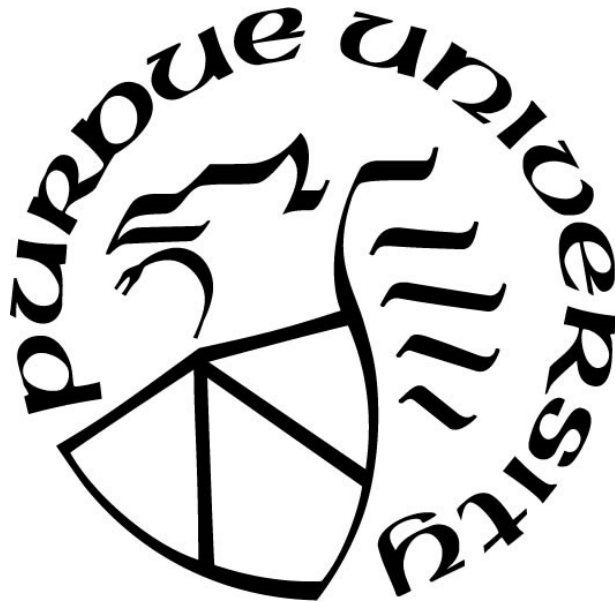
Asim Bikash Dey

A Dissertation

Submitted to the Faculty of Purdue University

In Partial Fulfillment of the Requirements for the degree of

Doctor of Philosophy



Department of Biology

Indianapolis, Indiana

May 2020

**THE PURDUE UNIVERSITY GRADUATE SCHOOL
STATEMENT OF COMMITTEE APPROVAL**

Dr. Simon J. Atkinson

Department of Biology

Dr. Mark C. Kowala

Eli Lilly and Company

Dr Ruben C. Aguilar

Purdue University

Dr. Guoli Dai

Department of Biology

Dr. Anthony J. Baucum II

Department of Biology

Approved by:

Dr. Theodore R. Cummins

Head of the Graduate Program

Dedicated to my family

ACKNOWLEDGMENTS

I greatly appreciate Dr. Simon Atkinson at IUPUI and Dr. Mark Kowala at Eli Lilly and Company, my supervisors, for their support and encouragement throughout my graduate work in parallel to my day job. Their unrelenting support and profound belief in me have been instrumental in completing this work. Special thanks to Dr. Kowala for his flexibility that made it easier to juggle graduate work and the demands of a full-time job.

I'm deeply indebted to Dr. Mark Rekhter whose unconditional support at all stages of my thesis made this a reality. Your insightful comments and input have helped me develop my critical analytical skills and help me become a better scientist. Completion of my experiments would not have been possible without your critical input, technical assistance and constant support over the last several years.

I also would like to thank my committee members, Dr. Guoli Dai, Dr. Claudio Aguilar, and Dr. AJ Baucum for their invaluable comments and suggestions during this process. Special thanks to Dr Baucum for graciously agreeing to serve as a member at the last minute and for a very thorough review of the writing. Thanks to Laura Flak and Anita Sale at the Graduate school for helping me with administrative and technical issues through my time at IUPUI.

I thank Leah Porras, Fang Li, Wayne Blosser, my co-workers at Lilly who has been very helpful in executing experiments. Big thanks to Dr Tao Wei, at Eli Lilly for his insightful bioinformatics help. My computational biology part would not been possible without his help. I learned a lot from him.

This arduous process of earning a doctorate and writing a dissertation would not be possible without the support of my family specially my wife my daughters who put up with a husband and a father missing in action all the time during this process. Without their constant support and understanding it would not have been possible to achieve my educational goals.

TABLE OF CONTENTS

LIST OF FIGURES	8
LIST OF TABLES	11
ABBREVIATIONS	12
ABSTRACT.....	14
CHAPTER 1. DIABETIC KIDNEY DISEASE: CHALLENGES AND POTENTIAL NOVEL MECHANISM	15
1.1 Introduction.....	15
1.2 Risk factors for diabetic kidney disease.....	16
1.2.1 Hemodynamic factors.....	16
1.2.2 Metabolic factors	18
1.3 Structural changes in diabetic kidney disease.....	19
1.4 Second messengers in chronic kidney disease.....	20
1.4.1 Cyclic nucleotide signaling in kidney.....	21
1.4.2 PDE family	22
1.4.3 Intracellular calcium and kidney disease.....	26
1.5 Use of computational biology in deciphering DKD	29
1.6 Conclusion	31
CHAPTER 2. ROLE OF PHOSPHODIESTERASE 1 IN SYSTEMIC HEMODYNAMICS AND POTENTIAL IN DIABETIC KIDNEY DISEASE	33
2.1 Introduction.....	33
2.2 Methods and materials	35
2.2.1 Animals.....	35
2.2.2 Generation of PDE proteins.....	36
2.2.3 Phosphodiesterase enzyme assays	37
2.2.4 IC50 calculation.....	37
2.2.5 Calcium-calmodulin dependent PDE enzyme assays.....	38
2.2.6 PDE enzyme assays using [3H]cAMP as substrate.....	38
2.2.7 PDE enzyme assays using [3H]cGMP as substrate.....	38

2.2.8	ReninAAV db/db uNx model for renal failure	39
2.2.9	Rat telemetry studies.....	39
2.2.10	Rat Ear temperature.....	40
2.2.11	Histopathologic Evaluation	42
2.2.12	Isolation of rat glomeruli.....	42
2.2.13	Enzyme-Linked Immunosorbent Assay (ELISA)	43
2.2.14	Urinary cAMP and cGMP measurement in rats.....	44
2.2.15	Measurement of apoptosis using Caspase-3/7 Green Detection Reagent	44
2.3	Results.....	45
2.3.1	Effect of LY1 on PDE1 activity	45
2.3.2	Development of rat model of vasodilation	45
2.3.3	LY1 lowered blood pressure in normal and spontaneously hypertensive rats	45
2.3.4	LY1 attenuated disease progression in the mouse model of DKD	50
2.3.5	LY1 improved histopathology in DKD mouse model.....	52
2.3.6	LY1 reduced fibrotic and inflammatory gene expression	54
2.3.7	LY1 reduced urinary bio markers of kidney injury	54
2.3.8	Acute effect of LY1 on cyclic nucleotides in the rat urine.....	57
2.3.9	Expression analysis of major calcium channels in patients with CKD	59
2.3.10	LY1 attenuated renal cell apoptosis induced by in vitro activation of TRPC6.....	59
2.4	Discussion.....	67
2.4.1	Hemodynamic effects of PDE1 inhibition.....	67
2.4.2	Renal benefits of PDE1 inhibition in diabetic nephropathy	72
2.4.3	Mechanism of PDE1 activation and reno-protective effects of PDE1 inhibition.....	77
CHAPTER 3. ROLE OF TRPC6 AND PDE1 IN THE CROSSTALK OF CALCIUM AND CYCLIC NUCLEOTIDE SIGNALING.....		80
3.1	Introduction.....	80
3.2	Methods and materials	83
3.2.1	Reagents.....	83
3.2.2	Cell Culture.....	83
3.2.3	Construction of recombinant plasmid and generation of TRPC6 stable cell line.....	83
3.2.4	Adenoviral construction of GCamp2 Ca sensor with hTRPC6.....	84

3.2.5	Membrane potential assay	84
3.2.6	Measurement of Calcium influx in cell using FLIPR calcium assay kit	85
3.2.7	DAG measurement	85
3.2.8	cAMP measurement.....	85
3.3	Results.....	86
3.3.1	Generation and selection of TRPC6-overexpressing stable cell line.....	86
3.3.2	Hyperforin 9 induced calcium flux in HEK293 cells in TRPC6-dependent manner	89
3.3.3	Several risk factors of DKD caused increased calcium influx in TRPC6-overexpressing cell line	92
3.3.4	Diabetic risk factors differentially activate TRPC6.....	92
3.3.5	Activation of TRPC6 caused depletion of cellular cAMP level.....	95
3.4	Discussion	96
CHAPTER 4. TRANSLATING ANIMAL TO HUMAN; USE OF COMPUTATIONAL BIOLOGY IN UNDERSTANDING DIABETIC KIDNEY DISEASE.....		103
4.1	Introduction.....	103
4.2	Methods and materials	105
4.2.1	Gene expression omnibus datasets.	105
4.2.2	Gene Ontology and Pathway Enrichment Analysis.....	106
4.2.3	Statistical Analysis Software	106
4.3	Results.....	108
4.3.1	Identification of common genes modulated in DKD patients	108
4.3.2	Gene Ontology analysis of DKD2000 genes.....	109
4.3.3	Correlations between clinical phenotype and expression data in diabetic nephropathy	112
4.3.4	Translatability assessment of animals to human DKD.....	115
4.4	Discussion	116
CHAPTER 5. GENERAL CONCLUSION		124

LIST OF FIGURES

Figure 1.1. Schematic outlining interactions between hemodynamic and metabolic factors and how their interactions trigger the downstream signaling system in mediating diabetic kidney disease..	17
Figure 1.2. Pathological lesions of DKD..	20
Figure 2.1. Inhibition of PDE1 enzyme activity by LY1..	46
Figure 2.2. Effect of LY1 on ear temperature in rats..	47
Figure 2.3. Effect of LY1 on the hemodynamics of SD rats.	48
Figure 2.4. Effect of LY1 on the hemodynamics of SHR rats.....	49
Figure 2.5. Effect of LY1 on the hemodynamics of SHR rats on top of enalapril..	51
Figure 2.6. Effect of PDE1 inhibition in DKD.	53
Figure 2.7. Histopathological changes in renin AAV db.db AAV uNx mice upon inhibition of PDE1.	55
Figure 2.8. Gene expression analysis of fibrotic and inflammatory markers..	56
Figure 2.9. Urinary level of NGAL is decreased in AV renin db/db uNx mice following PDE1 inhibition.....	58
Figure 2.10. Urinary level of KIM-1 is decreased in AAV renin db/db uNx mice following PDE1 inhibition.	58
Figure 2.11. Urinary level of MCP-1 is decreased in AAV renin db/db uNx mice following PDE1 inhibition.....	60
Figure 2.12. Urinary level of GDF15 is decreased in AAV renin db/db uNx mice following PDE1 inhibition.	61
Figure 2.13. Effect of PDE1 inhibition on urinary cyclic nucleotide in normal rats.....	62
Figure 2.14. Gene expression analysis of the calcium channels in the microdissected kidney samples of CKD patients in ERCB cohort.....	63
Figure 2.15. Effect of PDE1 inhibition on TRPC6 mediated apoptosis in human mesangial cell..	64
Figure 2.16. Effect of glomerular number on apoptosis. 96 well plate was seeded with different number of glomeruli and incubated in the media for 24hrs.....	65
Figure 2.17. Effect of PDE1 inhibition on TRPC6 mediated apoptosis in isolated rat glomeruli.	66
Figure 3.1. TRPC6 gene expression in the stable HEK293 cell line..	87

Figure 3.2. Comparison of fluorescent signal response of selected TRPC6 clones to membrane potential change during AngII stimulation.	88
Figure 3.3. Membrane potential assay.	88
Figure 3.4. TRPC6 inhibitor inhibits AngII mediated change in membrane polarization.....	89
Figure 3.5. Effect of cell density on the fluorescence response of membrane potential dye in TRPC6 clone 11 against different stimuli.....	90
Figure 3.6. TRPC6 inhibitor inhibits hyperforin 9 induced calcium influx in C11.....	91
Figure 3.7. Representative FLIPR traces showing changes in calcium influx in C11 in response to diabetic risk factors.	93
Figure 3.8. Hyperforin 9 induce transient intracellular diacylglycerol (DAG) in C11.....	95
Figure 3.9. N-acetyl cysteine (NAC) attenuates tetra butyl hydrogen peroxide (TBHP) induced ROS in C11.....	96
Figure 3.10. Differential response in DAG signal by diabetic risk factors in activation of TRPC6..	97
Figure 3.11. Differential response of TRPC6 activators in generating ROS in C11.....	97
Figure 3.12. ROS signal in isolated glomeruli as assessed by CEL ROX dye.....	98
Figure 3.13. Detection of cAMP using green upward cAMP sensor. A) C11 cells were infected with baculoviral construct containing cAMP biosensor..	98
Figure 4.1. Identification of 2040 (DKD2000) commonly changed DEGs from the four cohort profile data sets (GSE30528, GSE30529, GSE104954 and GSE50892).....	110
Figure 4.2. Ingenuity Pathway Analysis (IPA) top 10 canonical pathways for DKD 2000 DEG list. ($p < 0.001$).....	111
Figure 4.3. Significantly enriched A) disease and B) function pathway analysis of the DKD 2000 genes.	112
Figure 4.4. Schematic representation of the correlation density analysis of the DKD 2000 genes..	113
Figure 4.5. Density histograms of Pearson correlation coefficient between gene expression signature and clinical parameters of the DKD patients..	114
Figure 4.6. Density histograms of Pearson correlation coefficient between gene expression signature and histological parameters of the DKD patients.....	115
Figure 4.7. Model for cross species translation based on the correlation density analysis.	117
Figure 4.8. Density histograms of Pearson correlation coefficient between gene expression and histopathological parameters.	118

Figure 4.9. Density histograms of Pearson correlation coefficient between gene expression and histopathological parameters. 119

LIST OF TABLES

Table 1: Body weight, proteinuria and blood glucose level of the dbdb renin AAV mice	40
Table 2: Inhibition of PDE enzyme activity by LY1	46

ABBREVIATIONS

DKD	Diabetic Kidney Disease
PDE	Phosphodiesterase
ACR	Albumin to creatinine ratio
eGFR	Estimate glomerular filtration rate
ACE	Angiotensin converting enzyme
ARB	Angiotensin receptor blocker
TRPC	Transient receptor potential canonical
FSGS	Focal segmental glomerular sclerosis
DAG	Diacylglycerol
ROS	Reactive oxygen species
NFAT	Nuclear factor of activated T-cells
JAK/STAT	Janus kinase/signal transducers and activators of transcription
AngII	Angiotensin II
ET-1	Endothelin-1
KIM1	Kidney Injury Marker
NGAL	Neutrophil gelatinase associated lipocalin
SHR	Spontaneously hypertensive rats
DKD	Diabetic Kidney Disease
PDE	Phosphodiesterase
ACR	Albumin to creatinine ratio

eGFR	Estimated glomerular filtration rate
ACE	Angiotensin converting enzyme
ARB	Angiotensin receptor blocker

ABSTRACT

Diabetic Kidney Disease (DKD) is a major complication of diabetes. Incomplete understanding of its molecular mechanisms is highlighted by the limited treatments options. We hypothesized that inhibition of protective endogenous mechanisms plays major role in the pathogenesis of DKD. While renoprotection is mediated by cyclic nucleotides (cAMP and cGMP), phosphodiesterases (PDEs) lead to cyclic nucleotide degradation. Our investigation focused on the role of calcium/calmodulin activated PDE1 in DKD. Three isoforms of PDE1 are differentially expressed in vascular smooth muscle cells, renal tubular epithelial cells, podocytes, and mesangial cells. We used highly potent and selective PDE1 inhibitor LY1 to explore systemic hemodynamic and local renal role of PDE1. LY1 reduced systolic and diastolic blood pressure in normotensive and spontaneously hypertensive rats. Renal protection with PDE1 inhibition was tested in mouse model of DKD, featuring a combination of diabetes, nephron loss and arterial hypertension. In this model, a PDE1 inhibitor caused a significant improvement in renal function as evident by significant reduction of albuminuria, serum creatinine and several urine biomarkers of inflammation and injury. Histopathological analysis revealed substantial improvement in the pathology of DKD in the treated group that was associated with the reduction of gene expression related to inflammation and fibrosis. Thus, we revealed the role of calcium activated PDE1 in DKD. However, the source of calcium in this context remained obscure. Our bioinformatics analysis pointed out that calcium channel TRPC6 is likely to be involved. Further in vitro studies demonstrated that TRPC6 activation induced apoptosis in human mesangial cells and isolated rat glomeruli, which was attenuated by both TRPC6 and PDE1 inhibition, thereby suggesting a functional coupling between TRPC6 (as a source of calcium) and PDE1 activation. Moving upstream, we showed that several systemic risk factors of DKD (angiotensin II, endothelin 1 and glucose) activated TRPC6 in a different manner, through generation of either reactive oxygen species or diacylglycerol. The computational modeling to relate human transcriptomic and phenotype data demonstrated the pre-clinical findings of renal benefit upon PDE1 inhibition is translatable in human. Taken together, our results suggest mechanistic link among systemic risk factors, TRPC6, calcium flux and PDE1 activation in pathogenesis of DKD. As a corollary, PDE1 inhibition leads to direct and indirect renoprotective effects.

CHAPTER 1. DIABETIC KIDNEY DISEASE: CHALLENGES AND POTENTIAL NOVEL MECHANISM

1.1 Introduction

Diabetic Kidney Disease (DKD) is a microvascular complication of both type I and type II diabetes mellitus which often results in end-stage renal disease (ESRD) requiring either dialysis or renal transplantation. [1]. Patients with DKD have a high rate of mortality, high financial burden, as well as a very poor quality of daily life. Prevalence rates of DKD are increasing in parallel with the incidence rates of diabetes mellitus. Currently in the United States (US) about two hundred thousand patients receive ESRD care due to DKD, with fifty thousands new patients starting dialysis each year [2] and it is estimated that by 2030 the number of DKD patients will increase significantly due to the projected 54% increase in the prevalence of diabetes [3]. Primarily the increased prevalence of obesity, metabolic syndrome, and westernization of lifestyle are the drivers of diabetes but to what extent these factors contribute to DKD remains unknown. Clinically, a diabetic patient with an estimated glomerular filtration rate (eGFR) of less than 60 mL/min/1.73 m² and/or albuminuria greater than 30 mg/g creatinine would be diagnosed with DKD [4]. In the clinic angiotensin-converting-enzyme (ACE) inhibitors and angiotensin receptor blockers (ARB), the widely used blood pressure lowering drugs, are the current standard of care for DKD. But unfortunately, they can achieve only 20% reduction in risk of future ESRD, rendering it semi-effective option for the DKD patients [5]. Moreover, even with the best available clinical management, involving both glycemic and blood pressure control, it is only possible to achieve at most a 30% improvement in declining diabetic kidney [6-8]. In recent years the successful clinical trial of SGLT2 inhibitor and GLP agonist provided new therapeutic opportunity but still there is an urgent need for new interventions that will effectively delay or reverse CKD progression in patients with diabetic nephropathy (DN). To facilitate the discovery of new intervention understanding of the disease mechanism is crucial. The pathophysiology of DKD complex and multifactorial, that involves both genetic and environmental factors. The exact mechanism is not well understood. Although the initial trigger is hyperglycemia but in later stages several risk factors like obesity, hypertension, etc. contributes towards the progression of the disease. Although these risk factors are clearly important, the exact mechanism is still unknown. The mechanistic

understanding of how the systemic risk factors like high glucose, or other co-morbid factors translate into downstream intracellular signaling pathway and identifying the key players would provide new therapeutic opportunity for DKD.

1.2 Risk factors for diabetic kidney disease

Initially, hyperglycemia driven pathogenic pathways act as trigger but later the interaction of metabolic and hemodynamic factors plays a major role in the progression of the disease [2, 9]. These metabolic factors such as excess fatty acids, glucose etc resulted in enhanced oxidative stress, formation and buildup of advanced glycation end-products (AGEs) and renal polyol formation. The hemodynamic factors include both increased systemic and intraglomerular pressure, in addition to the activation of vasoactive hormone pathways including the renin angiotensin system and endothelin-1 signaling pathways [10]. In the presence of chronic diabetes, both of these factors feed into and triggers common pathogenetic mechanisms that ultimately lead to increased renal albumin permeability resulting in proteinuria and extracellular matrix deposition resulting in glomerulosclerosis and ultimately tubulointerstitial fibrosis.

1.2.1 Hemodynamic factors

Hemodynamic factors like increased systemic blood pressure and intraglomerular pressure driven by the activation of several vasoactive hormone pathways like renin angiotensin system and endothelin-1 are major contributors to the disease [10].]. The role of hemodynamic factors in DN was emphasized first by Brenner et al, when they observed several intrarenal abnormalities including increased intraglomerular pressure, increased single nephron GFR and preferential vasodilation of the afferent, over the efferent, arteriole through micropuncture studies in diabetic rats. In the same study they also demonstrated that ACE inhibitor reduced intraglomerular pressure that is associated with reduced renal injury, thereby emphasizing the role of renin-angiotensin system (RAS) in DN. Moreover, in an in vitro system, glucose has been shown to upregulate angiotensinogen (converts renin to angiotensin II) in proximal tubular cell [10] and in mesangial cell stimulated angiotensin II production that is associated with increased TGF β accumulation [11]. However, the role of RAS in DN still remains somewhat controversial as plasma measurement of various components of RAS showed low to normal in diabetes, although the distribution of these

components in various compartments cannot be ruled out. Moreover data demonstrating renal benefit in both diabetic and non-diabetic model of renal injury by modulating TGF β expression and a range of intracellular mediators like PKC and NF- κ B indicate some non-hemodynamic component of RAS system [10, 12]. In addition to angiotensin, several other vasoactive hormones like Endothelin-1, vasopressin has been attributed to the renal injury. These hormones have been shown to have differential effects on efferent and afferent arterioles thereby affecting the intraglomerular pressure. Recent success with Atrasentan, an endothelin-1 inhibitor, in DKD patients (SONAR trial), clearly emphasize the role of local hemodynamics in DKD [13]. Contrary to vasoconstrictors, a wide range of vasodilatory substances like bradykinin, atrial natriuretic peptide, certain prostaglandins, and nitric oxide have been shown to modulate glomerular vascular tone [10]. Neutral endopeptidase (NEP) is an enzyme that degrades natriuretic peptides as well as

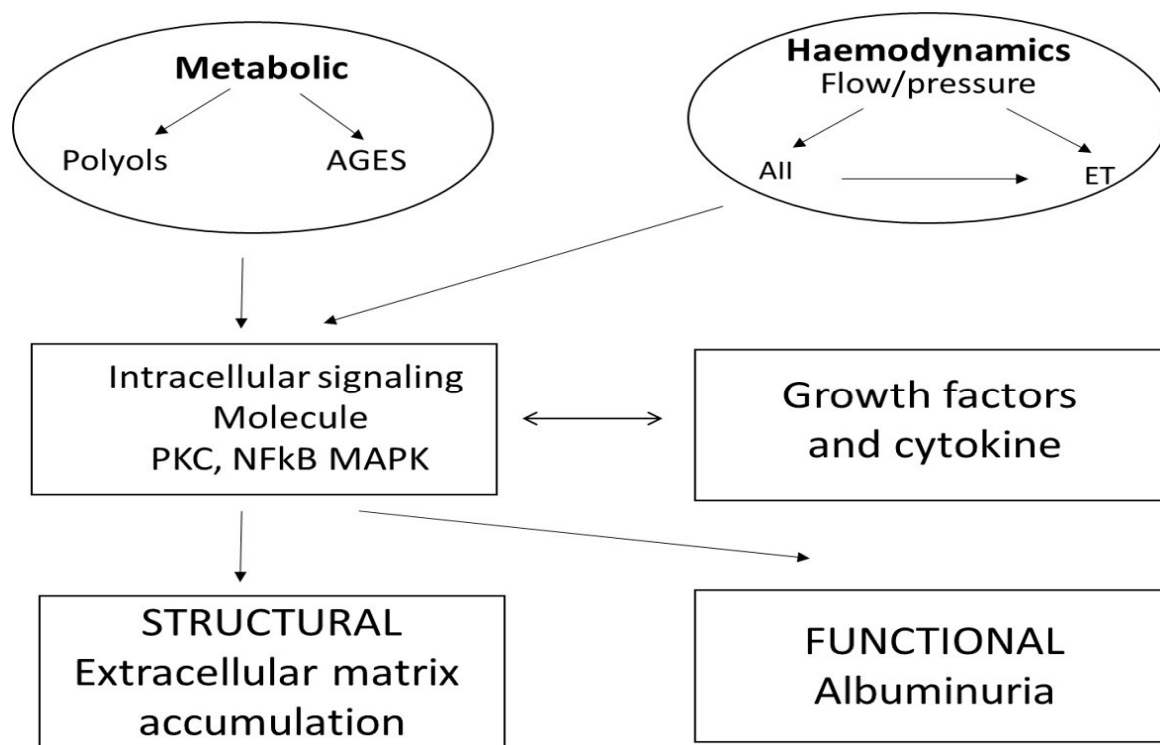


Figure 1.1. Schematic outlining interactions between hemodynamic and metabolic factors and how their interactions trigger the downstream signaling system in mediating diabetic kidney disease.

Modified from Copper et al. 2001.

bradykinin and endothelin converting enzymes. Combination of NEP inhibitor and ACE inhibitor

in the PARAGON trial demonstrated renal benefit in heart failure patients [14]. This further illustrated that approach to increase vasodilation that would lead to have a greater anti-hypertensive effect is renoprotective in both diabetic and non-diabetic condition.

1.2.2 Metabolic factors

Brownlee in 2001 described how hyperglycemia leads to increased glycolysis generating excessive by-products that feed into four pathways; the polyol pathway, hexosamine pathway, production of AGEs, and activation of protein kinase C [15]. In the initial stage of glycolysis, glucose is broken down to 1,3 diphosphoglycerate by the enzyme glyceraldehyde-3-phosphate dehydrogenase (GADPH), which is a critical step as in the state of abundant glucose superoxide produced by electron transport chain that causes an upregulation of upstream components of glycolysis. The excess amount of glucose can be shunted through polyol pathway and reduced to fructose. This further cause decrease of glutathione resulting in increase of oxidative stress leading to increased cellular stress-mediated apoptosis. As the NADH:NAD⁺ ratio increases, it also increases the formation of methylglyoxalate and diacylglycerol, both of which are reported to be abundant in DKD patients ([16, 17]. It has been shown that in hyperglycemia, diacylglycerol (DAG) is chronically upregulated and contributes to sustained activation of protein kinase C (PKC), which contributes to DKD through several signaling pathways [18]. Activation of PKC can also contribute to the local hemodynamics by prostaglandin E2 and nitric oxide mediated vasodilation of afferent arterioles which then causes augmentation of angiotensin II-mediated vasoconstriction of efferent arterioles thereby contributing to glomerular hyperfiltration[19]. By products of increased activity of hexosamine pathway contribute to the increased renal cell hypertrophy and mesangial matrix accumulation that are the hallmark of DKD (34, 35 of Atta). Lastly irreversible glycation of proteins in presence of excessive glucose resulted in AGEs that is known to contribute to DKD in multiple ways. For example, AGEs have been shown to modify both laminin and type IV collagen thereby causing increased permeability of the glomerular basement membrane (GBM). In addition to that, increased concentrations of AGEs are known to dose-dependently increase density and expansion of the extracellular matrix activation by contributing to the increased expression of fibronectin and collagen types I and IV.

1.3 Structural changes in diabetic kidney disease

One of the hallmarks of DKD is proteinuria, which occurs when the glomerular filtration barrier fails to retain the macromolecules, like albumin, within intravascular space. The glomerular filtration apparatus consists of three components-glomerular endothelial cells, visceral epithelial cells (podocytes), and glomerular basement membrane. It has been suggested that early changes in renal glomeruli are critical for the subsequent histopathological feature and nephron loss. Podocytes with their unique interdigitating foot processes are highly specialized terminally differentiated cells that sit on the glomerular basement membrane (GBM). In a normal healthy human the shape and integrity along with the charge barrier properties of the GBM is maintained by intricate network of glomerular endothelial cells and podocytes which are compromised in the diabetic glomerulus [1]. Chronic exposure to hyperglycemia induces ‘patho-adaptive’ progressive changes in podocytes, including cytoskeletal rearrangement, de-differentiation, causing retraction and flattening (known as effacement) that ultimately detaches them from the slit diaphragm and eventually drop out [1]. Thickening of the GBM is regarded as one of the earliest and most characteristic of all glomerular changes in diabetes and can be seen via electron microscope within few years of diagnosis [20]. Under hyperglycemia, mesangial cells are also altered, undergoing proliferation and hypertrophy thereby producing more matrix proteins leading to structural features of DKD. Diabetes-induced changes in the local environment resulted in recruitment of activated leukocytes, especially T cells and macrophages into the glomerulus and tubulointerstitium. Although this influx of inflammatory cells is due to tissue injury, the secreted cytokines, chemokines, activated complement and reactive oxygen species further mediate DKD [1]. In the early stage of diabetes, increased glucose load to the tubule induces maladaptive hypertrophy and hyperplasia that causes increased absorption of glucose and activation of the tubule-glomerular feedback that leads to increased hyperfiltration. The cumulative effect of the above changes is activated myofibroblasts, atypical collagen, inflammatory cells, and loss of capillary architecture that results in tubulointerstitial fibrosis [21]. These progressive changes in the different components of the kidney present a heterogeneous range of pathological features, that includes nodular or diffuse glomerulosclerosis, tubulointerstitial fibrosis, tubular atrophy and renal arteriolar hyalinosis, alone or in combination.

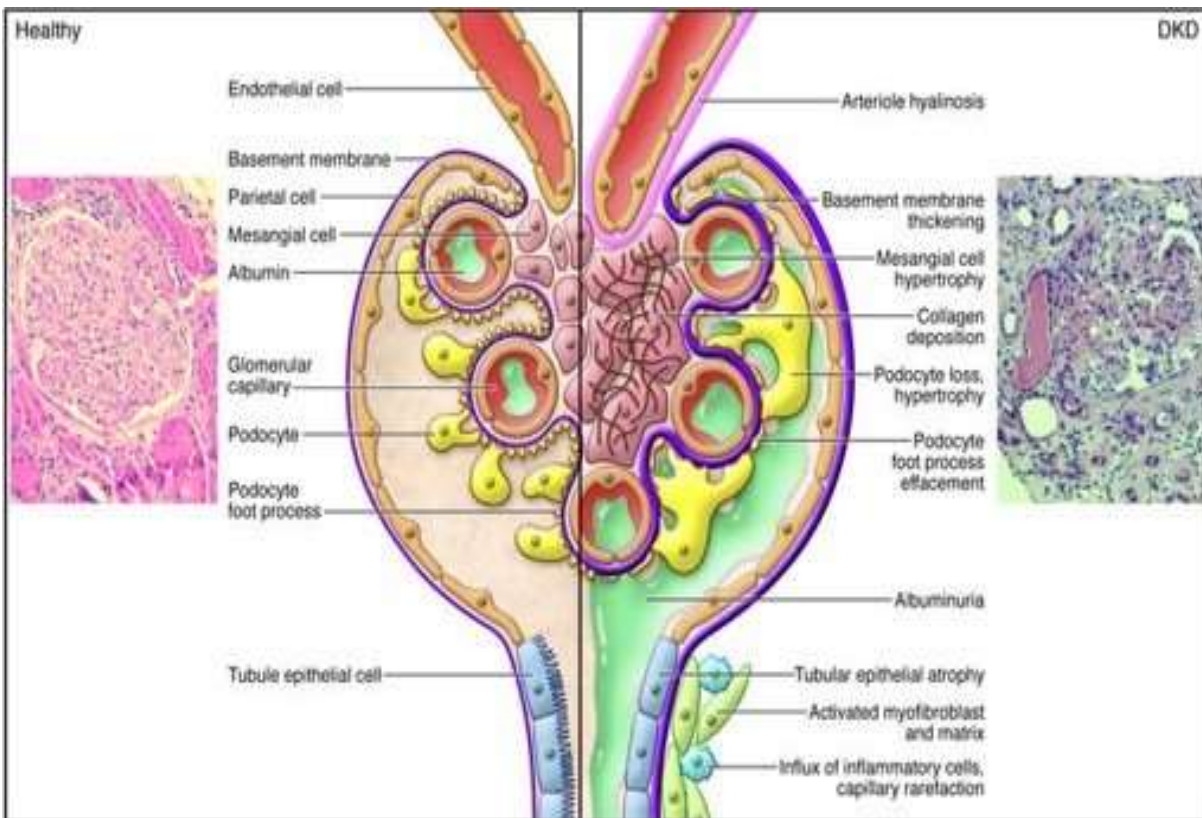


Figure 1.2. Pathological lesions of DKD. In normal human albumin is retained in the blood through an elaborate network of endothelial cells, basement membrane, podocytes, parietal epithelial cells that is called glomerular filtration barrier. In contrast, the diabetic glomerulus displays several histopathological features like arterial hyalinosis, mesangial expansion, collagen deposition, basement membrane thickening, podocyte loss and hypertrophy, that is clinically translated in high albuminuria, decreased glomerular filtration and ultimately lead to end stage renal failure. Modified from Kimberly et al. 2014.

1.4 Second messengers in chronic kidney disease

Any systemic risk factors either hemodynamic or metabolic can act as ligands and bind to specific cellular receptors that alter protein confirmation to stimulate nearby effector proteins. These effectors can catalyze the production of molecules or in case of ions, increase the influx of ions that are called second messengers. They further diffuse rapidly to their targets elsewhere within the cell thus altering the activities as a response to the new information received by the receptors [22]. There are four classes of second messengers: cyclic nucleotides that signal within the cytosol; lipid messengers and ions like calcium that signal within and between cellular compartments and

gases and free radicals. Each of these second messengers can bind to specific protein targets, to modulate downstream signals by altering their activity. Given their importance in physiology, second messengers are tightly controlled to ensure precision in cellular signaling.

1.4.1 Cyclic nucleotide signaling in kidney

Cyclic nucleotides, cyclic adenosine monophosphate (cAMP) and cyclic guanosine monophosphate (cGMP) are important intracellular second messengers that are involved in the transduction of a diverse array of physiologic stimuli. They play prominent roles in the development and progression of renal disease, including mitogenesis, inflammation, and fibrosis. A wide variety of G-coupled receptor mediated activation of adenylyl cyclase is responsible for generation of cAMP, whereas both receptor-associated and soluble guanylyl cyclase (sGCs) generates cGMP [23, 24]. Once produced they engaged the effector molecules to activate the downstream signaling pathways. For cAMP the effector molecule is predominantly cAMP-dependent protein kinase A (PKA) and for cGMP it is protein kinase G (PKG). In addition to that cAMP-regulated guanine nucleotide exchange factors (cAMP-GEF, or EPACs), and cyclic nucleotide gated channels (9, 10) also act as effector molecules. Catabolism of cyclic nucleotides is always directed by phosphodiesterases (PDEs). The balance between synthesis and catabolism of cyclic nucleotides basically plays a pivotal role in regulating the amplitude, duration, and localization of cyclic nucleotide signaling. Preservation of cGMP either by activating the enzymes involved in the synthesis or inhibition of the enzyme that degrades them have been shown to have therapeutic benefits in kidney disease. Several lines of evidence suggested that both sGC stimulators or sGC activators increase intracellular level of cGMP and reduce kidney fibrosis in several different model of kidney fibrosis by inhibiting the TGF β pathway. For example clinically approved drug Riociguat, a sGC stimulator alone or in combination with an inhibitor of the angiotensin-II type 1 receptor (AT1R) improved renal function in a diabetic model of kidney disease by attenuating progression of renal fibrosis [25]. Moreover, in another rodent model where the disease was driven by volume and pressure overload it improved renal function by renal fibrotic tissue remodeling and reduced expression of several profibrotic markers [26]. Cinaciguat, a sGC activator improved renal function by targeting sGC and increasing intracellular cGMP in a nephron loss model of CKD in rats [27]. Similarly, PDE5 inhibitors that specifically hydrolyze cGMP has

been shown to have renoprotective effects in multiple studies via their antiapoptotic and antioxidant properties. The PDE5 inhibitor sildenafil has been tested in both fibrosis and nephron loss model of kidney disease and shown improved renal function by increasing cGMP level and decreasing several key mediators of fibrosis pathway [28, 29]. Tadalafil was shown to prevent kidney dysfunction by preserving the renal structure and reducing several injury markers like KIM1 and NGAL in an ischemia-reperfusion injury model [30, 31]. Preservation of cAMP has been shown to have anti-fibrotic effect by blocking TGF β mediated gene transcription. The therapeutic options for enhancing cAMP are adenylate cyclase stimulators, PDE inhibitors, cyclosporine, or adrenomedullin; however, most of the data showing effect on kidney exist with PDE inhibitors. Roflumilast, a selective PDE4 inhibitor has shown renoprotective effect in streptozotocin-induced diabetic model of kidney disease by reversing pathology and attenuating apoptosis [32]. Pentoxifylline, a non-specific PDE inhibitor, has demonstrated renal benefits in various rodent model of kidney disease as well in clinical trial with type 2 diabetics and chronic kidney disease (CKD) by lowering the decline of estimated glomerular filtration rate in addition to RAS blockade [33]. Besides their direct effect as anti-fibrotic and anti-apoptotic cyclic nucleotides has been shown to induce vasorelaxation in the vascular system, which also can contribute to beneficial effects in the kidney by modulating the local and systemic hemodynamics. All of this evidence suggests that preservation of cyclic nucleotide has potential renal benefits.

1.4.2 Cyclic nucleotide phosphodiesterase (PDE) and chronic kidney disease

1.4.2 PDE family

PDEs are a large family of enzymes that can hydrolyse cAMP and/or cGMP to their inactivated noncyclic nucleotides 5'-AMP and 5'-GMP. They are the only cellular mechanism for degrading cAMP and cGMP, there by playing a major role in regulating the intracellular levels of these second messengers and, subsequently, modulating cellular activities. Based on their structure, primary sequence, substrate specificity and their pharmacological properties, PDEs are currently classified into eleven families. Majority of PDE families comprise more than one gene (~20 PDE genes), generating multiple protein products (> 50 PDE proteins) by alternative 5' mRNA splicing [34]. The international nomenclature of PDE designated the gene families (types) of PDE by a capital letter to designate the product of a single PDE isogene also called "PDE subtype" and the

isoforms or variants are expressed by a numerical number. For example, for PDE1A1: gene family 1 (type), gene A (subtype), and variant 1 (isoform). PDE family members have unique substrate specificity with PDE4, PDE7 and PDE8 hydrolyzing only cAMP, PDE5, PDE6, and PDE9 hydrolyzing cGMP and PDE1, PDE2, PDE3, PDE10 and PDE11 hydrolyzing both [35].

Despite differences, the different PDE isoforms share similar structural features. The catalytic domain of all mammalian PDEs is highly conserved, containing consensus sequences and motifs along with two consensus Zn binding sites. In addition, it also contains sequences specific to the family, determine the substrate affinities, and sensitivity to inhibitors. On the contrary the 'regulatory domain' located in NH₂-terminal vary widely among PDEs in structure and contain sequences targeted for different regulatory components. These include phosphorylation sites for different protein kinases like PKA or PKG, non-catalytic sites for cGMP and binding site for Ca²⁺/calmodulin. The small C-terminal domain of PDEs has recently been reported to have some MAPK dependent regulatory functions [23]. PDE family members largely differ in tissue distribution, inhibitor specificity and in mode of regulation. Although intracellular cyclic nucleotide concentration are major regulator but their activities can depend on the binding of Ca²⁺/CaM, phosphorylation, interaction with regulatory proteins or subcellular compartmentalization [35]. PDEs plays a vital role in balancing the concentration of cyclic nucleotides thereby modulating multiple signal transduction pathways to fine tune the physiological and pathophysiological processes that is now widely demonstrated in the literature such as erectile dysfunction, asthma, pulmonary hypertension, atherosclerosis, heart failure, and diabetes. Here we will review the role of PDEs in the context of renal disease with special emphasis on PDE1 as a potential therapeutic target for DKD.

1.4.2.1 Role of PDEs in vascular contraction

In 1970 Kukovetz and Poch first described the role of PDE in vascular contraction when they observed the vasodilator papaverine inhibits cAMP-PDE in vessel [36]. Since then, using specific PDE inhibitors several studies have reported the vasodilatory role of PDE1, PDE4 and PDE5 in isolated aorta from several species including human [37]. Using precontracted rat aorta with or without endothelium and specific PDE inhibitors it has been demonstrated that vasorelaxation induced by PDE3 is endothelium independent but PDE4 requires endothelium [38]. PDE4 has

been reported to be abundant in renal vasculature and Ro 20-1724, a PDE4 inhibitor has been shown to prevent endotoxin induced renal vascular resistance [39]. Moreover chronic infusion of the PDE4 inhibitor in zymosan-induced model of multiple organ dysfunction syndrome, a chronic inflammation induced organ failure model in mice, has shown to decrease mesenteric vascular resistance as well as improve renal function by preserving glomerular filtration rate and preserving cAMP [40]. PDE5, which is mainly present in vascular smooth muscle also participates in vascular contraction. Specifically, the PDE5 inhibitor, Zaprinast, mediates relaxation in rat and rabbit aorta in an endothelium-dependent manner [38, 41]. In kidney, PDE5 has been reported to express in vessel walls, glomeruli, mesangial cells, cortical tubules, and inner medullary collecting duct cells of rat kidney [42]. Several PDE5 inhibitors, like sildenafil and tadalafil, demonstrated renal benefit that is attributed to the vasodilatory feature of PDE5 inhibition. Sildenafil has demonstrated renal benefit in both a diabetic and non-diabetic pre-clinical model of CKD. In both mouse and rat model of diabetic nephropathy PDE5 inhibition by sildenafil showed improvement in renal function by reducing glomerular hyperfiltration. It also demonstrated renal benefit in a rat 5/6 uninephrectomy model by preventing glomerular hypertension and hyperfiltration [43]. This evidence clearly demonstrates that PDEs play an important role in maintaining the local vascular tone and thus exert its influence in controlling either local or systemic hemodynamics.

1.4.2.2 Role of PDEs in inflammation and fibrosis

Preservation of cyclic nucleotides by inhibiting PDEs has been shown to reduce inflammation and fibrosis in several diseases including renal disease. In rat mesangial using isoform-specific inhibitors, Chini et al demonstrated functional compartmentalization of intracellular pools of cAMP that are differentially regulated by PDEs [44]. They found that cAMP regulated by PDE3 suppressed cell proliferation by inhibiting Ras-Raf MEK-ERK pathway whereas a PDE4-regulated cAMP pool suppresses cell inflammation by inhibiting MCP-1. Using both specific and nonspecific inhibitors, the role of PDEs in inflammation and fibrosis has been demonstrated in non-hemodynamic dependent models of CKD in animals. Roflumilast, a selective PDE4 inhibitor has shown antifibrotic and antiapoptotic capability in streptozotocin induced type-1 diabetic nephropathy [45]. PDE5 inhibitors sildenafil and tadalafil showed renal benefit in several different acute kidney injury model through their antiapoptotic and anti-fibrotic properties. After treatment

with sildenafil for 14 days in acute unilateral ureter obstruction model, it reduced renal TGF β 1/smad signaling along with mRNA expression of α -SMA, collagen type 1 and type III [28]. In a 5/6 renal ablation model sildenafil also improved renal function by reducing renal cell inflammation and apoptosis [46]. In both studies the renal improvement was associated with the preservation of cGMP. In a renal ischemia-reperfusion model, tadalafil has been shown to prevent renal damage as evidenced by decreased kidney injury marker (KIM-1) and neutrophil gelatinase-associated lipocalin (NGAL), well-known kidney injury markers [45]. Besides these, pentoxifylline, a non-specific PDE inhibitor has been reported to ameliorate proteinuria by reducing interstitial inflammation and fibrosis in rat nephron loss model [35]. These evidences showed that apart from their effect on vascular contraction, PDEs also have other mechanism to influence the pathophysiology of renal disease.

1.4.2.3 PDE1 and its potential role in renal biology

Among all 11 PDEs, PDE1 is the only phosphodiesterase that is activated by a Ca²⁺/CaM-binding domain and has affinity for both cAMP and cGMP. The PDE1 family members consists of three isoforms that are encoded by three distinct genes, PDE1A, 1B, and 1C. Although dual substrate specific, PDE1A and PDE1B have higher affinity for cGMP than cAMP, whereas, PDE1C hydrolyses cGMP and cAMP with equal efficiency [47]. For PDE1A, at least seven splice-variants have been reported, among which PDE1A1 and PDE1A2 have been isolated from bovine heart and brain. PDE1B is particularly high in the striatum and so far only one gene product has been identified whereas five splice variants of PDE1C has been reported that localized in brain cerebellum, olfactory neurons, heart and testis [48]. All three isoforms, PDE1A, B and C are found to be expressed in pulmonary vasculature and aorta and mesenteric arteries in rats [49-51]. In rat cardiomyocytes and vascular smooth muscle cells, PDE1A was found to primarily regulate cGMP where as PDE1C regulates cAMP in aortic and pulmonary smooth muscle cells. PDE1C has been reported to be upregulated in the vasculature of rats with pulmonary hypertension whereas increased activity of PDE1A was found in rats with angiotensin II-induced systemic hypertension [49, 52]. Moreover, PDE1A has been linked to the development of hypertrophy and fibrosis in the hypertrophic rat heart [53]. All these evidences indicate PDE1 being a major player in regulating systemic hemodynamics. Several studies with specific and non-specific PDE1 inhibitors have

clearly showed improvement in vascular resistance and blood pressure both in vivo and ex vivo. Selective PDE1 inhibitors demonstrated blood pressure lowering effect in normal rats [52]. The role of PDE1C has been well characterized in the pathological cardiac remodeling and dysfunction. Using genetic and pharmacological approaches, Knight et al, demonstrated that inhibition of PDE1 attenuated cardiac remodeling and dysfunction by antagonizing cardiac myocyte hypertrophy and death [54]. The non-hemodynamic properties of PDE1 has also been described in other tissue type including vascular smooth muscle. For example in rat aortic smooth muscle cells and in patient derived pulmonary arterial smooth muscle cells, genetic knock down or inhibiting the activity using a small molecule resulted in inhibition of cell proliferation and induced apoptosis [55, 56]. Expression of PDE1 isoforms have been reported to alter time of activation and differentiation of inflammatory cells which indicates PDE1's potential role in inflammatory response. Indeed ITI-214, a very potent PDE1 inhibitor has been shown to reduce LPS-induced increases in TNF- α , IL-1 β and MCP-1 in microglia [57]. This is not surprising as being dual substrate specific, suppression of PDE1 can preserve cAMP which is a negative modulator of inflammatory cell responses including cytokine secretion and leukocyte as well increase availability of cGMP to attenuate LPS induced responses.

In the kidney, PDE1A is expressed in the tubules, PDE1C is expressed in the glomeruli and tubules, and PDE1B is not expressed in either location [58]. Both the vasodilatory mechanism and anti-inflammatory feature of PDE1 inhibition as seen in other tissue could potentially result in renal benefit. To date, no functional role of PDE1 has been reported in the kidney. Moreover, in diabetic nephropathy several risk factors like AngII, ET-1, and high glucose can increase intracellular calcium that might drive the upregulation of PDE1, thus implicating it to the pathophysiology of DKD.

1.4.3 Intracellular calcium and kidney disease

Calcium is an important intracellular messenger that engages in a wide range of cellular functions by direct binding to target proteins or stimulation of calcium sensors that then activate different downstream responses [59]. Either imported from the extracellular milieu or mobilized from intracellular stores it not only bridges extracellular and intracellular signal transduction as a second

messenger but also can regulate enzyme activity as a cofactor and modulate action potential [60]. Being so versatile in nature, intracellular calcium concentration is tightly controlled by an assortment of channels, pumps, transporters, buffers and effector moieties. Entry of calcium from external milieu is controlled by Ca^{2+} permeable channels such as transient receptor potential (TRP) and voltage gated Ca^{2+} channels. Calcium is also stored internally in different organelles like endoplasmic reticulum, Golgi, sarcoplasmic reticulum and acidic organelles of the endo-lysosomal system. Calcium has always been thought to related with the bone health but lately calcium homeostasis has been shown to be important in the regulation of insulin secretion from beta cells in the pancreas [61]. Increased intracellular calcium is thought to contribute to reduced β -cells function thereby promoting altered glucose homeostasis. In adipocytes and skeletal muscle, high cytosolic calcium has been inked to insulin resistance [62]. Moreover at least three studies have demonstrated that serum calcium level is higher in diabetic patients than non-diabetes [63-65]. The kidney plays an important role in maintaining the total body Ca^{2+} balance by filtering and reabsorbing calcium. Disruption in calcium signaling has been reported to result in kidney disease. The most relevant example is the evidence of gain and/or loss-of-function mutations in transient receptor potential canonical (TRPC) 6 (TRPC6) causing focal segmental glomerulosclerosis, which is manifested by severe albuminuria. Also mutation in polycystin 1/polycystin 2 genes has been linked to polycystic kidney disease and mutation in TRPM6 channels are found to be associated with hypomagnesemia, a condition that has been correlated with cardiovascular disease and all-causes of mortality in end-stage renal disease patients [66]. The discovery of these genetic mutations in calcium channels associated with hereditary kidney diseases signifies the importance of calcium signaling in the kidney disease although their role in DKD is not clear yet.

1.4.3.1 Role of TRPC channel in kidney disease

Podocyte health is crucial in maintaining the filtration capability of the kidney as it is key in regulating glomerular permeability. Elevation of intracellular calcium is regarded as one of the main pathological factors that drive the pathological changes in glomerular morphology and permeability. The transient receptor potential canonical (TRPC) channel belong to a superfamily called TRP channels that are non-selective cation channel with high Ca^{2+} permeability. They exist as tetramer with each subunit containing intracellular NH_2 and COOH termini, six transmembrane

domains (S1–S6), and a pore loop between the S5 and S6 segments[67]. To date it is widely known TRPC channels are one of the major ion channel classes that regulate calcium influx inside the cell. Among seven structurally related family members, the importance of TRPC6 has been emphasized by the discovery of genetic mutation associated with focal segmental glomerulosclerosis (FSGS) which displays similar renal injury like loss of the glomerular filtration barrier cells and progressive albuminuria seen in DKD [68]. Studies have shown that overexpression of either wild type or any of the reported mutant version of TRPC6 in mice resulted in FSGS like disease [69]. Moreover, several studies have suggested that TRPC6 can be activated by molecules that are reported to be increased in disease conditions, especially in diabetes, and could potentially enhance calcium influx and trigger proteinuria. For example, one of the key mechanisms of TRPC6 activation involves DAG, that is generated by GPCR mediated stimulation of PLC [70]. Besides Gq mediated production, increased levels of glycolytic intermediates can also stimulate de novo synthesis of DAG. Many studies have shown that DAG levels are high in various tissues including glomeruli. Serum level of DAG has been reported to be elevated in diabetic patients [71]. Moreover, Gq receptors can be activated by multiple ligands: angiotensin II, Endothelin-1, thromboxane, prostaglandin E2 which are also reported to be elevated in diabetic condition [72-74]. Reactive oxygen species that is highly produced in diabetic conditions due to metabolic abnormality is another factor that has been reported to activate TRPC6. It has been demonstrated that ROS in particular hydrogen peroxide generated from NADPH oxidase is required for TRPC6 activation. In both podocyte and mesangial cells multiple studies have shown ROS mediated activation of TRPC6 resulted in injury of the cells [75]. In addition, TRPC6 expression has been found to be elevated in various animal models of DKD. In streptozotocin induced rat model of diabetes in the background of both normal and hypertension, upregulation of TRPC6 was associated with high proteinuria and renal histopathology that is similar to human DKD [75, 76]. Wang et al using genetic approaches recently showed that TRPC6 KO resulted in attenuated tubule injury and reduced proteinuria until the later stages of the disease process in type 1 Akita mice [77]. Although these data implicate TRPC6 as a major player in type-1 diabetic nephropathy, no data exist related to type-2 nephropathy.

The downstream signaling pathway for TRPC6 has been extensively studied in podocyte and several signaling pathways has been linked to the phenotype related to glomerular disease. Several

authors have already demonstrated that activation of TRPC6 results in the apoptosis of podocyte via calcineurin-NFAT mediated signaling pathway [78, 79] without explaining the mechanism. It is well known that TRPC6 mediated calcium influx activate calcineurin-NFAT pathway whereby upon dephosphorylation NFAT goes into nucleus and activate a plethora of genes whose products can be other transcription factors, signaling proteins, secretory proteins, cell surface receptors, and other effector proteins any of which can be attributed to apoptosis. Multiple reports have indicated that NFAT mediated apoptosis might involve activation of intracellular signaling pathways or production of secreted proteins. The role of intracellular molecules in podocyte apoptosis as a result of calcineurin NFAT activation has been demonstrated by several authors [80, 81]. In those studies, they have identified NFAT dependent COX2 mediated ROS generation and an enhanced calcineurin/NFAT/Bax2 signaling pathway as one of the downstream effectors for podocyte apoptosis. It is fairly established that intracellular activation of COX2 or Bax/Bak signaling pathway leads to apoptosis but if TRPC6-mediated cell death involves either of these pathways is still unknown. In addition, activation of TRPC6 was shown to activate RhoA-Ras pathway and leads to cytoskeleton remodeling [66]. Given the number of calcium responsive proteins these mechanisms do not exclude the possibilities of other pathways that might be linked to similar disease phenotype.

1.5 Use of computational biology in deciphering DKD

Over the past several years tremendous progress has been made in understanding the pathophysiology of DKD, yet a clear mechanistic understanding is still lacking. The use of gene expression profiling has become a popular tool due to the availability of large amount of molecular, clinical and histopathological data from DKD patients. This created a new approach called system biology approach to understand DKD. In this approach using a set of experimental and computational tools, molecular changes are first identified in the whole kidney or more precisely in different interrelated kidney cells. Then these changes in cellular networks are then used to identify associations among the many molecular changes that might predict, enhance, or ameliorate disease progression in DKD patients. For the past several years, several authors reported either a new and novel mechanism or validated previously known mechanism using this approach. For example, Woroniecka et al. in their transcriptome analysis of human DKD, reported

vascular endothelial growth factor (VEGF) implicated in DKD, confirming the known biology, at the same time they also reported integrin pathway involved in the DKD pathogenesis [82]. They found that in both glomeruli and tubulointerstitium from DKD patients there is an increase in inflammation and fibrosis related gene expression. Data from other studies suggested that there is a cascade of activation of inflammatory genes with the progression of disease. For example in one study pathway mapping suggested that out of 138 known NF- κ B responsive genes only one gene is enhanced in early disease where 54 are upregulated in progressive disease, thus emphasizing the progressive activation of inflammatory pathways in DKD [83]. Transcriptome analysis at tissue compartment level also helped deciphering mechanisms at tissue level. Transcriptomic analysis using glomeruli and tubulointerstitial tissues from patients with both early DKD and progressive DKD demonstrated differential activation of the JAK-STAT signaling pathway in glomeruli versus tubule. They reported that at early stage most of the JAK-STAT genes were expressed at substantially higher levels in the glomeruli; whereas, tubulointerstitial JAK-STAT gene expression was not elevated in early DKD but was higher in the patients with more progressive DKD [84]. One of the key limitations of all these studies is that they don't point to a specific cellular phenotype. Moreover, with the availability of additional datasets, it would be interesting to delineate how much overlap exists in all of the data set to give a consensus sets of genes that are common in all DKD patients. Finding such consensus sets of genes and understanding their collective role in DKD pathogenesis might help to find a common mechanism.

Although transcriptome analysis alone can help to have mechanistic understanding of the disease, sometimes alterations in a gene do not necessarily lead to proportionate changes in protein expression. In that case it becomes harder to link the molecular changes to a phenotype. Another approach of system biology might be to associate the molecular changes to cellular morphology or clinical phenotype. DKD is still confirmed by histopathological evaluation, thus emphasizing the role of structural changes as the hallmark of disease progression. The overarching goal of such approach would be to define the correlation of molecular changes to early-stage structural damage in DKD and their association with long-term outcomes. Using cortical interstitial fractional volume (VvInt), an index of tubule-interstitial damage and compartment-specific gene expression profiling from CKD patients Nair et al demonstrated the early molecular signature can be linked to the long-term disease progression [85]. In a separate study, Beckerman et al. in an effort to identify key

driver modules in kidney expression data and correlate this with phenotypic outcomes found that molecular signature correlates well with structural changes rather than GFR [86]. These data demonstrate that relating transcriptomic data with histological features by correlating genotype to phenotype would provide better understanding of DKD pathogenesis rather than relying on only molecular data alone.

1.6 Conclusion

Despite the advancement of our understanding the mechanism of DKD, the available option for treating DKD is still to use an antagonist against ACE or ARB. Although with recent success of SGLT2 inhibitor and the observation of renal benefit of Glucagon like peptide 1 (GLP1) agonist and ET-1 antagonist might open up new therapeutic intervention; however, with ever increasing numbers of diabetic patients there is an urgent need for new therapeutic interventions. Preservation of cyclic nucleotides has been shown to be beneficial in renal disease [23, 43, 87]. Using multiple different preclinical renal disease models, several investigators have shown the beneficial role of cyclic nucleotides in the context of PDE4, that uses cAMP as substrate, and PDE5, that uses cGMP as substrate, by using class-specific inhibitors. In this context the question becomes, is preservation of both nucleotides beneficial for kidney? Moreover, the complex nature of DKD indicates that addressing multiple pathological changes such as alterations in hemodynamics or inflammation, concurrently, might offer greater benefits than focusing on a single pathology. From these perspectives PDE1 hypothetically fits nicely as its hemodynamics and anti-inflammatory features were shown by several investigators [39, 51, 52]. Moreover, according to the human protein atlas, PDE5 is not well expressed in glomeruli or tubule whereas PDE1 is highly expressed in both glomeruli and tubule thereby indicating its potential greater role in renal biology. Yet no single data exist exploring PDE1s role in renal biology. Among the 11 mammalian PDEs, PDE1 is the only PDE activated by calcium which is critical due to the calcium dysregulation observed in DKD patients. This fact also provide a strong rational to investigate the role of PDE1 in the context of diabetic renal disease as several of the risk factors in the diabetic milieu are known to activate ion channels, especially calcium channels. Yet no data exist about the relative abundance of calcium transporters in DKD patients. In cardiomyocytes it has been reported that TRPC3 associated calcium activates PDE1 and cause apoptosis. Similar mechanism has not been demonstrated in

any renal cell type [88]. The role of TRPC6 in FSGS has been clearly demonstrated and it is known to be present in all major type of renal cells. So, it would be interesting to see if TRPC6 is a major calcium channel associated with PDE1 activation. Finally, a severe limitation in finding a therapeutic intervention is a lack of animal models that recapitulate human CKD or DKD. Not only that animal models do not reflect the heterogeneity of human DKD but also often times the outcome measured in two species do not match. For example, in the search for agents to reduce fibrosis and progression of CKD, the efficacy readouts in animal would be multiple histological, histochemical and biochemical parameters, whereas in man the more restrictive end points would be mortality, glomerular filtration or proteinuria. One of the major reasons for failure in clinical trials is such kind of cross-species differences in translational research. Therefore, there is an urgent need to develop methodologies for reducing the gap between cross-species translational research.

CHAPTER 2. ROLE OF PHOSPHODIESTERASE 1 IN SYSTEMIC HEMODYNAMICS AND POTENTIAL IN DIABETIC KIDNEY DISEASE

2.1 Introduction

DKD is a major microvascular complication of diabetes that often results in either dialysis or kidney transplantation and poses a major global burden to healthcare. Approximately half of type-2 and one-third of type-1 diabetic patients will develop DKD, which is clinically defined by the presence of impaired renal function as indicated by declining glomerular filtration or elevated urinary albumin excretion, or both [1]. Although the pathophysiology of DKD is multifactorial, the link with hemodynamic and metabolic factors is well established [10]. The initial driver for DKD is associated with a dysregulated metabolic milieu such as hyperglycemia, hyperlipidemia and insulin resistance. However, several clinical trials achieving metabolic benefits still failed to demonstrate improvement in renal disease, thus indicating involvement of other factors [2]. Hemodynamic factors like increased systemic blood pressure and intraglomerular pressure driven by the activation of several vasoactive hormone pathways like renin angiotensin system and endothelin-1 are also major contributors to the disease [89]. The current standard of care, ACE or ARB inhibitor and the recent successful SONAR trial [13] emphasized the role of hemodynamics in the pathophysiology of DKD. Moreover, the positive renal outcome seen in the CRDENCE trial with SGLT2 inhibition indicated that the renal benefit extends beyond the glycemic control and could be due to its effect in renal hemodynamic [90]. Despite the recent therapeutic advances there remains an unmet need for innovative treatment strategies to prevent, arrest, treat, and reverse DKD. Chronic metabolic and hemodynamic disturbances lead to the activation of several autocrine and paracrine factors that further cause structural changes in the kidney. Decades of research towards the understanding of the molecular mechanisms of DKD pathogenesis has made it possible to identify numerous new targets that open up opportunities for new therapeutic intervention.

A major factor underlying kidney dysfunction involves defects of second messenger signaling, including cyclic nucleotides. Many renal functions, like solute transport and regulation of vascular tone has been shown to be modulated by cyclic nucleotides. Arginine-vasopressin mediates increases in cyclic adenosine monophosphate (cAMP) and atrial natriuretic factor induced cyclic

guanine monophosphate (cGMP) have been shown to be critical in the regulation of sodium and water retention [23]. The regulation of cyclic nucleotides in the cell is a balance between the synthesis of these molecules by adenylate cyclase and guanylate cyclase and catabolizing enzymes the cyclic 3', 5'-nucleotide phosphodiesterases (PDEs) that play a pivotal role in regulating the amplitude, duration, and localization of cyclic nucleotide signaling. In kidney, unique cellular and tissue distribution of PDEs contribute to cyclic nucleotide compartmentalization. Using PDE isoform specific inhibitors, several investigators have shown that PDEs exert different downstream effects by regulating the compartmentalization of cyclic nucleotides. For example, in mesangial cells, it has been demonstrated that although cAMP hydrolysis is directed by PDE3 and PDE4 but they play different function in terms of cellular physiology. Using using spatially restricted probes for cAMP, they have shown that the PDE3-regulated cAMP pool inhibits mitogenesis, whereas the PDE4-regulated cAMP pool regulates reactive oxygen species generation and monocyte chemoattractant protein-1 expression [91, 92]. Pharmacological intervention studies in pre-clinical models of both DKD and CKD have further demonstrated the functional role of several PDE isoforms in renal biology. Roflumilast, a selective PDE4 inhibitor, demonstrated renal benefits in streptozotocin induced type1 diabetic nephropathy. Specifically, Roflumilast reduced oxidative stress, deposition of extracellular matrix proteins such as fibronectin and collagen, and inhibited apoptosis. PDE5 has been reported to be expressed in different parts of the kidney. In addition to tubule and glomeruli they also have been reported in inner medullary collecting duct cells, and mesangial cells. PDE5 inhibitors, including sildenafil and tadalafil, were renoprotective in pre-clinical models of CKD and DKD through its vasodilatory, antiapoptotic and antioxidant properties [46]. This also translated in humans as PF-00489791, a long acting PDE5 inhibitor, reduced albuminuria in DKD patients [93]. In a small clinical trial of 90 type-2 diabetic patients, a selective inhibitor of PDE3, has proven to be effective in improving albuminuria and the expression of adhesion and pro-inflammatory molecules [94]. Although all isoforms of PDEs have been reported to be expressed in kidney [58] the functional role of other PDEs (beyond PDE 3, 4 and 5) is still largely unknown.

Among all 11 PDEs, PDE1 is the only phosphodiesterase that is activated by a Ca²⁺/calmodulin-binding domain and has affinity for both cAMP and cGMP. All three isoforms, PDE1A, B and C are found to be expressed in pulmonary vasculature, aorta and mesenteric arteries in rats [49-51].

PDE1A regulates cGMP in rat cardiomyocytes and vascular smooth muscle cells, whereas PDE1C regulates cAMP in aortic and pulmonary smooth muscle cells [52]. In vitro and ex vivo experiments have demonstrated the role of PDE1 in vasodilation. A selective pan-PDE1 inhibitor demonstrated blood pressure lowering effect in normal rats [52]. The role of PDE1C has been well characterized in pathological cardiac remodeling and dysfunction. Using genetic and pharmacological approaches, Knight et al, demonstrated that inhibition of PDE1 attenuated cardiac remodeling and dysfunction by antagonizing cardiac myocyte hypertrophy and death [54]. In the kidney, PDE1A is expressed in the tubules, PDE1C is expressed in the glomeruli and tubules, and PDE1B is not expressed in either location [58]. Both the vasodilatory mechanism and anti-apoptotic feature of PDE1 inhibition could potentially confer renal benefit. As of yet, the functional role of PDE1 in the kidney has not been defined. Moreover, in diabetic nephropathy several risk factors like AngII, ET-1, high glucose can increase intracellular calcium that might drive the upregulation of PDE1. In mouse cardiomyocytes, calcium channel TRPC3 drove PDE1 upregulation that lead to apoptosis of cardiomyocytes [95]. No such studies are known to exist in the context of renal biology. Therefore, we were prompted to investigate the role of PDE1 in kidney, especially in the context of diabetes. Herein, we describe a potent pan-PDE1 inhibitor and show in vivo its vasodilatory function using a novel method. Using the same pharmacological tool, we also demonstrate its beneficial role in diabetic kidney disease using a DKD model driven by diabetes, hypertension, and nephron loss. We demonstrate that the functional beneficial effect of PDE1 inhibition was associated with reduction of inflammation and fibrosis. We also demonstrate that PDE1 inhibition lead to lowering of blood pressure in both normal and hypertensive animals. Taken together, these observations strongly suggest potential therapeutic application of PDE1 inhibition in DKD.

2.2 Methods and materials

2.2.1 Animals

The animal care and experimental protocols in this study were conducted under the supervision of a veterinarian and in accordance with the Eli Lilly and Company's Animal Care and Use

Committee. Whenever possible, procedures in this study are designed to avoid or minimize discomfort, distress, and pain to animals. Animals were purchased from the following vendors: Harlan (db/db KS with or without vendor-performed surgical removal of one kidney at 4–5 weeks of age), or Taconic (SD rats and SHR rats). Mice were fed ad libitum a standard 5008 diet (Lab Diets). Rats were fed with standard 2014 diet (Lab diets). Females were used in the obese type 2 models to prevent risk of pyelonephritis.

2.2.2 Generation of PDE proteins

The nucleotide sequences encoding full-length human PDE1A (NP_001003683.1), PDE1C (NP_005011.1), PDE5A (NP_001074.2), PDE7B (NP_061818.1) and PDE9A (NP_002597.1) were inserted into pFastBac1 (Invitrogen) vector with an N-terminal HIS tag. The nucleotide sequences encoding full-length human PDE4D (NP_006194.2) and the catalytic domain (residue 641-1141) of PDE3A (NP_000912.3) were inserted into pFastBac1 (Invitrogen) vector with a C-terminal HIS tag. The nucleotide sequences encoding full-length human PDE8A (NP_002596.1) and PDE11A (AAI12394.1) were inserted into commercially available pFastBac1 (Invitrogen) vector with a Flag tag at N-terminal. The nucleotide sequences encoding full-length human PDE10A (AAD32595.1) were inserted into pFastBac1 (Invitrogen) vector with a C-terminal Flag-His tag. The nucleotide sequences encoding full-length human PDE6A (NP_000431.2) and PDE6B (AAH00249.1) were inserted into pFastBacDual1 (Invitrogen) vector with an N-terminal HIS tag and N-terminal Flag tag, respectively, for production of PDE6A/6B dimer. Baculovirus generation and protein expression in Sf9 cells were carried out according to the protocol of Bac-to-Bac Baculovirus Expression system (Invitrogen). The nucleotide sequences encoding full-length human PDE1B (NP_000915.1) and PDE2A (NP_002590.1) were inserted into pIEX4 (Novagen) with a C-terminal HIS tag, and both protein productions were carried out in Sf9 cells according to the vendor's protocol (Novagen). The HIS tagged PDE proteins were purified using Ni-NTA agarose (Qiagen) followed by size exclusion chromatography on a SUPERDEX® 200 column (GE Healthcare) in storage buffer (20 mM Tris-HCl, pH7.5, 150 mM NaCl, 10% Glycerol). The Flag tagged PDE proteins including PDE6A/6B were purified using anti-Flag M2-agarose (Sigma), after purification through NiNTA column chromatography and eluted in storage buffer

(50 mM Tris-HCl, pH7.5, 150 mM NaCl, 10% Glycerol, 0.1 mg/ml Flag peptide). All purified proteins were stored at -80° C. in small aliquots.

2.2.3 Phosphodiesterase enzyme assays

All 3', 5' cyclic nucleotide phosphodiesterase (PDE) enzyme activities are measured with a radiometric enzyme assay based on SPA detection system (scintillation proximity assay). Compounds to be tested were diluted in pure dimethyl sulfoxide (DMSO) using ten-point concentration response curves. Maximal compound concentration in the reaction mixture was either 10 or 100 μ M. Compounds at the appropriate concentration were pre-incubated with either of the PDE enzymes for 30 minutes before the reaction is started by the addition of substrate. Reactions are allowed to proceed for 60 minutes at room temperature. Next, reactions were stopped by addition of SPA beads. Samples were read 12 hours later in a MICROBETA™ TRILUX® Counter. "IC50" refers to the concentration of the compound that produces 50% of the maximal inhibitory response possible for that compound. IC50 values are calculated by plotting the normalized data vs. log [compound] and fitting the data using a four-parameter logistic equation.

2.2.4 IC50 calculation

For each test compound, % Inhibition is calculated using the equation below:

$$\% \text{ Inhibition} = 100 - \left[\frac{\text{Test Compound} - \text{Median Min}}{\text{Median Max} - \text{Median Min}} \right] \times 100$$

where the signals are defined as:

Test Compound = signal for test compound

Min = signal in the absence of agonist

Max = signal in the presence of agonist

% Inhibition (Y-axis) is plotted against log concentration of test compound (X-axis) and analyzed using a 4-parameter nonlinear logistic equation (ABase Equation 205) as shown below:

$y = \frac{A + (B - A) / (1 + (C/x)^D)}{1}$ where, y = % specific inhibition A = Bottom of the curve, B = Top of the curve, C = Relative IC50 = concentration causing 50% inhibition based on the range of the data from top to bottom and D = Hill Slope = slope of the curve.

2.2.5 Calcium-calmodulin dependent PDE enzyme assays

PDE1A, PDE1B, and PDE1C were cloned and purified in house following standard protein generation procedures. The assay buffer is prepared to give a final concentration of 50 mM Tris-HCl, 50 mM MgCl₂, 4 mM CaCl₂, 0.1% Bovine serum albumin and 6 U/ml Calmodulin in water, at pH 7.5. The final enzyme concentration is 0.25, 0.074 and 0.0012 nM, for PDE1A, PDE1B, and PDE1C, respectively. The reactions were started by addition of the substrate, [3H]cAMP, at a final concentration of 47 nM.

2.2.6 PDE enzyme assays using [3H]cAMP as substrate

The following phosphodiesterase activities were measured using [3H]cAMP as reaction substrate: PDE3A (catalytic domain), PDE4D, PDE7B and PDE8A. All these enzymes were cloned and purified in house following standard procedures. The assay buffer is prepared to give a final concentration in the assay of 50 mM Tris-HCl, 8.3 mM MgCl₂, 1.7 mM ethylenediaminetetraacetic acid (EDTA) and 0.1% Bovine serum albumin at pH 7.5. Final enzyme concentrations are 0.008, 0.021, 0.5 and 0.06 nM for PDE3A, PDE4D, PDE7B and PDE8A respectively. Reactions are also started by addition of the substrate, [3H]cAMP, to give a final concentration of 47 nM.

2.2.7 PDE enzyme assays using [3H]cGMP as substrate

The following phosphodiesterase activities are measured using [3H]cGMP as reaction substrate: PDE2A, PDE5A, PDE6A/6B, PDE9A, PDE10A and PDE11A. The catalytic active form of PDE6 is a dimer composed of a (PDE6A) and b subunits (PDE6B). The dimer of PDE6A/6B is produced by the expression and purification strategy, using two purification steps, i.e., NiNTA and anti-FLAG Sepharose chromatography. The rest of the enzymes are cloned and purified in house following standard procedures. The assay buffer is prepared to give a final concentration in the assay of 50 mM Tris-HCl, 8.3 mM MgCl₂, 1.7 mM EDTA and 0.1% Bovine serum albumin at pH 7.5. Final enzyme concentrations are 0.2, 0.002, 5, 1, 0.03 and 0.03 nM for PDE2A, PDE5A, PDE6AB, PDE9A, PDE10A and PDE11A, respectively. The reactions are started by addition of

the substrate, [3H]cGMP, to give a final concentration of 80 nM in the case of PDE2A, PDE10A, PDE5A, PDE6AB and PDE11A assays, whereas for PDE9A 20 nM of [3 H]cGMP is used.

2.2.8 ReninAAV db/db uNx model for renal failure

In vivo assessment of DKD Progression in ReninAAV and corresponding control LacZAAV were obtained as previously described [96]. In brief, Mice received a single retro-orbital injection of ReninAAV (5 X 10¹⁰ GC per animal) or LacZAAV at approximately 12 weeks of age. Body weight, blood glucose levels, and proteinuria were measured after 4wks to evaluate the disease progression. Once the disease establishment was confirmed by their albuminuria mice were randomized based on the above parameters. Mice were treated with either vehicle or PDE1 inhibitor for 6wks. Urine was collected bi-weekly. At the end of the study mice were euthanized, and the half of the remaining kidney was collected and fixed in 10% neutral buffered formalin for histologic processing and the remaining half was snap frozen for RNA processing. Serum and plasma were collected at necropsy for measurement of serum creatinine (enzymatic creatinine using a protocol validated by HPLC).

2.2.9 Rat telemetry studies

Male Sprague Dawley rats, Spontaneous Hypertensive rats (Charles River Laboratories, USA), implanted with Data Science International transmitters (HD S10) for collection of blood pressure (BP) and heart rate (HR) data in aseptic conditions. The transmitters that was implanted in animals by the vendor, are capable of transmitting a signal via a pressure catheter inserted into the abdominal aorta. Baseline was established and recorded. After they were randomized based on their baseline hemodynamic parameters each rat was then removed from its recording cage and was dosed twice a day by p.o. gavage with vehicle or compound, and the animals were then returned to the recording cage. Data sampling for blood pressure and heart rate was carried out in intervals at selected time points for 24hours.

2.2.10 Rat Ear temperature

Male Sprague Dawley rats were purchased from Taconic Biosciences at 6 to 7 weeks of age. They were dosed orally by p.o. gavage with different doses of LY1, the pan PDE1 inhibitor was formulated in 1% hydroxyethylcellulose (Dow Corning, Midland, MI) (w/v), 0.25%

Table 1: Body weight, proteinuria and blood glucose level of the dbdb renin AAV mice

Group	Proteinuria (mg/g)	Body weight (g)	Blood glucose (mg/dl)
DbDb Renin AAV-Vehicle	10716.25	39.2	253.5
DbDb Renin AAV-Vehicle	32678.57	44	247
DbDb Renin AAV-Vehicle	32821.92	52.9	358
DbDb Renin AAV-Vehicle	33757.01	51.8	447.5
DbDb Renin AAV-Vehicle	42547.17	53.02	510
DbDb Renin AAV-Vehicle	43229.17	41.6	253
DbDb Renin AAV-Vehicle	45375	50.1	255.5
DbDb Renin AAV-Vehicle	50075.95	44.8	202
DbDb Renin AAV-Vehicle	53720.93	50.4	311
DbDb Renin AAV-Vehicle	66126.44	57.2	313.5
DbDb Renin AAV-LY1-0.3mg/kg	10071.43	58.3	273
DbDb Renin AAV-LY1-0.3mg/kg	17784.72	43.3	449
DbDb Renin AAV-LY1-0.3mg/kg	27176.8	43.3	231.5
DbDb Renin AAV-LY1-0.3mg/kg	28806.72	50.2	274
DbDb Renin AAV-LY1-0.3mg/kg	35355.56	49.7	425
DbDb Renin AAV-LY1-0.3mg/kg	43985.4	46.5	287.5
DbDb Renin AAV-LY1-0.3mg/kg	48818.79	49.1	172
DbDb Renin AAV-LY1-0.3mg/kg	49508.77	54.6	505
DbDb Renin AAV-LY1-0.3mg/kg	54395.06	42.4	271.5
DbDb Renin AAV-LY1-0.3mg/kg	61094.49	49.2	183.5
DbDb Renin AAV-LY1-1 mg/kg	12891.72	44	127.5
DbDb Renin AAV-LY1-1 mg/kg	15862.07	46.7	281
DbDb Renin AAV-LY1-1 mg/kg	26285.71	56.3	239.5

Group	Proteinuria (mg/g)	Body weight (g)	Blood glucose (mg/dl)
DbDb Renin AAV-LY1-1 mg/kg	34142.86	49.9	294.5
DbDb Renin AAV-LY1-1 mg/kg	41811.76	54.5	260
DbDb Renin AAV-LY1-1 mg/kg	43359.55	42.4	489.5
DbDb Renin AAV-LY1-1 mg/kg	45276.6	49.8	207.5
DbDb Renin AAV-LY1-1 mg/kg	54216.56	45.6	531.5
DbDb Renin AAV-LY1-1 mg/kg	68552.63	43.1	480.5
DbDb Renin AAV-LY1-1 mg/kg	71627.27	48.4	272.5
DbDb LacZ	1464.84	48.9	246
DbDb LacZ	3136.45	48.6	316
DbDb LacZ	2071.25	59.6	585
DbDb LacZ	3734.26	58.3	295.5
DbDb LacZ	883.95	52	120
DbDb LacZ	2234.18	47.6	261.5

polysorbate 80 (Sigma-Aldrich, St. Louis, MO) (v/v), and 0.05% antifoam (v/v; Dow Corning, Midland, MI) in purified water. Following dosing, ear temperature was measured by using a k-type thermocouple probe digital thermometer every hour for 6 hrs and then at 24 hrs. Blood samples for plasma exposure measurement were obtained at the same time. Blood was collected via a tail snip directly into a 20- μ L EDTA-coated capillary and immediately spotted onto a Whatman DMPK-C DBS card (GE Healthcare Bio-Sciences, Piscataway, NJ). Tail snips were performed by removing approximately 1 mm of the tail by using a scalpel. Blood flow was initiated by gentle squeezing of the tail. No analgesia or anesthesia was used during blood collections. A single sample and spot were collected per time point. The DBS cards were allowed to dry for approximately 2 h at room temperature, after which the cards were placed in a zip-top bag, stored, and shipped at ambient temperature.

2.2.11 Histopathologic Evaluation

The histopathological evaluation of the kidneys were done as described previously [97]. Kidneys fixed in 10% formalin were transversely trimmed, processed, paraffin embedded, microtome sectioned at a thickness of 5mm. They were then stained with either hematoxylin and eosin, or Masson trichrome, or periodic acid–Schiff. After required incubation and washing steps as per the protocol tissue sections were examined by light microscopy. A board certified veterinary pathologist assigned scores for several histopathological parameters like tubular regeneration, tubular protein, tubular dilation, and interstitial inflammation. Glomerular injury, expansion of the mesangium, and integrity of tubular basement membranes were evaluated based on the Periodic acid–Schiff-stain in similar manner. Masson trichrome–stained slides were evaluated for interstitial and glomerular fibrosis. A score from zero to five (normal to severe, respectively) was used to describe the histological changes in compound treated group compared with controls. Following are the description of the individual scores:

no changes or changes consistent with spontaneous background finding in the age, sex, and/or strain; minimal (score one)

0%–10% affected; slight (score two):

10%–25% affected; moderate (score three):

25%–50% affected; marked (score four):

50%–75% affected; and severe (score five)

2.2.12 Isolation of rat glomeruli

Before the experiment, a fresh solution of RPMI1640 with 5% bovine serum albumin (BSA) was made and referred to as solution A. SD rat was euthanized using CO₂ followed by a secondary method of killing. After perfusion using a needle through the ventricle, the kidneys were removed and de-capsulated. Pelvis and medulla were removed as much as possible along with the perirenal adipose tissue . Kidney was cut in half sagittal with a single edged razor and place it in a petri plate on ice. The cortex was isolated using a curved scissor. It was finely minced with razor blade in a small amount of PBS in the petri plate and rinse pieces onto #140 sieves presoaked in solution A (only the area to be used was soaked to minimize the use of solution A) resting on a collection pan using the PBS from the wash bottle. The pieces were gently pushed through sieve mesh using

circular motion with the spatula. The underside of #140 sieve was rinsed with the wash bottle and allowed to drain briefly into a pan. A #80 sieve was placed on top of #200 sieve in sink, holding both at a 45° angle. The suspension was poured over sieves, using only the lower 1/3 of the total area. The collecting pans were rinsed with 100 ml aliquots of PBS 2-3 times, pouring over sieves. Finally, the glomeruli were collected with the BSA coated pipette tip and transferred to a 50 ml conical flask. They were centrifuged at 600-100RPM for 5 minutes, and PBS was carefully aspirated off. The glomeruli were re-suspended in appropriate volume of PBS and used for subsequent experiments.

2.2.13 Enzyme-Linked Immunosorbent Assay (ELISA)

Direct ELISA was performed to detect urinary NGAL, Kim-1, MCP-1 and GDF-15 using commercial kits and following their direction. Briefly, urine samples were thawed approximately 1 h before the assays were performed. For all measurements, 100 µL of diluted urine sample was analyzed in duplicate. For quantification, an 8-point standard curve was prepared by a 1:3 dilution of a premixed standard containing all analytes of a specific panel. The recommended dilution of 500-fold was optimal for the detection of NGAL and KIM-1, whereas no dilution was required for the detection of Kim-1 and GDF-15. Urinary antigens were bound to the wells of microtiter plates by incubation of 100 µL urine samples for 1 h at 37°C. Wells were blocked with buffer containing 5% BSA. The primary antibody was mouse monoclonal against mouse NGAL (MLCN20; Quantikine ELISA, R&D Systems), mouse Kim-1 (MKM100; Quantikine ELISA, R&S Systems), mouse MCP-1 (MJE00; Quantikine ELISA, R&S Systems) and mouse GDF 15 (MGD150; Quantikine ELISA, R&S Systems). Incubation was followed by treatment with horseradish peroxidase-conjugate was added for color development. 30 minutes later the reaction was stopped by adding 100ul of HCl. The plate was then read at 450 nm with a Benchmark Plus microplate reader (Bio-Rad, CA, USA). The urinary creatinine (Cr) concentration was used to normalize all analyte measurements to account for the influence of urinary dilution on its concentration. Urinary levels of biomarkers were expressed as analytes/Cr ratio in ng/mg creatinine.

2.2.14 Urinary cAMP and cGMP measurement in rats

To evaluate the acute effect of PDE1 inhibition on urinary cyclic nucleotides male Sprague Dawley rats were dosed with either vehicle or PDE1 inhibitor and a 24-hr urine was collected by placing them in metabolic cage. Urinary cAMP and cGMP were measured using the respective ELISA kit (for cAMP kit cat#501040, for cGMP cat# 501040) from Caymen chemicals following their instruction. Briefly urine samples were thawed approximately 1 h before the assays were performed. For all measurements, 100 μ L of diluted (1:500) urine sample was analyzed in duplicate. For quantification, an 8-point standard curve was prepared by a 1:2 dilution of a premixed standard. The urinary Cr concentration was used to normalize all analyte measurements to account for the influence of urinary dilution on its concentration.

2.2.15 Measurement of apoptosis using Caspase-3/7 Green Detection Reagent

Cellular apoptosis was detected by using CellEvent™ Caspase-3/7 Green ReadyProbes™ Reagent from Thermo-Fisher Scientific (cat# R37111). For the human mesangial cells about 20K cells per well were plated in 96-well black walled plate. The next day, cells were treated with hyperforin 9 at different doses along with DMSO and incubated for 4 hrs at 37°C. A solution of CellEvent™ 3/7 caspase dye was made by adding 2 drops/ml of PBS. Hoechst stain solution was made by adding 2.5 μ L of 2mg/ml solution in 10ml PBS. Thirty minutes before the 4-hr incubation period ended, both dyes were added in total of 200 μ L volume. After 30 minutes of incubation, cells were fixed with 4% paraformaldehyde. For rat glomeruli isolation, about 80 glomeruli per well were plated in 96 well black walled plate. They were incubated in RPMI 16 medium with 10% fetal bovine serum (FBS) overnight. Next they were treated with hyperforin 9 and incubated for 24 hrs. In case of compound treatment, isolated glomeruli were pre-incubated for 1 hr. Before measuring the signal, the glomeruli were incubated with both caspase and nuclear dye for 30 minutes. Images were captured using a high throughput imaging Arrayscan VTI and analyzed with the Target Activation BioApplication using two channels at a magnification of $\times 10$. An algorithm was used to identify objects by nuclear staining with Hoescht dye at 365nm, and caspase signal was captured at 475 nm wavelength. All fluorescent intensities are displayed as relative fluorescent units.

2.3 Results

2.3.1 Effect of LY1 on PDE1 activity

Using a radiometric enzyme assay based on scintillation proximity assay (SPA) detection system LY1 was tested against all recombinant PDE enzymes. LY1 inhibited all three isoforms of PDE1 with very comparable half maximal inhibitory concentrations (IC₅₀) (1.74nM, 2.44nM and 1.20nM for PDE1A, PDE1B and PDE1C, respectively) (Fig. 2.1), while other PDEs were only affected at μ M concentrations (Table 2).

2.3.2 Development of rat model of vasodilation

We used ear temperature measurement to examine if PDE1 inhibition would cause vasodilation in the rats' ear. The hypothesis behind the ear temperature method was the assumption that PDE1 inhibition-induced vasodilation would increase the blood flow in the rat ear that would subsequently increase the surface temperature. Sprague Dawley rats were administered orally a single dose of LY1 at 0.03, 0.1, 0.3, 1 or 3 mg/kg and ear temperature was measured every hour for up to 6 hrs and then finally at 24 hrs. Indeed, there was a significant rapid increase of ear temperature, 14% at the highest dose of 3 mg/kg within 1 hr of dosing compare to the vehicle control as shown in figure 2.2A. Also, a significant dose-dependent increase in ear temperature was observed at 0.1, 0.3 and 1 mg/kg. The calculated ED₅₀ was 0.14 mg/kg (Fig. 2.2B). The response in ear temperature sustained for almost 3 hrs in all groups except the lower dose groups and returned to baseline by 6 hrs. The pharmacokinetic analysis of LY1 correlated with the observed change in ear temperature and calculated the half-life as 4 hrs (Fig. 2.2D). The calculated percent target engagement based on the unbound drug concentration demonstrated about 65% target engagement (TE) at the lowest dose at 1hr and saturated after 0.3mg/kg (Table 2).

2.3.3 LY1 lowered blood pressure in normal and spontaneously hypertensive rats

Vasodilation is an integral part of the regulation of systemic hemodynamics. In general, any dilation of arteries and arterioles leads to an prompt decrease in arterial blood pressure. To evaluate

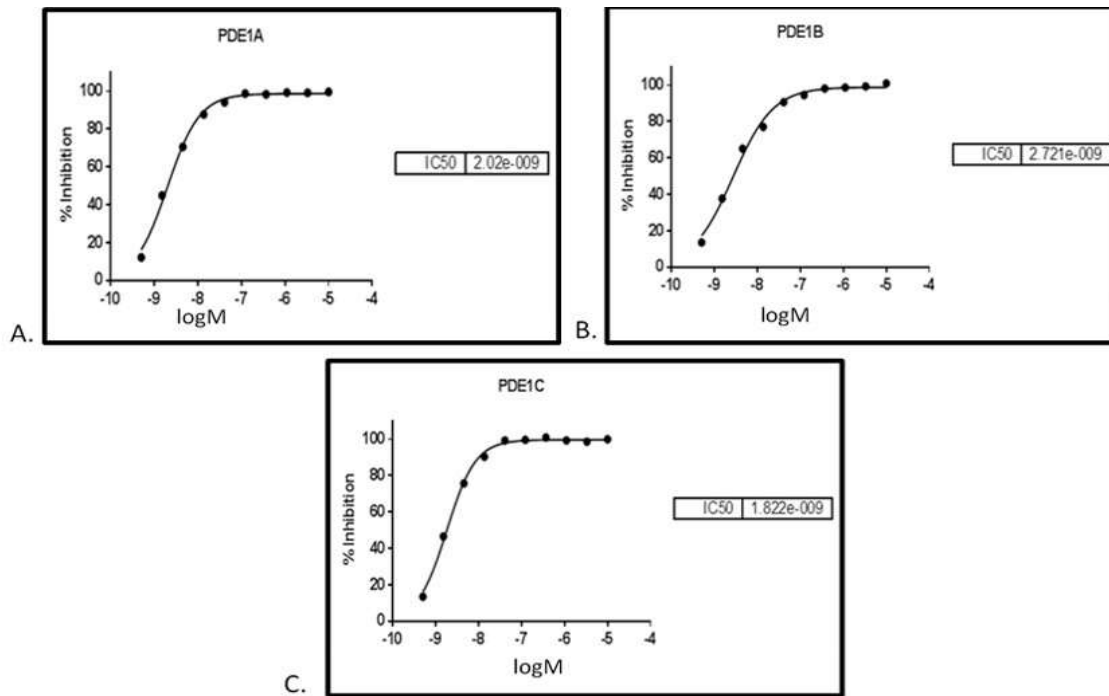


Figure 2.1. Inhibition of PDE1 enzyme activity by LY1. LY1 was pre-incubated with different recombinant PDE1 isoforms for 30 minutes before the addition of the substrate. After incubating at room temperature for 60 minutes reactions were stopped by addition of SPA beads. cAMP levels were measured after 12 hrs. “IC50” refers to the concentration of the compound that produces 50% of the maximal inhibitory response possible for that compound. IC50 values of A) PDE1A, B) PDE1B and C) PDE1C were calculated by plotting the normalized data vs. log [compound] and fitting the data using a four-parameter logistic equation.

Table 2: Inhibition of PDE enzyme activity by LY1

LSN3191567	IC50 (nM)
PDE1A	1.37 (mean of N=10)
PDE1B	1.45 (mean of N=10)
PDE1C	1.20 (mean of N=10)
PDE3A	>10000
PDE4D	7060
PDE5A	>10000
PDE6A/6B	>10000
PDE7B	2180
PDE8A	>10000
PDE9A	>10000
PDE10A	>10000
PDE11A	2970

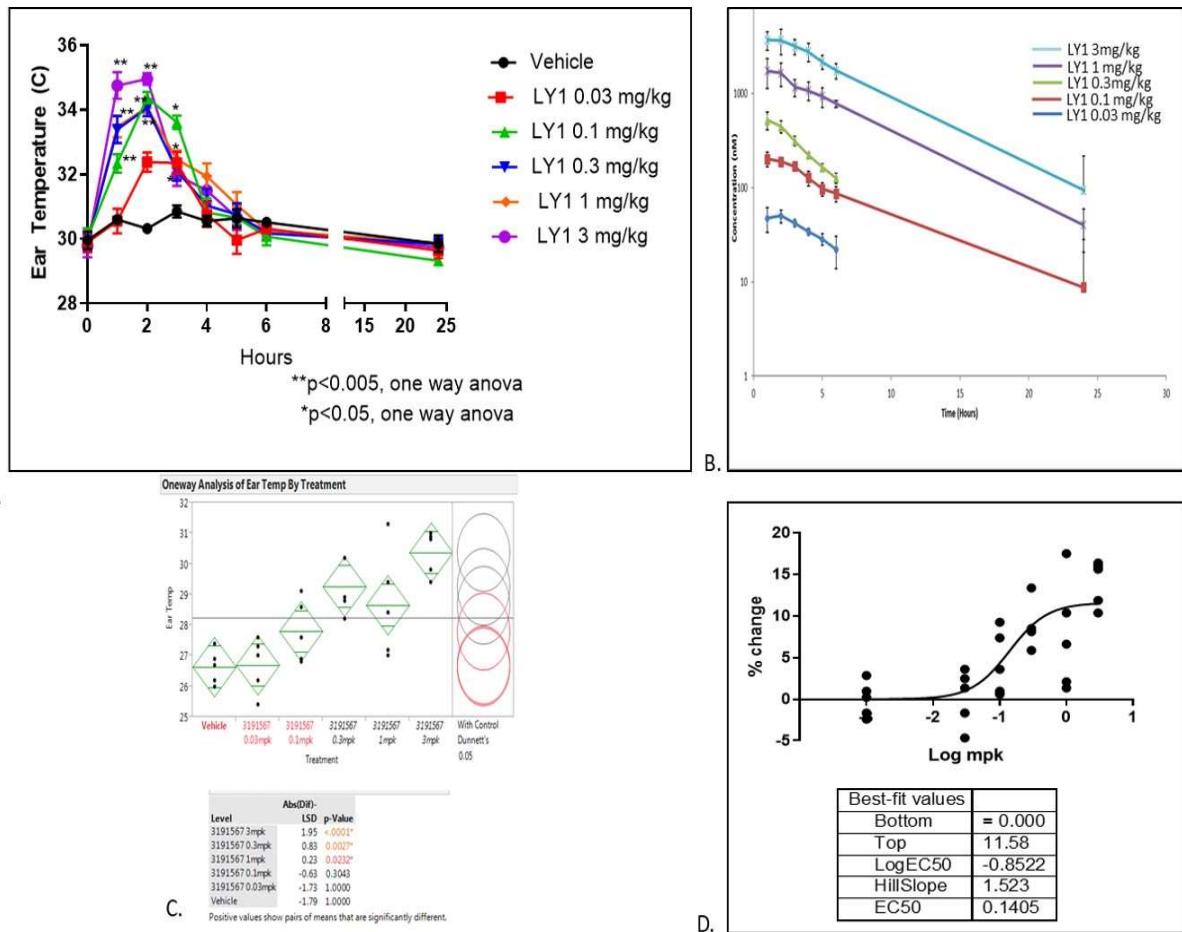


Figure 2.2. Effect of LY1 on ear temperature in rats. Sprague Dawley rats were orally dosed with 0.03, 0.1, 0.3, 1 or 3mg/kg of LY1 and the temperature of the pinnae measured with a K-probe thermometer at every hour for up to 6 hrs and then at 24 hrs after dosing. A) Ear temperature was plotted against time, B) an ED50 of 0.14 was calculated at the 1hr time point. Data are given as mean \pm SEM (N=5). C) One-way ANOVA analysis demonstrating significant change in ear temperature in rats with PDE inhibition. Data represents mean of group average with N=5 and the p-value calculated compared to the vehicle group. D. Pharmacokinetic profile of LY1. Plasma concentrations of LY1 were determined after a single oral administration of 0.03, 0.1, 0.3, 1 and 3 mg/kg of the compound to male Sprague Dawley rats. Data are given as mean \pm SEM (N=5).

the blood pressure lowering effect of PDE1 inhibition in normotensive animals, LY1 was administered in freely moving telemetered Sprague Dawley (SD) rats. Rats were dosed at 1 and 3 mg/kg twice daily via oral gavage, and data were captured every hour for 24 hrs. Figure 2.3 demonstrates a rapid reduction in blood pressure that was sustained for several hours. A decrease

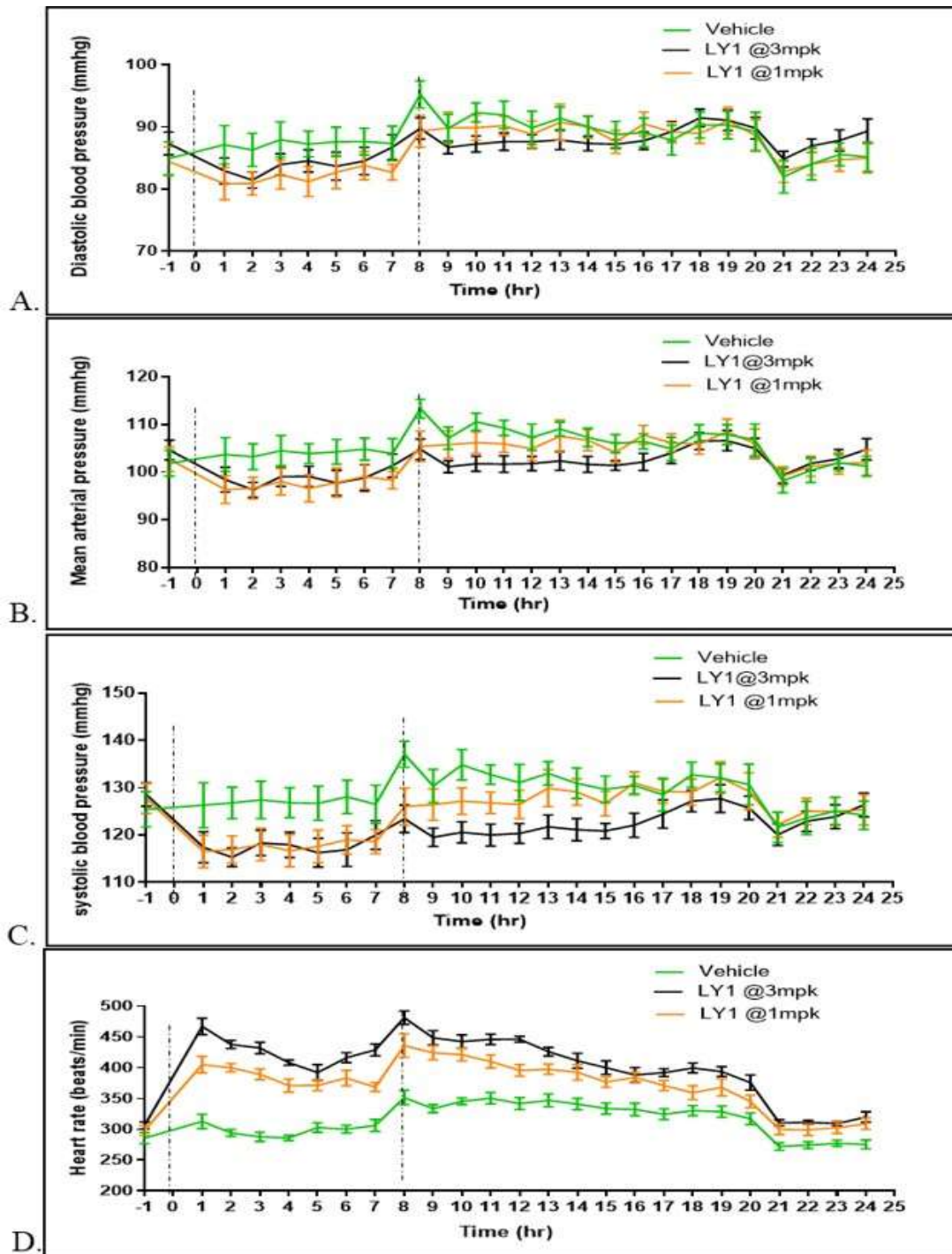


Figure 2.3. Effect of LY1 on the hemodynamics of SD rats. Telemeterized SD rats were dosed twice daily and A) diastolic blood pressure, B) mean arterial pressure, C) systolic blood pressure and D) heart rate were recorded for 24 hrs. Dotted line represents the timing of doses. All the data represented here as SEM.

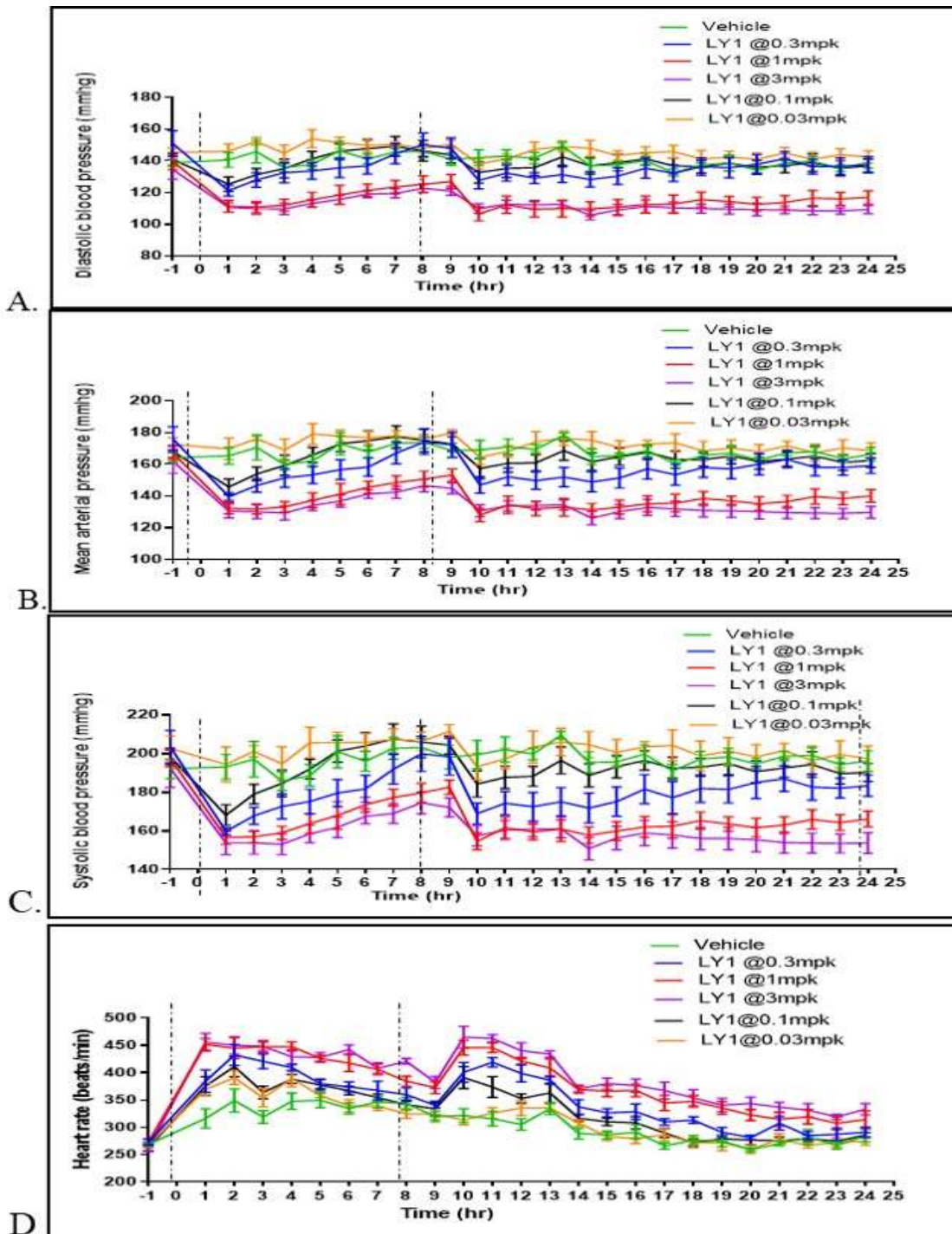


Figure 2.4. Effect of LY1 on the hemodynamics of SHR rats. Telemeterized SHR rats were dosed twice daily and A) diastolic blood pressure, B) mean arterial pressure, C) systolic blood pressure and D) heart rate were recorded for 24hrs. Dotted line represents the timing of doses. All the data represented here as SEM.

of about 5 mm Hg was observed in both groups within 1hr of the first dose compared to the vehicle. In general, the blood pressure lowering effect was sustained for longer in high dose group and returned to baseline 7hrs after the second dose. A dose-dependent increase in heart rate was also observed that returned to baseline towards the end of the time of recording. The blood pressure lowering effect of PDE1 inhibition as observed in normal rats suggested that this might be beneficial in the context of hypertension. In order to test this, telemetered genetically spontaneous hypertensive rats (SHR) that exhibit spontaneous hypertension were dosed twice orally with either LY1 at 0.03, 0.1, 0.3, 1 and 3 mg/kg or a vehicle, and cardiovascular parameters were recorded for 24 hrs. As shown in Figure 2.4, a dose-dependent decrease in blood pressure was observed along with increase in heart rate. Within the first hour of dosing, an acute decrease of about 30 mmHg was observed in 1 and 3mg/kg dose groups compared to only 5 mmHg drop in normal SD rats at the same dose level. A dose dependent increase in heart rate was also evident in SHRs with relatively greater magnitude compare to SD rats at the same dose level. The lowest dose of 0.03mg/kg did not show any effect in both BP and heart rate.

The magnitude of blood pressure lowering effect was much greater in SHRs than in normal rats when compared at the same dose level. ACE inhibitors are used as standard of care for the clinical management of hypertensive patients. In order to evaluate the additive effect of PDE1 inhibitor with ACE inhibitor, SHRs were orally dosed twice a day with either 3 mg/kg enalapril alone or in combination with 0.3 mg/kg of PDE1 inhibitor, and cardiovascular parameters were recorded for 24 hrs. As expected, enalapril lowered the mean arterial pressure by 15% without affecting the heart rate (Fig. 2.5). The co-administration of LY1 with enalapril, an ACE inhibitor lowered mean arterial pressure by almost 20% with significant increase in heart rate which sustained for almost 5hrs but came down to baseline.

2.3.4 LY1 attenuated disease progression in the mouse model of DKD

To determine the role of PDE1 in the pathogenesis of DKD we used a mouse model of severe diabetic nephropathy. Following unilateral nephrectomy at 4-5 weeks old, dbdb mice were injected with AAV virus carrying a renin gene at 12-13 weeks of age. The combination of unilateral

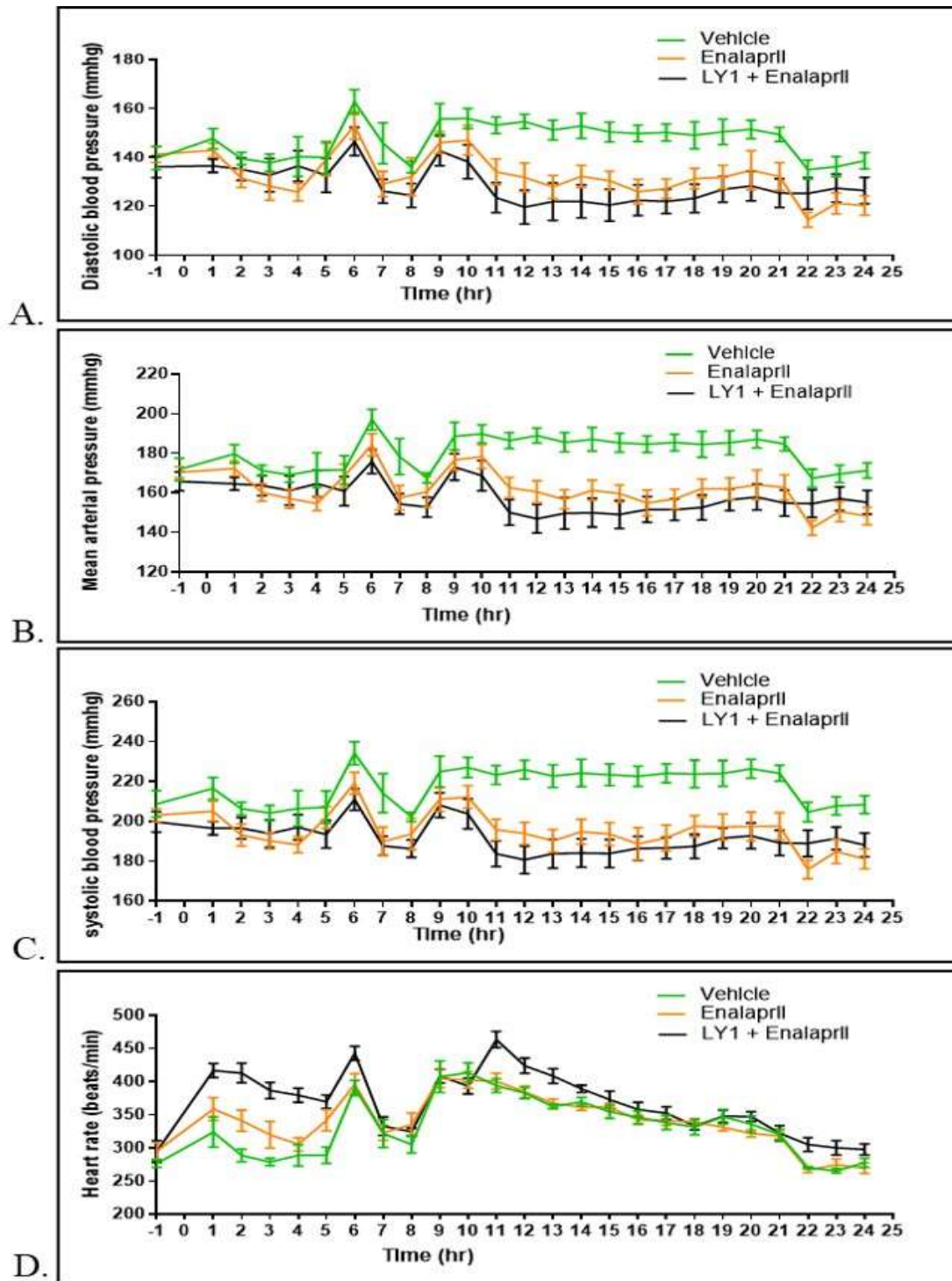
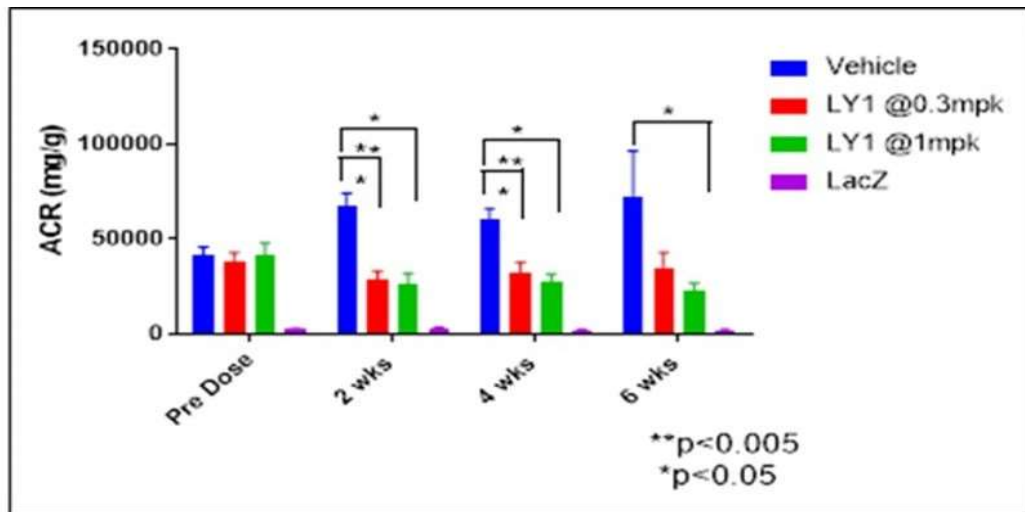


Figure 2.5. Effect of LY1 on the hemodynamics of SHR rats on top of enalapril. Telemeterized SHR rats were dosed twice daily and A) diastolic blood pressure, B) mean arterial pressure, C) systolic blood pressure and D) heart rate were recorded for 24hrs. All the data represented here as SEM.

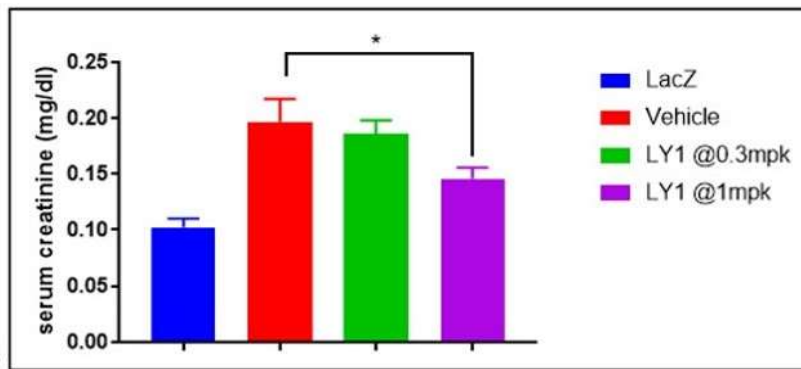
nephrectomy and induction of renin-mediated hypertension resulted in about 18-fold increase in albuminuria compare to the AAV-lacZ control animals. Following randomization based on albuminuria, body weight and blood glucose level, the animals were administered either LY1 twice a day orally at 0.3 or 1 mg/kg for 6 wks or vehicle. Dosing with the PDE1 inhibitor led to significant dose dependent decrease of albuminuria that was evident as early as 14 days and sustained for 6 weeks of treatment (Fig 2.6A). LY1 treated group showed a reduction in urine ACR of about 51% and 69% at 0.3mg/kg and 1mg/kg group, respectively, compared to vehicle after 6 weeks of treatment. Interestingly, in the 1 mg/kg dose group LY1 not only attenuated disease progression but also significantly reduced albuminuria (by 45%) when compared to the pre-dose albuminuria which suggests a possible restoration of kidney function beyond the baseline. The reduction of albuminuria was significant at each time point collected for both doses except in low dose group at the 6-week time point. We also measured serum creatinine to evaluate kidney function. As expected, the AAV renin mice demonstrated an almost two-fold increase in serum creatinine compare to the AAV-lacZ treated animals. Treatment with LY1 for 6 weeks reduced serum creatinine significantly compares to the vehicle treated group (Fig 2.6B). The lower dose group did not show any change in serum creatinine. Administration of AAV renin increased heart weight significantly compared to the lacZ group which was dose dependently decreased with LY1 treatment which indicates a potential cardiovascular benefit. There was no significant change in kidney weight in observed across all groups. (Fig. 2.6C).

2.3.5 LY1 improved histopathology in DKD mouse model

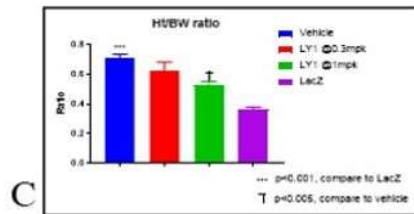
Renal histopathology was evaluated in db/db UNIX-AAV-Renin mice treated with 0, 0.3, and 1 mg/kg of LY1. As reported earlier [97], overexpression of renin in uninephrectomized db/db induced severe pathological changes compared to the AAV-lacZ mice. The vehicle-treated group demonstrated significantly increased deposition of mesangial matrix, intraglomerular fibrosis, periglomerular fibrosis/inflammation, and dilated kidney tubules. Though renal morphologic variability existed within and between treatment groups, mice treated with 1 mg/kg of LY1 had less severe kidney changes when compared to untreated AAV-Renin mice. The changes observed included significantly fewer dilated tubules with proteinaceous filtrate, less glomerular matrix,



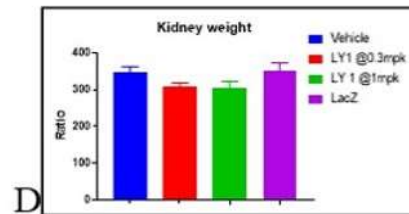
A



B



C



D

Figure 2.6. Effect of PDE1 inhibition in DKD. Four weeks after the induction of renin-dependent hypertension in the unilateral nephrectomy model in db/db mice, they were treated twice with either vehicle or two different doses of LY1 for 6 weeks. Treatment with the PDE1 inhibitor markedly decreased A) albuminuria and B) serum creatinine compare to the vehicle group. Mice treated with the PDE1 inhibitor showed reduced C) heart weight and D) kidney weight after normalized with brain weight. All the data represented here as mean±SD, with N=10 in each group.

decreased glomerular and peri-glomerular fibrosis and sclerosis, and less renal inflammation (Fig 2.7).

2.3.6 LY1 reduced fibrotic and inflammatory gene expression

Histopathological evaluation of the study indicated increased fibrosis and inflammation in the dbdb AAV renin model which improved upon PDE1 inhibition. To further identify relevant gene expression profile associated with the improvement in histopathology, microarray analysis of gene expression was performed using the mRNA isolated from the kidney. The preliminary gene chip data demonstrated a change in the set of genes involved in inflammation, fibrosis and innate immunity signaling pathways in LY1 treated animals compared to control but did not reach significance. The list of genes modulated were further followed up with RT PCR using low density gene expression array card. Several fold increase in some key inflammatory genes were seen in the vehicle control group compare to LacZ group, thereby confirming increased inflammatory response in the disease model (Fig 2.8A). PDE1 inhibition significantly attenuated the inflammatory response (almost to the baseline) at 1mg/kg dose. Similarly, there was a several fold increase in fibrotic gene expression in the control group which were attenuated by PDE1 inhibition. Ingenuity pathway analysis (IPA) revealed that the top three canonical pathways associated with the total number of genes downregulated upon PDE1 inhibition. As expected, one of the pathways was associated with acute phase response. Interestingly a number of affected genes was associated with Liver X receptor/Farnesoid X receptor activation and prothrombin activation pathway. A number of genes that were downregulated by PDE1 inhibition are reported to be associated with renal inflammation, renal tubule injury and kidney failure (Fig 2.8B).

2.3.7 LY1 reduced urinary bio markers of kidney injury

Having seen such a significant improvement in the renal pathology and corroborating changes in the gene signature in the LY1 treated animals, we explored several non-invasive biomarkers indicative of kidney injury. Several urinary biomarkers like NGAL, KIM1, MCP1 and GDF15 were measured via ELISA to evaluate the effect of PDE1 inhibition in this preclinical model of DKD. The urinary neutrophil gelatinase-associated lipocalin (NGAL), which is widely regarded as a marker for renal tubular damage progressively increased in the AAV renin treated animals compare to the lacz control. Urine collected at a 2 week time point demonstrated a 5-fold increase in urinary NGAL in the AAV renin treated animals compare to lacz animals, which progressively

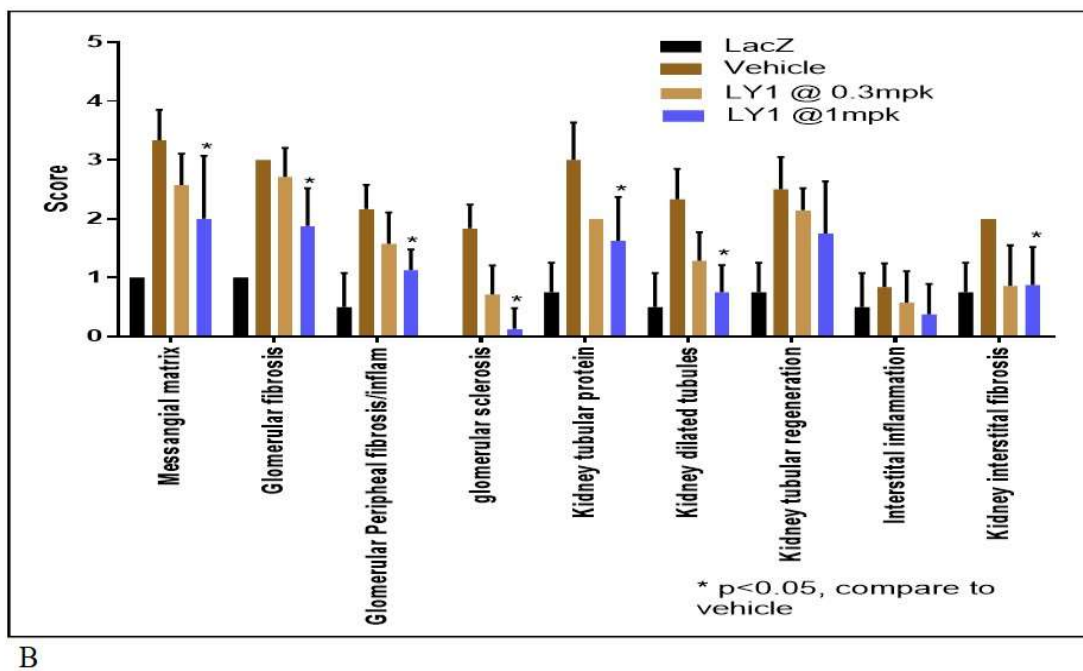
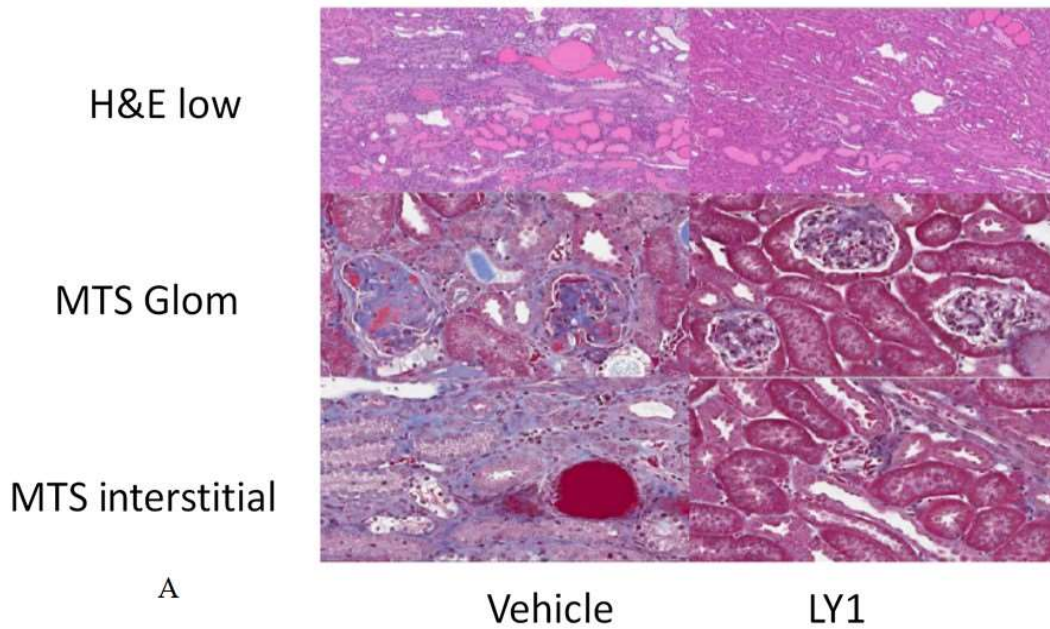
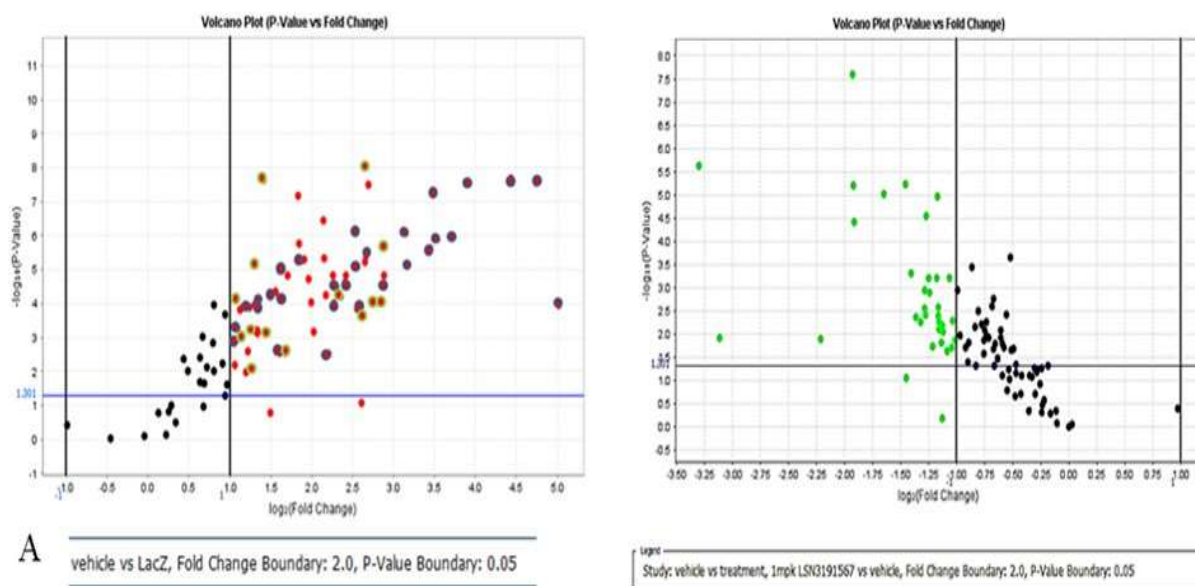


Figure 2.7. Histopathological changes in renin AAV db.db AAV uNx mice upon inhibition of PDE1. A) Representative images of kidney sections stained with H&E , Masson Trichrome (MTS) and periodic acid-Schiff (PAS) from mice treated with either vehicle or LY1 for 6wks. Renin AAV db/db uNx mice treated with LY1 showed reduction in glomerular matrix, decreased glomerular and peri-glomerular fibrosis and sclerosis, and less renal inflammation compared to vehicle treated group. B) Quantification of pathological changes.



LacZ vs Vehicle		Vehicle vs LSN treated	
Gene	Fold change	Fold change	Pathway
<i>Saa1</i>	32.4	0.365	Inflammation
<i>Lcn2</i>	26.7	0.264	
<i>Ccl2</i>	21.5	0.488	
<i>Vcam1</i>	15.1	0.423	
<i>Fgb</i>	13	0.388	
<i>C3</i>	11.6	0.447	
<i>Smpd13b</i>	11.1	0.42	
<i>Fga</i>	10.9	0.409	
<i>Ctss</i>	8.9	0.399	
<i>Clec7a</i>	8.8	0.364	
<i>Lrg1</i>	7.4	0.455	
<i>C1qc</i>	6.3	0.377	
<i>S100a8</i>	5.9	0.457	
<i>Cd14</i>	5.8	0.263	
<i>Col3A1</i>	5.4	0.445	
<i>Col1a2</i>	4.1	0.471	
<i>Fn1</i>	3.3	0.477	

Figure 2.8. Gene expression analysis of fibrotic and inflammatory markers. Taqman analysis using Gene expression array card showing changes in the inflammatory and fibrotic genes in AAVrenin db/db mice compare to lacZ and LY1 treatment reduced the expression of those gene. A) volcano plot B) List of genes that are changed in inflammation and fibrosis pathway.

increased and showed a 17-fold increase at 6 weeks. PDE1 inhibition by LY1 significantly attenuated the elevation of urinary NGAL as early as within 2 weeks and maintained it for 4 weeks in dose-independent manner (Fig 2.9).

Kidney Injury Marker (KIM-1) is a well validated marker for acute kidney injury. Urinary KIM-1 was highly elevated in a 2-week urine sample in the AAV renin treated group compare to the lacZ animals which demonstrated significant kidney injury in this model. The elevation in KIM1 was progressive and reached as high as 18-fold elevation in the diseased animal in 6 weeks. PDE1 inhibition by LY1 significantly attenuated the progressive elevation of urinary KIM1 as early as 2 weeks and maintained it for 2 weeks. At 6 weeks, the high dose group still showed significant reduction in KIM-1 although the low dose group lost the significance. Reduction of urinary KIM-1 was significantly associated with albuminuria ($R^2= 0.78$, p val <0.0001) after 6wks of treatment with PDE1 inhibitor (Fig 2.10).

Monocyte chemoattractant protein 1 (MCP-1) belongs to a group of inflammatory chemokines which is reported to be elevated in DKD. In the vehicle treated AAV renin mice, there was a massive increase (about 64-fold) in urinary MCP-1 compare to the lacZ control as early as 2 weeks. MCP-1 progressively increased during the study. Inhibition of PDE1 by LY1 attenuated the increase of MCP-1 as early as within 2 weeks after dosing, and that was maintained during the study. At 6wks, reduction of MCP-1 was found to be associated with ACR ($R^2=0.78$, p val <0.0001) (Fig 2.11). Interestingly, neither KIM-1 nor MCP-1 showed any significant change in the blood, although KIM-1 showed a trend in treated animals compare to the vehicle group (fig 10 and 11). Urinary growth differentiating factor 15 (GDF-15) has been found to be increased about 4-fold within 2weeks and progressively increased up to 7-fold in 6wks in diseased animals compare to the lacZ. Inhibition of PDE1 significantly reduced the level of GDF15 within 4-6 weeks (Fig 2.12) which also correlates with albuminuria.

2.3.8 Acute effect of LY1 on cyclic nucleotides in the rat urine

In order to explore the effect of PDE1 inhibition on the urinary cyclic nucleotides, normal SD rats

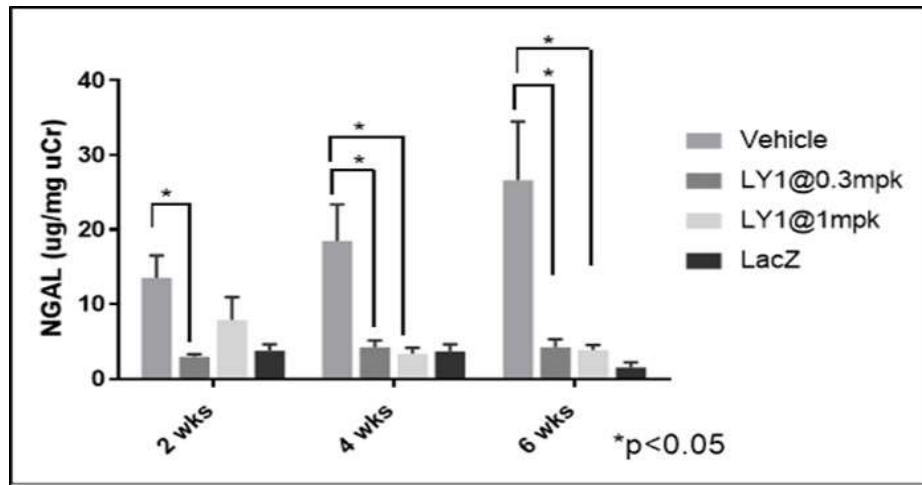


Figure 2.9. Urinary level of NGAL is decreased in AV renin db/db uNx mice following PDE1 inhibition. Mice were treated with 0 (vehicle), 0.3 or 1mg/kg of LY1 for 6wks. Biweekly urine was collected and urinary NGAL was measured using commercially available ELISA kit. Vehicle treated AAVrenin db/db mice showed significant increase in uNGAL which is reduced significantly upon treatment with LY1.

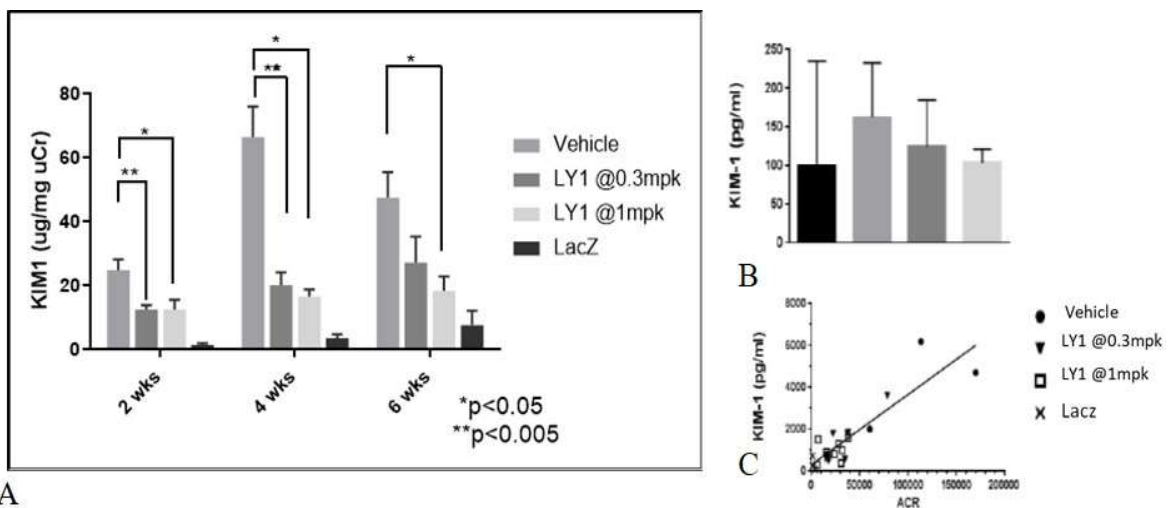


Figure 2.10. Urinary level of KIM-1 is decreased in AAV renin db/db uNx mice following PDE1 inhibition. Mice were treated with 0 (vehicle), 0.3 or 1mg/kg of LSN3191567 for 6wks. Biweekly urine was collected and urinary KIM-1 was measured using commercially available ELISA kit. Blood was collected at the end of the study and KIM-1 was measured in the serum using ELISA. A) Vehicle treated AAVrenin db/db mice showed significant increase in KIM-1 which is reduced significantly upon treatment with LSN3191567. B) Serum KIM-1 showed a trend but did not reach significance. C) Scatter plot showing correlation between urinary KIM-1 and proteinuria ($r^2=0.77$, $p<0.001$) at 6wks.

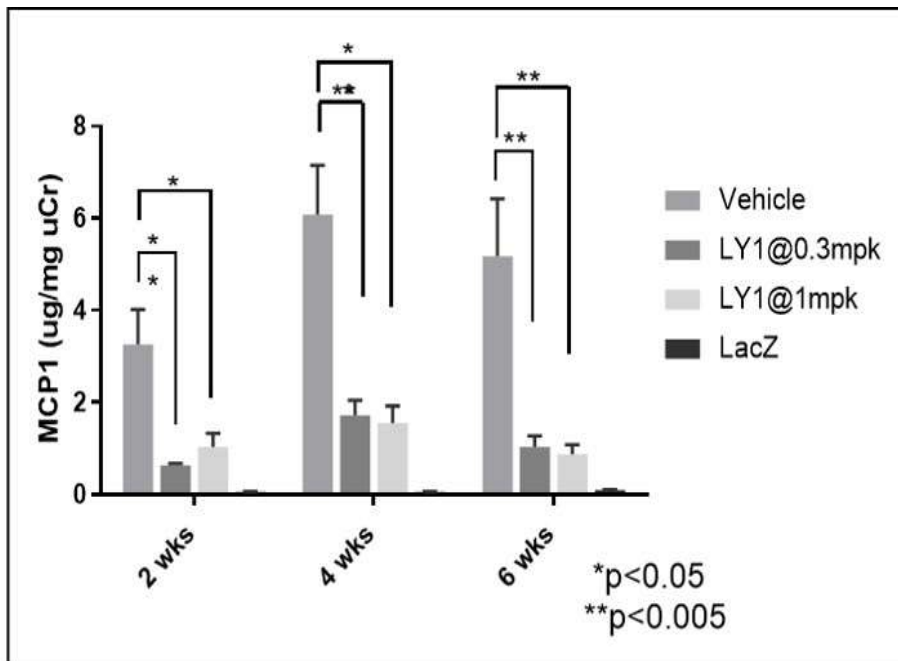
were orally dosed twice daily with LY1 either at 0.3 or 3mg/kg and urine was collected for 24 hrs using metabolic cage. A significant increase in the urine volume was observed in both dose groups that corroborated reduction in urinary creatinine (fig 13). This increase in urine volume demonstrates a potential diuretic effect of PDE1 inhibition. For the cyclic nucleotide levels, a trend of increasing cAMP level in the urine has been observed which did not reach significance. However, a significant increase in cGMP has been observed in LY1 treated rats compare to the vehicle group (Fig 2.13).

2.3.9 Expression analysis of major calcium channels in patients with CKD

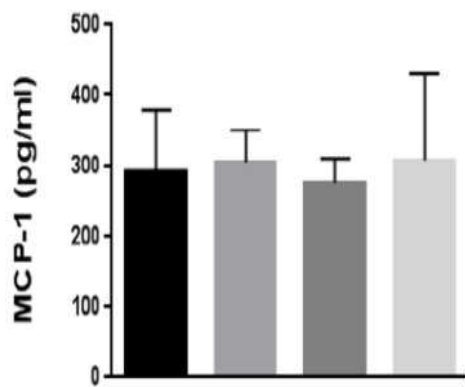
Thus, we have demonstrated that PDE1 inhibition provided significant therapeutic benefits in the animal model of DKD. On the flipside, it means that PDE1 activity is critical for disease pathogenesis. PDE1 is activated by calcium-calmodulin. However, the source of calcium for PDE1 activation in this context is unknown. To narrow down the list of calcium channels that are important in kidney disease we first did a literature search and found about 11 channels so far reported to contribute in calcium signaling in the kidney. Majority of the channels falls into the category of transient receptor potential canonical channel (TRPC) and voltage-gated channels. The channels that are found to play a role in several cellular function in kidney by modulating calcium signaling are TRPC1, TRPC3, TRPC5 TRPC6, TRPV4, TRPV5, PKD1/PKD2, Voltage gated channels Cav3.1, v3.2, v1.2 and v2.1. To further rank them based on their differential expression in different compartments of the kidney, we analyzed their gene expression in CKD patients database. Differential expression analysis of these 11 genes were done using the ERCB patient dataset which contained microarray data of micro dissected kidney biopsy samples from 199 CKD patients. In the tubular compartment, we found no change in the expression of the 11 channels (Fig 2.14). On the other hand, the glomerular gene expression data revealed that TRPC6 is the most upregulated gene among 11 channels in all five different CKD types including DKD (Fig 2.14). This data signifies the importance of TRPC6 as major channel that is involved in the kidney disease pathophysiology.

2.3.10 LY1 attenuated renal cell apoptosis induced by in vitro activation of TRPC6

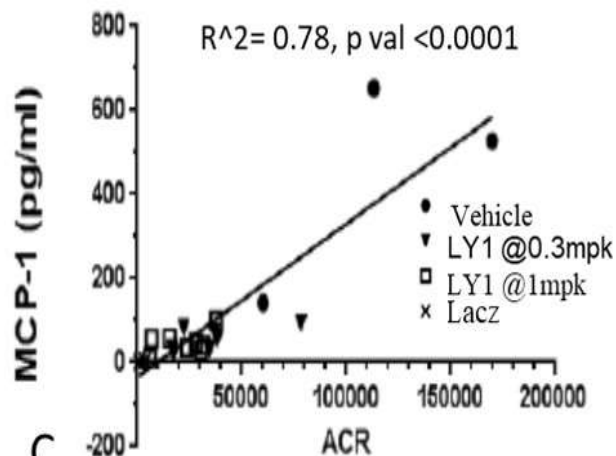
To investigate whether TRPC6 mediated activation of PDE1 plays a direct role in renal cell



A.



B.



C.

Figure 2.11. Urinary level of MCP-1 is decreased in AAV renin db/db uNx mice following PDE1 inhibition. Mice were treated with 0 (vehicle), 0.3 or 1mg/kg of LY1 for 6wks. Biweekly urine was collected and urinary KIM-1 was measured using commercially available ELISA kit. Blood was collected at the end of the study and KIM-1 was measured in the serum using ELISA. A) Vehicle treated AAVrenin db/db mice showed significant increase in KIM-1 which is reduced significantly upon treatment with LY1. B) Serum KIM-1 showed a trend but did not reach significance. C) Scatter plot showing correlation between uKIM-1 and proteinuria ($r^2=0.78$, $p<0.001$) at 6wks.

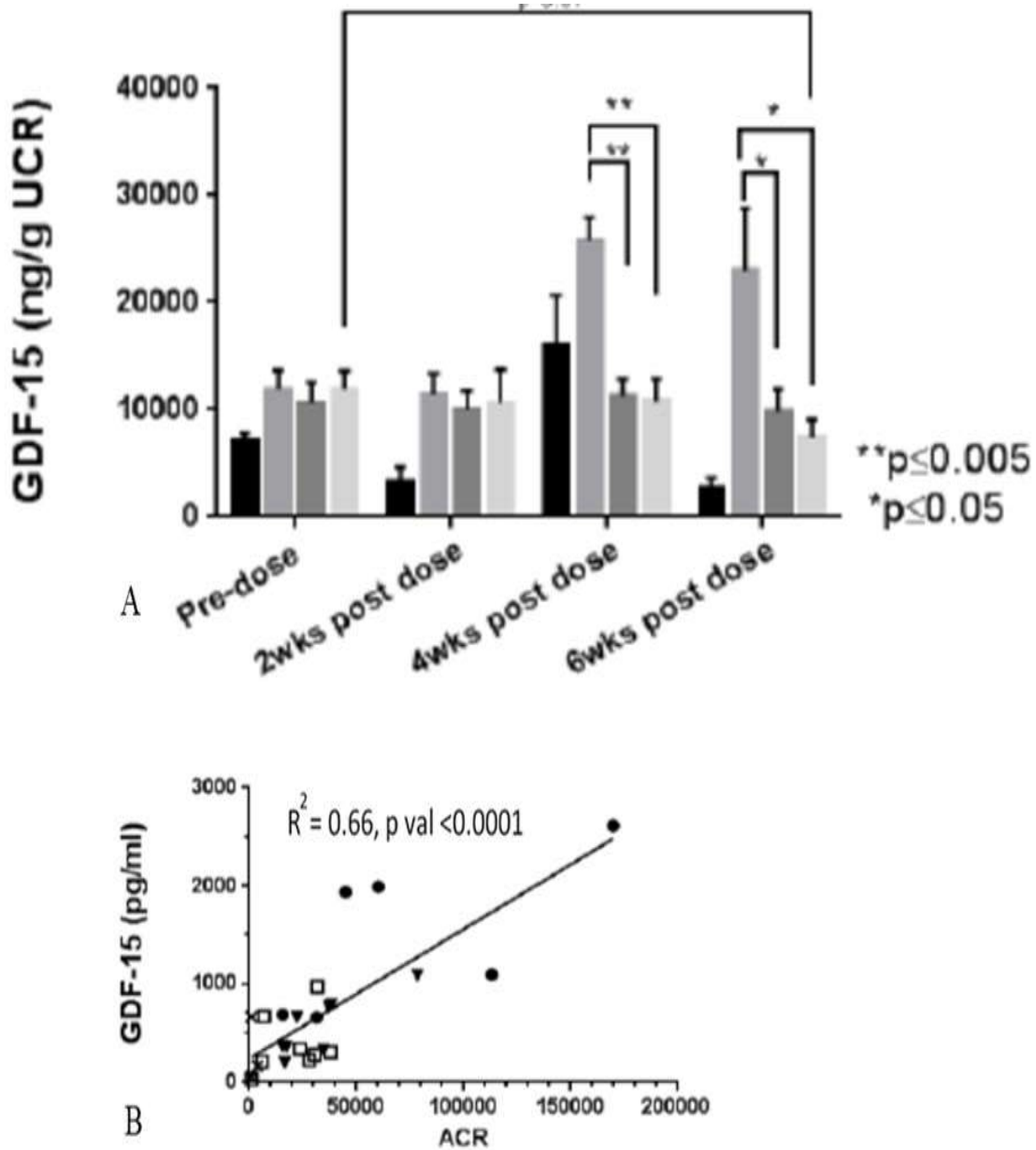


Figure 2.12. Urinary level of GDF15 is decreased in AAV renin db/db uNx mice following PDE1 inhibition. Mice were treated with 0 (vehicle), 0.3 or 1mg/kg of LY1 for 6wks. Biweekly urine was collected and urinary GDF15 was measured using commercially available ELISA kit. A) Vehicle treated AAV renin db/db mice showed significant increase in GDF15 which was reduced significantly upon treatment with LY1. B) Scatter plot showing correlation between GDF15 and proteinuria ($r^2=0.66$, $p<0.001$) at 6wks.

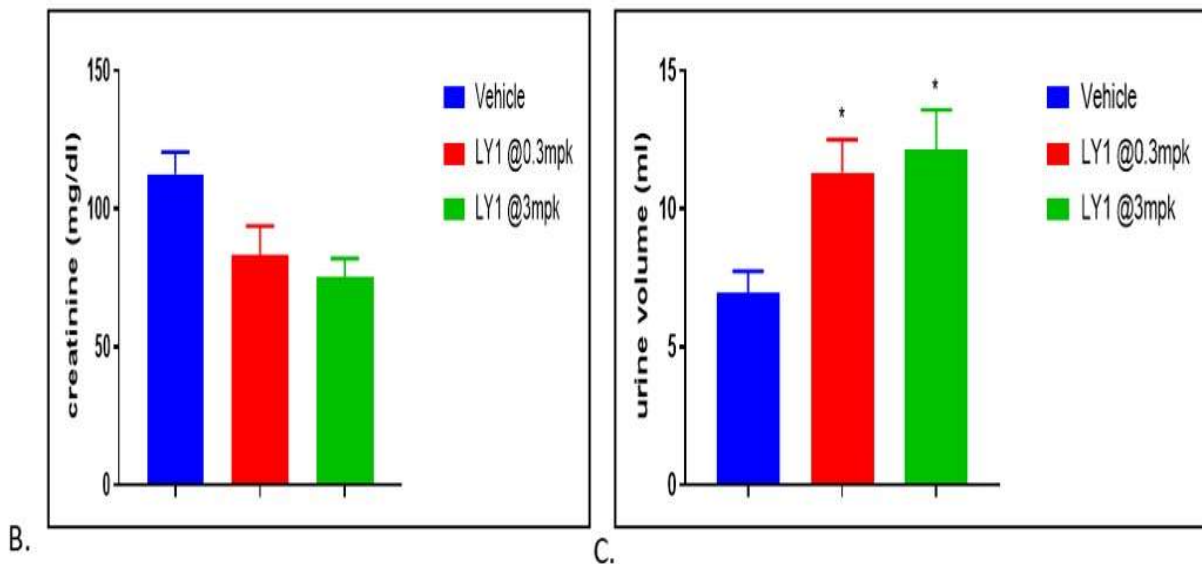
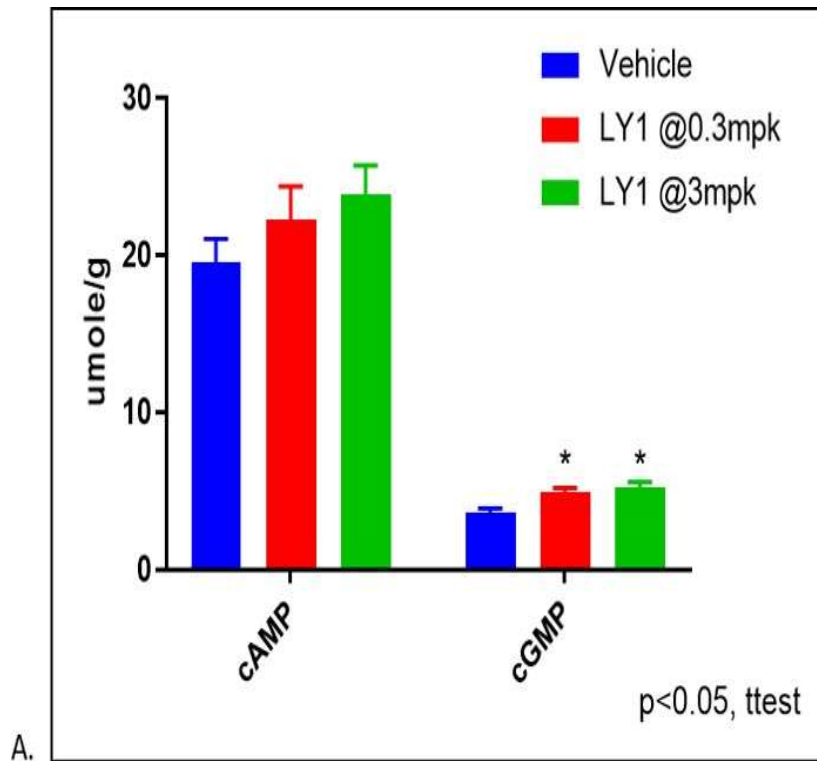


Figure 2.13. Effect of PDE1 inhibition on urinary cyclic nucleotide in normal rats. Sprague Dawley rats were dosed with either 0.3 or 3 mg/kg of LY1. Rats were kept in metabolic cage following first dose and urine were collected for 24hrs. Urinary cyclic nucleotides were measured using ELISA. A) LSN3191567 treated animals showed a significant increase in cGMP but a trend in increase in cAMP. B) Dose dependent increase in urine volume upon LY1 with concomitant decrease in urinary creatinine.

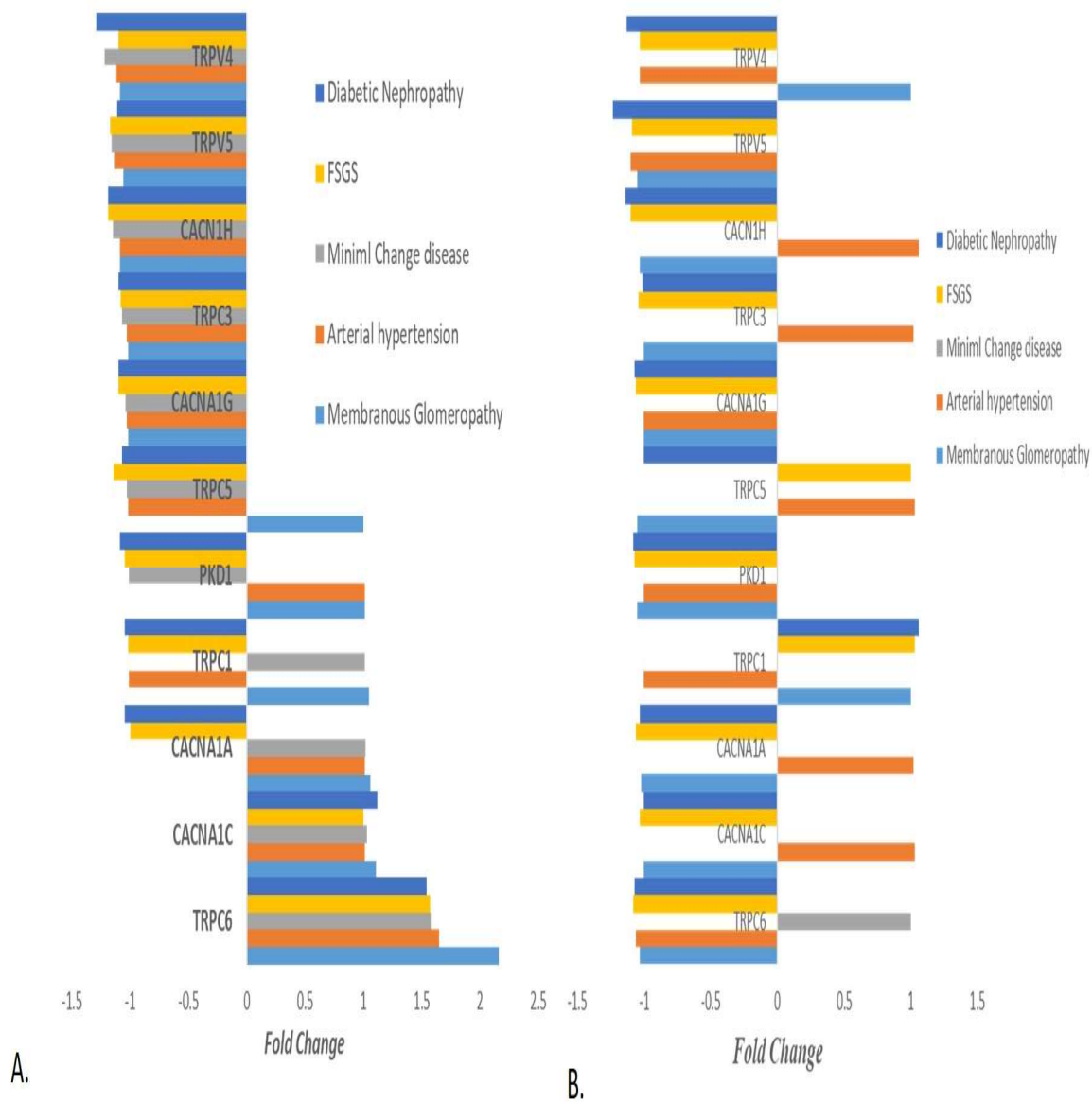


Figure 2.14. Gene expression analysis of the calcium channels in the microdissected kidney samples of CKD patients in ERCB cohort. Bar chart showing the A) glomerular and B) tubular gene expression of calcium channels in CKD patients.

apoptosis, we used TRPC6-specific activator in primary human mesangial cell and measured cleaved caspase 3/7 activity as a marker of apoptosis. Primary human mesangial cells were treated with different doses of hyperforin 9 or in some cases they were pre-treated with small molecule of TRPC6 or PDE1 inhibitor for 1hr and then treated with hyperforin 9 for 6hrs. Cellular apoptosis

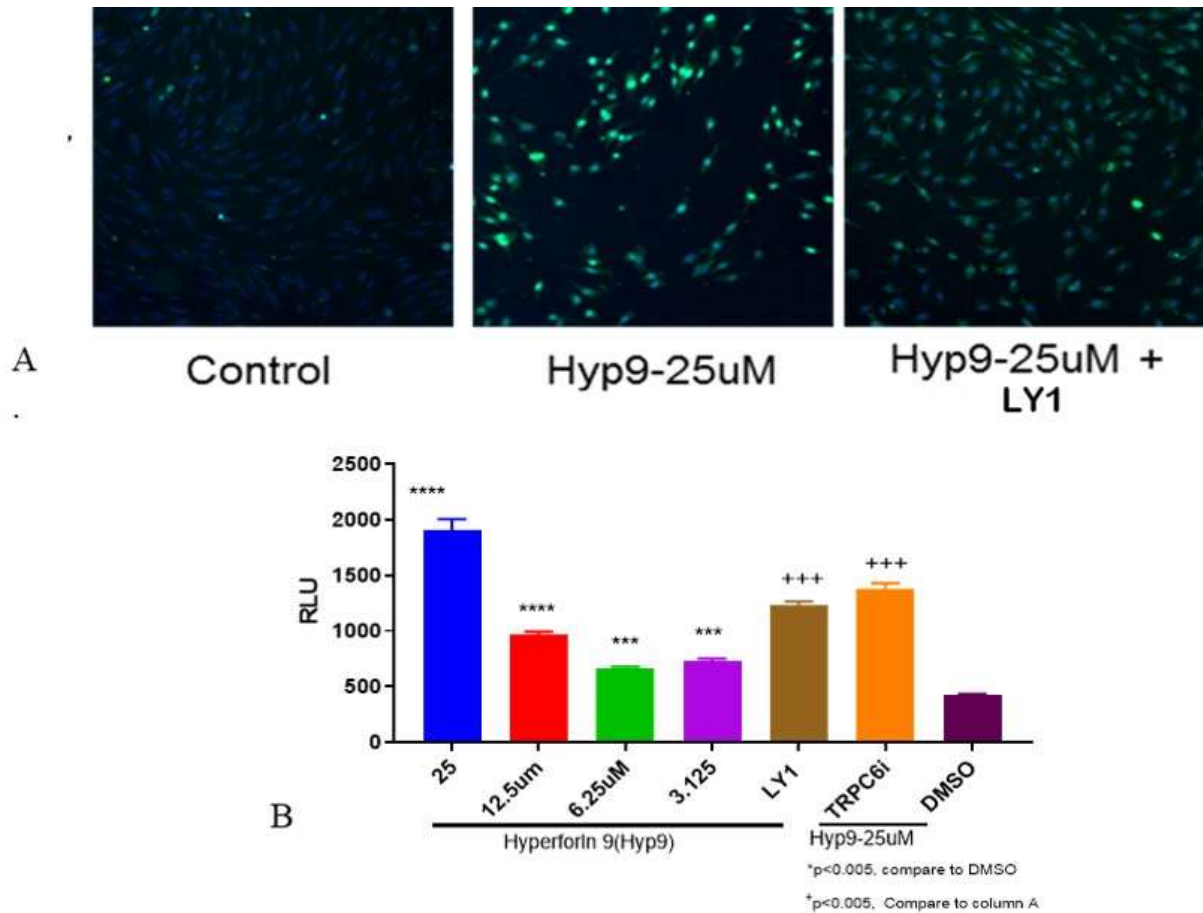


Figure 2.15. Effect of PDE1 inhibition on TRPC6 mediated apoptosis in human mesangial cell. Primary human mesangial cells were treated with different doses of hyperforin 9 for 24hrs. In other experiments hMS cells were pre-incubated with either small molecule of TRPC or PDE1 inhibitor for 1hr and then treated with 25uM hyperforin 9 for 6hrs. A) Confocal microscopic imaging of caspase 3/7 activity in cells at 10X magnification. B) Quantitative representation of the caspase activity. All data was represented as standard error of mean.

was measured by caspase 3/7 activity as detected using high throughput imaging platform using caspase 3/7 specific dye.

Hyperforin 9 treatment induced significant apoptosis in dose-dependent manner in mesangial cell, which can be blocked by TRPC6 inhibitor (Fig 2.15). In addition, PDE1 inhibition also attenuated hyperforin 9 induced apoptosis thereby positioning PDE1 as a downstream mediator of TRPC6 induced apoptosis.

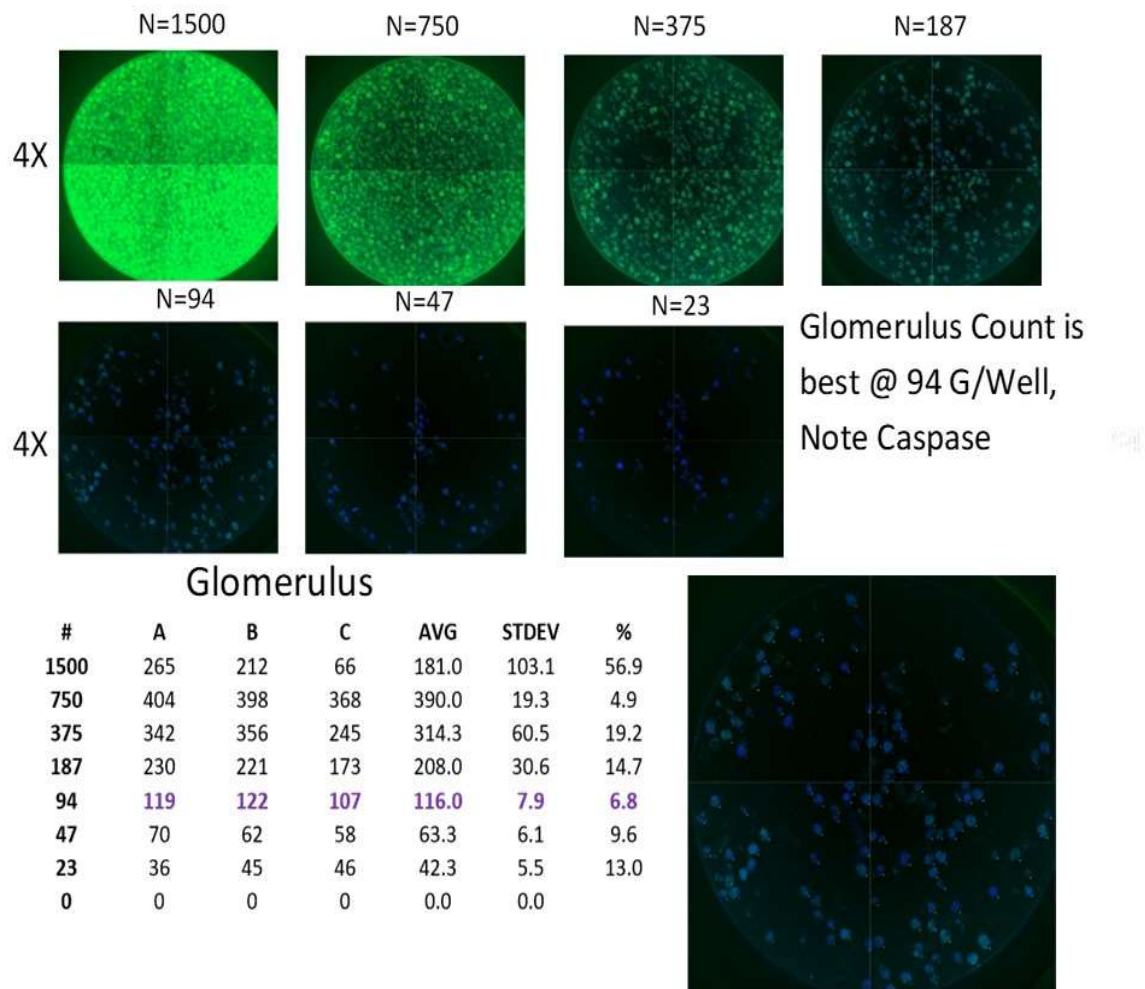


Figure 2.16. Effect of glomerular number on apoptosis. 96 well plate was seeded with different number of glomeruli and incubated in the media for 24hrs. Following 24hrs incubation caspase activity was measured using Cell Evet caspase 3/7 green dye. Confocal microscopic images taken at 4X showing the optimum number of glomeruli that did not induce any apoptosis.

Next, we wanted to investigate this phenomenon in more complex cellular system using isolated rat glomeruli. Our preliminary data demonstrated that the level of apoptosis could depend on the number of glomeruli per well. Therefore, first, we decided to optimize the glomeruli number that is enough for our study without any spontaneous apoptosis. After isolating the rat glomeruli using the method described in the material and methods section, different numbers of rat isolated glomeruli were plated on a 96-well plate. They were incubated for 24 hrs, and the next day caspase activity was measured using the same technique. We found that a high number of glomeruli was

indeed associated with spontaneous apoptosis, and a count of 94 glomeruli per well is the optimum number for plating (Fig 2.16).

As described earlier, 96-well plate was plated with the optimum number of isolated rat glomeruli and treated with different dose of hyperforin 9 or in some cases they were pre-treated with either PDE1 or TRPC6 inhibitor for 1 hr and then treated with 100 μ M of hyperforin 9 for 24hrs. Cellular apoptosis was measured by caspase 3/7 activity. Hyperforin 9 dose dependently significantly induced caspase activity which can be attenuated by TRPC6 inhibitor or PDE1 inhibitor in dose dependent manner (Fig 2.17).

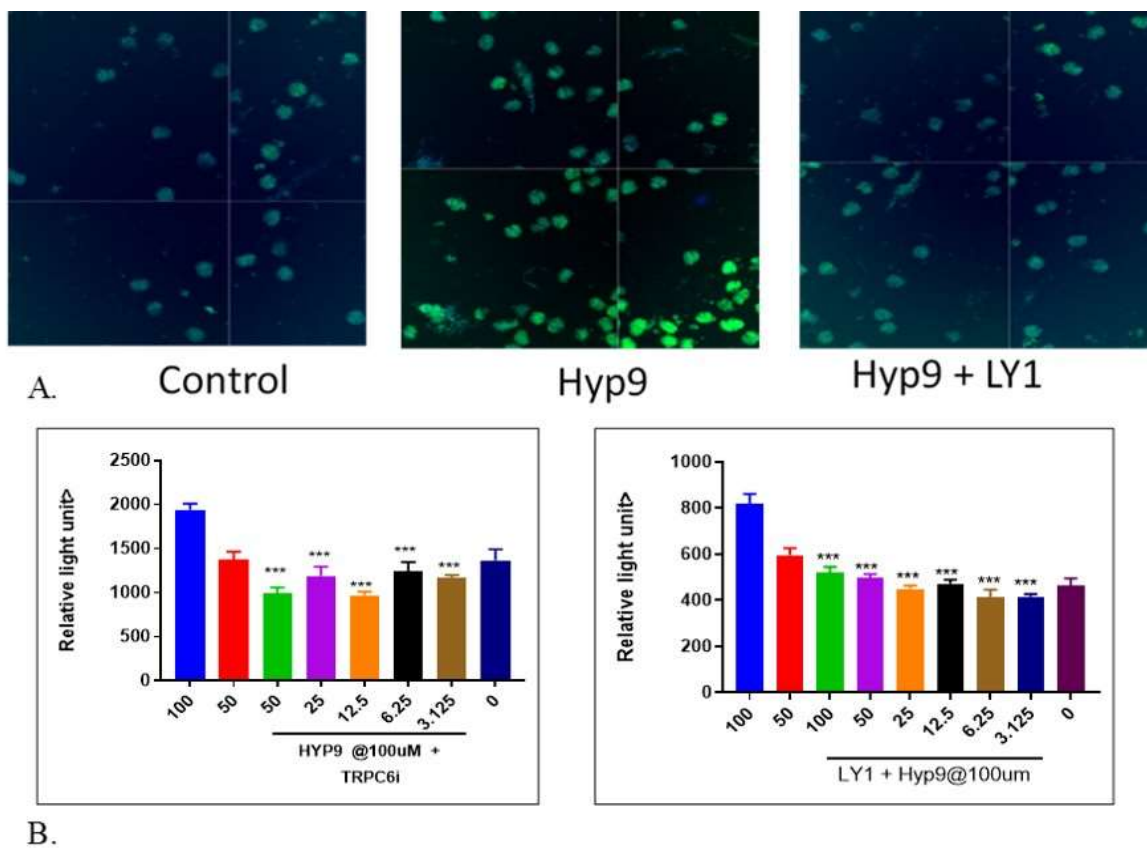


Figure 2.17. Effect of PDE1 inhibition on TRPC6 mediated apoptosis in isolated rat glomeruli. Rat isolated glomeruli were treated with different doses of hyperforin 9 for 24hrs. In other experiments rat glomeruli were pre-incubated with either small molecule of TRPC or PDE1 inhibitor for 1hr and then treated with 100uM hyperforin 9 for 24hrs. A) Confocal microscopic imaging of cleaved caspase 3/7 activity in rat glomeruli at 4X . B) Quantitative representation of the caspase activity. All data was represented as standard error of mean.

2.4 Discussion

In this chapter, using a novel technique, for the first time we demonstrated evidence of PDE1 dependent vasodilation in vivo using a small molecule inhibitor. We also have demonstrated its blood pressure lowering effect in both normal and spontaneously hypertensive rats and demonstrated additive effect to the standard of care treatment. We also used the same pharmacological approaches in vivo to explore the role of PDE1 in DKD and shown that inhibition of PDE1 improved renal function in an animal model of DKD that closely resembles human DKD. The renal benefit was manifested by significant reduction in proteinuria, improved glomerular filtration rate along with improved histopathological features compare to the vehicle treated animals. Molecular and urinary biomarker analysis revealed the renal benefit might be exerted by inhibition of inflammation and fibrosis. To the best of our knowledge, this is the first time demonstration of the role of PDE1 in DKD. Using both in vitro and ex vivo technique, we further demonstrated that calcium channel is the likely source of calcium responsible for activation of renal PDE1. TRPC6 mediated activation of PDE1 caused renal cell apoptosis. Overall, these data indicate that PDE1 may be a potential player in the progression of diabetic kidney disease, and inhibition of this phosphodiesterase presents a potential therapeutic opportunity.

2.4.1 Hemodynamic effects of PDE1 inhibition

PDE1 attracted interest in the context of arterial hypertension when, in human genetics study, an association of PDE1A single nucleotide polymorphism with diastolic and mean blood pressure was described [98]. At a fundamental level, the study of hemodynamics is concerned with the distribution of pressures and flows in the circulatory system. In its simplest form, the flow of blood through the blood vessel depends on the pressure exerted by heart and the peripheral resistance. In other words, to increase blood flow, one could either increase the cardiac force or decrease the systemic vascular resistance [99, 100]. The vascular resistance largely depends on the size and the shape of the blood vessels which is maintained by the contraction of the vascular wall mediated by the contraction of smooth muscle cell.

Cyclic nucleotides are ubiquitous second messengers that are known to play an important role in regulating vascular tone. PDE1 is expressed in smooth muscle cell (SMC) and can lead to

degradation of both cAMP and cGMP [47]. All three isoforms, PDE1A, B and C are found to be expressed in pulmonary vasculature, aorta and mesenteric arteries in rats [49, 56, 101]. PDE1A has been shown to regulate cGMP in rat cardiomyocytes and vascular smooth muscle cells [102], whereas PDE1C was shown to regulate cAMP in aortic [103] and pulmonary smooth muscle cells [56]. Lately Khammy et al. using in situ hybridization demonstrated that relative expression of PDE1A in VSMC of the vascular wall of rat mesenteric arteries is higher than the other two isoforms [51]. Giachini et al, showed that arteries from Ang II-infused hypertensive rats, display increased PDE1 expression and activation compared to control rats, and pharmacological inhibition of PDE1 abolished differences in the contractile responsiveness between the groups [49]. Recently Laursen et al showed selective inhibition of PDE1 induced relaxation in mesenteric as well as in femoral arteries from rats [52].

Although these ex-vivo studies demonstrated vasodilatory role of PDE1, in vivo demonstration of vasodilation relies on invasive techniques or sophisticated methods using ultrasound or imaging under anesthesia. For example, Cheng et. Al. has shown the niacin induced vasodilation in mouse using a laser doppler imaging technique [104]. Regardless, no such data exist showing in vivo vasodilation for PDE1. Here, for the first time, we demonstrated in vivo vasodilatory effects of a novel selective PDE1 inhibitor using very simple and reproducible method. The idea of using ear temperature as a surrogate for vasodilation came from the observation during dosing of LY1 in rats for an unrelated study. We observed the rapid reddening of the rat ear followed by concurrent warming of the rat ear after the dosing of the compound. As we measured the temperature using a thermometer equipped with k-probe thermocouple, indeed we saw about 12% increase in rat pinna temperature in the highest dose of LY1 treated animals compare to vehicle group. We also have demonstrated a dose dependent increase in ear temperature and the phenomenon repeated in other active compounds (data not shown). The pharmacokinetic analysis demonstrated sufficient exposure of the compound with a projected half-life of about 4hrs. It also revealed that we obtained about 64% target engagement with the minimum dose of 0.03mpk and saturated the target at 0.3mpk. The PK/PD analysis shown that the linear relationship between change in ear temperature and corresponding target engagement ratio remained linear for one hour.

The phenomenon of cutaneous relaxation or hot flushing is associated with many drugs, like PDE5 inhibitor [105], niacin [106], selective serotonin reuptake inhibitors (SSRIs), and few others [107]. In all cases patients have demonstrated redness or warmth of the face, neck or chest area. Although differ in initial stimulus, in general all these treatments lead to the same phenotypic response, i.e. 'hot flushing' associated with vasodilation. Intuitively, we associated the increase in temperature with this phenotypic response and went ahead to measure the temperature of rat pinna as the hot flush was remarkably evident in that area. Thus, the ear temperature has been used as surrogate marker of vasodilation. However, relationships between compound exposure and ear temperature are more complex. While at the early time points after the dosing ear temperature directly correlated with compound plasma concentration, the effect on ear temperature started to disappear at 3hr whereas the half-life of the compound is almost 4hrs. One explanation could be the homeostatic mechanism involved in the control of body temperature. LY1 at high dose demonstrated about 12-14% increase in ear temperature. In case of such increase in body temperature some negative feedback mechanism, independent of vasodilatory effect of PDE1 inhibition, might play a role in bringing down the temperature. It is well recognized that changes in skin blood flow played an important role in maintaining core body temperature within a very narrow range [108]. One such mechanism involves arterio-venous anastomoses (AVA) [109] which in human are abundant in finger and toes. Hoyer et al suggested its importance in temperature regulation in mammals. It has been shown that with the rise in body temperature induced AVA dilation to distribute the heat throughout the body [110]. Usually, this regulatory feedback acts instantly but the fact that rat ear don't have AVA but tail does might explain the delay in response [111]. Due to this reason and the fact that the linear relationship between change in temperature and target engagement ratio (TER) stayed only for an hour, the ear temperature might be a useful surrogate for vasodilation within that time frame. Taken together, LY1, a potent and selective PDE1 inhibitor with appropriate pharmacokinetic properties demonstrated vasodilation using a novel noninvasive method.

When blood vessels dilates, decrease in vascular resistance results in increase of blood flow [112]. Therefore, dilation of small arteries and arterioles leads to an instantaneous decrease in arterial blood pressure [113]. Several non-selective PDE1 inhibitors like IBMX, SCH51866, zaprinast or vinpocetine have shown blood pressure lowering effect in both normal or AngII infused rats [102,

114, 115]. The lack of specificity in those molecules makes it harder to implicate PDE1s role in hemodynamics. For example, vinpocetine has also been shown to inhibit PDE7B in micro molar range [116]. Furthermore, vinpocetine directly inhibits BKCa channels [117], and recently vinpocetine was found to have a PDE independent mechanism to inhibit NF-kB dependent inflammation [118]. However, very recently selective PDE1 inhibitor has been shown to reduce blood pressure in rats [52]. In our study we also have seen a dose dependent decrease in mean arterial pressure in normal rats that coincides with an increase in heart rate. We also demonstrated similar phenomenon in spontaneously hypertensive rats, a genetic model of hypertension. The magnitude of blood pressure lowering effect is higher in SHR rats and can be achieved with much lower dose compare to normal animals. ACE inhibitors are regarded as standard of care in the clinic for hypertensive patients. Our data clearly demonstrated a significant synergistic effect in lowering blood pressure when combined with LY1. Interestingly while enalapril did not increase the heart rate, the combination raised the heart rate to an extent that is higher than seen with compound alone in SHR animal.

PDE1 is likely to be involved in multiple mechanisms regulating blood pressure. Our data strongly suggest that peripheral vasodilation could play critical role. Literature data suggested relaxation of pre-constricted aortic rings with both specific and non-specific PDE1 inhibitors [52, 119]. Our in vivo findings complement these in vitro observations. We have shown that LY1 increased rat ear temperature in a dose-dependent manner. This change in temperature is likely a result of increased local blood flow driven by vasodilation. Importantly, plasma levels of the compound and, hence, tissue exposure, were comparable with compound concentrations in vitro that induced vasodilation and exceeded IC₅₀ for PDE1A. Given that diameter of small arteries and arterioles is directly related to peripheral vascular resistance, and the latter, together with the pumping capacity of the heart and blood volume, ultimately defines blood pressure, we surmise that vasodilation could be the main mechanism of antihypertensive effects of PDE1 inhibitors.

Since PDE1A is the major isoform expressed in arterial smooth muscle cells [49, 51], it is highly likely that blood pressure lowering activity of LY1 is primarily driven by its inhibition of PDE1A. Preferred substrate of PDE1A is cGMP that is produced in vascular smooth muscle cells (SMC) by nitric oxide-induced soluble guanylate cyclase or natriuretic peptide-activated particulate

guanylate cyclase [34]. Downstream, cGMP signaling is associated with activation of protein kinase G, ultimately leading to smooth muscle cell relaxation. When PDE1 is activated, it degrades cGMP and hence impedes vasorelaxation. PDE1 is the only phosphodiesterase activated by calcium [120]. Calcium signaling is enhanced in arterial hypertension [121]. Therefore, it is reasonable to suggest that PDE1A activation serves as one of the major mechanisms associated with increased peripheral vascular resistance, and its inhibition would have significant therapeutic benefit.

PDE1 inhibition, however, could also be responsible for an observed increase in heart rate. Tachycardia is not unique to LY1. It is likely to be the class effect since structurally unrelated PDE1 inhibitors increased heart rate in different species of experimental animals [122]. Precise mechanism of PDE1-induced tachycardia needs to be further investigated. However, it likely has both extracardiac and intracardiac components. The former could be a result of baroreflex, an activation of sympathetic signaling induced by blood pressure lowering [123] that, to some degree, is germane to any peripheral vasodilator [124]. The latter is likely to be specifically associated with inhibition of PDE1A. Lukyanenko et al. reported that PDE1 is expressed in the rabbit sinoatrial node. While cGMP is a preferred substrate of this enzyme, PDE1 is also capable of binding to (albeit with lower affinity) and degrading cAMP. cAMP, in turn, can stimulate calcium signaling resulting in increased pacemaker activity [119]. It is still unknown whether this mechanism is involved in tachycardia in the rat, and, most critically, is translatable to the human. ITI-214, a PDE1 inhibitor with similar potency and selectivity, has finished Phase II clinical trial for Parkinson's disease (ClinicalTrials.gov Identifier: NCT03257046). Although no data related to heart rate were published, the very fact that this compound is moved to Phase II is indicative of an overall beneficial safety profile. Thus, tachycardia could remain primarily pre-clinical finding. However, more detailed translational studies are needed.

In general, cross-species translation remains an issue given significant difference in the patterns of PDE1 expression in the heart. Recent paper by Hashimoto et al [122] demonstrated that PDE1 inhibition in the dog was simultaneously associated with positive inotropic effects (most likely driven by inhibition of PDE1C in cardiomyocytes) and peripheral vasodilation (most likely driven by inhibition of PDE1A in vascular SMCs). This “ino-dilation” provides intriguing prospects for

PDE1 inhibitors which could pave the way for new therapeutic approach in hypertension or related disease like chronic kidney disease.

Association of vascular resistance with CKD is well established. In participants of the US National Health and Nutrient examination Survey (NHANES), hypertension in women was strikingly associated with decline of kidney function [125]. Later Varaniemi K et al demonstrated that there is an independent association between systemic vascular resistance induced hypertension and lower eGFR [126]. Having seen the vasodilatory effect in both ex vivo and in vivo along with lowering of blood pressure we wanted to investigate the role of PDE1 in the context of CKD. Among different types of CKD, the prevalence of DKD constitutes about more than 50% and in both type 1 and 2 diabetic patients intracellular calcium has been reported to be higher than normal[127].

2.4.2 Renal benefits of PDE1 inhibition in diabetic nephropathy

To recapitulate human diabetic nephropathy and explore the role of PDE1 we used an animal model that has combination of hypertension and nephron loss on the background of type 2 diabetes. In this severe mouse model of diabetic nephropathy, we demonstrated that small molecule PDE1 inhibitor attenuates the progression of diabetic nephropathy as indicated by reduction in albuminuria, serum creatinine, and several urinary biomarkers like NGAL, KIM1, MCP-1 and GDF-15. We also demonstrated marked reduction in glomerular sclerosis, interstitial fibrosis, and mesangial matrix accumulation in the PDE1 inhibitor treated group compare to the vehicle. Gene expression analysis demonstrated that PDE1 inhibition also attenuated the upregulation of several genes related to inflammation and fibrosis. Taken together, these data provide first pre-clinical demonstration of renal benefit of PDE1 inhibitor in the context of diabetic kidney disease.

The biology of PDE1 has been investigated in heart and brain extensively but, to the best of our knowledge, no data exist describing its role in diabetic kidney disease. According to human protein atlas data, PDE1A is largely expressed in tubules, and PDE1C is expressed in both tubules and glomeruli, while PDE1B is not expressed in the kidney. Although nothing is known about the primary role of PDE1 in the context of DKD, it certainly can influence several components of the disease pathophysiology. For example, the course of disease in DKD can be influenced by local

hemodynamics. One major factor regulating hemodynamics is over activation of renin angiotensin system (RAS). Activation of the RAS leads to increased angiotensin II levels which subsequently cause efferent arteriolar vasoconstriction thus increasing intra glomerular pressure[18]. Increased levels of angiotensin II are associated with high albuminuria and nephropathy in both humans and mice [128, 129]. This is further validated by a long track record of ACEIs and ARBs in reducing the doubling rate of creatinine, albuminuria, and progression to nephropathy, ESRD, and death both in human and animal [130-133]. The vasodilatory and blood pressure lowering effect of PDE1 inhibition led us to explore the role of PDE1 in the context of diabetic nephropathy.

The animal model used in this study is characterized by severe albuminuria, increased serum creatinine and histopathological changes that are very similar to human DKD[97]. In this model, hypertension is induced by the AAV mediated overexpression of renin, and renal insufficiency is induced by unilateral nephrectomy on the background of type 2 diabetes. We demonstrated that treatment with PDE1 inhibitor significantly and dose dependently decreased albuminuria within two weeks of dosing, and this beneficial effect persisted for 6 wks. This was accompanied by the significant reduction in serum creatinine in the high dose group after chronic treatment. The improvement in albuminuria in the early phase of the treatment might be due to the modulation of glomerular hemodynamics exerted by the vasodilatory mechanism of PDE1 inhibition.

Persistent albuminuria is one of the salient features of DKD and is clinically recognized as a marker of the severity of chronic kidney disease. Recent study showed that patients with higher albuminuria are prone to cardiovascular death even in some cases where they were in range that was otherwise known as at 'normal' albumin excretion range [134]. Reduction in albuminuria in both diabetic and non-diabetic patients with renal disease translates into a protection from renal function decline [135, 136] Like albuminuria, serum creatinine is also a well-established biomarker of any renal disease. Traditionally, eGFR is used to characterize kidney function and to determine the stage of kidney disease.

Chronic exposure to hyperglycemia and hemodynamic changes that modulates various intracellular pathways can induce structural abnormalities in the glomerular and tubular compartments of the kidney which were reported in the model used in our studies.

Histopathological analysis demonstrated severe pathological changes that include mesangial expansion, interstitial fibrosis, glomerulosclerosis and increased tubular protein in the vehicle group which were significantly improved upon PDE1 inhibition. Shannon et al. showed that the histopathological changes in this model were associated with the upregulation of genes involved in inflammation and fibrosis [97]. In order to further understand the improvement in pathology upon PDE1 inhibition, we performed microarray analysis which demonstrated a reduction in expression of genes related to inflammation and fibrosis. However, while directionally consistent, these changes did not reach significance. To follow up in a more quantitative fashion, we designed a custom gene array focusing on the genes that were up-regulated in the disease state and down-regulated by the compound treatment. Using RT PCR with pre-configured Taqman array card, we demonstrated significant changes in the expression of several genes related to inflammation pathway like CCL2, LCN2, SAA1 and VCAM1. They were highly upregulated in the vehicle group but were significantly down-regulated upon PDE1 inhibition. Genes related to fibrotic pathway like COL1A1 and COL1A2, COL3A1, and FN1 were significantly downregulated in PDE1 inhibitor treated group compare to vehicle. These data suggest potential role of PDE1 in inflammation and fibrosis apart from its vasodilatory function that might have contributed to the renal benefit.

The role of PDE1 in inflammation and fibrosis has been reported in several other organ system. Initial evidence of potential role of PDE1 in inflammation came from the investigation of a non-selective PDE1 inhibitor vinpocetine. Recently, a highly selective PDE1 inhibitor ITI-124 demonstrated a regulatory role of PDE1 in inflammatory response in microglia [57]. The authors demonstrated that inhibition of PDE1 resulted in >50% reduction in LPS induced increase of TNF α , IL-1b, and CCL2 mRNA expression both in BV2 microglial cell and also in mice specially in brain regions with high PDE1 expression (striatum, cortex and hippocampus). Our data extended the scope of anti-inflammatory effects of PDE1 inhibition to the realm of diabetic kidney disease.

Although albuminuria and serum creatinine are widely used as primary endpoints for DKD, these markers are lacking direct association with the severity of morphological changes in kidneys and cannot be considered ideal prognostic markers [5]. The ACCORD study demonstrated that intensive pharmacological glycemic control can reduce the incidence of albuminuria but did not prevent development of CKD or progression of CKD to end-stage renal disease. Furthermore both

VADT or ADVANCE, which evaluated the benefits of heart disease upon intensive glycemic control, failed to show a statistically significant benefit for reducing HbA1c to less than 7% in T2DM patients. These findings underscore the necessity to predict incident and progressive CKD in type 2 diabetes (ACCORD trial). Faced this discrepancy, several potential prognostic and surrogate endpoint biomarkers for advanced DKD has received major interest. Although DKD has been regarded primarily a glomerular disease, recent data suggested that tubulointerstitial injury may have an important role in pathogenesis and progression of the disease. On that basis, KIM1 and NGAL [137-139] have been proposed as potential candidates for tubular damage markers and shown to be associated with faster decline in eGFR [140]. In CKD, including DKD, NGAL is considered a diagnostic and prognostic marker. Bolignano et al. observed that uNGAL increased and correlated with the advancement of kidney disease in patients with DKD both with and without albuminuria [141]. Both type 1 and 2 diabetic patients showed not only higher level of urinary NGAL but also showed a positive correlation with albumin/creatinine ratio [142, 143]. In the post-hoc analysis of dapagliflozin clinical trial, reduction of KIM1 has been associated with the renoprotective effect [144]. In our study, we found that both urinary KIM1 and NGAL were elevated in the AAV/Renin model and were significantly reduced (almost to the basal level) with PDE1 inhibitor. Interestingly, ACE inhibitor, the current standard of care for DKD, did not show any reduction in tubular injury markers in diabetic nephropathy patients [137]. These findings not only suggested that PDE1 inhibition mediated improvement of renal function, likely associated with direct protection of the renal tubules, but also offer either better or additive benefit with the standard of care.

Monocyte chemoattractant protein-1 (MCP-1) and growth differentiation factor-15 (GDF-15) are well known cytokines that are increased in tissue injury and inflammatory states and have been associated in both cardiac and renal disease [145-147]. It has been shown in animal studies that in diabetic renal injury, increases in urinary GDF-15 were associated with proximal tubule injury [148]. Urinary MCP-1 levels have been reported to be significantly higher in diabetic patients. They correlated with albuminuria and with increased severity of tubulointerstitial lesions along with urinary NGAL which might suggest that MCP-1 may reflect advanced tubulointerstitial lesions in diabetic patients [149]. In our study, we have seen a significant progressive increase in both urinary MCP-1 and GDF-15 in vehicle control group which significantly reduced in the PDE1

treated group. Interestingly, reduction in urinary MCP-1 was observed as early as in 2wks, whereas it took 4wks to see an effect on GDF-15. We did not see any change in serum MCP-1 in our mouse study that corroborates others findings [149]. Both markers demonstrated good correlation with albuminuria which corroborates previous findings [148]. These data provide another confirmation that renal benefits as seen in this model with PDE1 inhibition might be due to the protection of renal proximal tubule cells.

While the above urine markers provide useful prognostic information, molecular readout more proximal to the molecular target (PDE1) would be very useful as pharmacodynamic marker at the clinical drug development stage. In this context, it is reasonable to focus on cyclic nucleotides since they serve as direct substrates of PDE1 enzymatic activity. However, primary intracellular localization of cyclic nucleotides makes this task extremely challenging. cAMP and cGMP can exit the cell and thus can be detected in plasma or urine but regulation of these processes is poorly understood. Therefore, we have attempted quantification of cyclic nucleotides in urine and explored potential correlation of their levels with plasma concentration of PDE1 inhibitor. While in the relatively simple experimental system (acute effects on cyclic nucleotide levels in the urine of normal rat), we have found increased concentration of urine cyclic nucleotides as a result of treatment with PDE1 inhibitor, these relationships were not evident in the far more complex experimental system (chronic compound administration in the mouse model of DKD). Molecular mechanisms of this phenomenon are unclear. It is possible though that urine cAMP and cGMP concentration could be mechanistically associated with modification of secretion or reabsorption in the tubular cells and, therefore, with diuretic effects of PDE1 inhibitors. Indeed, we have found that PDE1 inhibition induced acute increase of urine volume in the normal rats. In the model of DKD, though, profound polyuria, typical for diabetes, has likely masked this physiological response. Thus, clinically important relationships between pharmacokinetic and pharmacodynamic parameters need further investigation.

In summary, we have shown for the first time in a very severe preclinical model of diabetic nephropathy that inhibition of PDE1 provides renal protection associated with lowering albuminuria, reduction in serum creatinine levels and marked improvement in renal histopathology likely driven by suppression of inflammation and fibrosis as evident by gene expression analysis.

The urinary biomarker panel demonstrated that the improvement in renal function is primarily due to the protection of renal proximal tubule. While we clearly demonstrated therapeutic benefits of PDE1 inhibition, it is still unclear how renal PDE1 is activated in the context of DKD and what are the downstream mechanisms of these benefits. We addressed these two questions by adopting some bioinformatics tools and through in vitro experimentation.

2.4.3 Mechanism of PDE1 activation and reno-protective effects of PDE1 inhibition

In this section we demonstrated that TRPC6 mediated calcium influx is responsible for PDE1 activation, and inhibition of PDE1 prevented renal cell apoptosis induced by TRPC6 activation. By using bioinformatics tools and publicly available CKD patients' database we demonstrated that TRPC6 is upregulated in the glomerular compartment of several types of CKD including DKD. Using a TRPC6-overexpressing cell line, we demonstrated that activation of TRPC6 resulted in PDE1 activation as evident by decrease in cAMP. By using a TRPC6 small molecule inhibitor we demonstrated that hyperforin 9, a widely used activator is specific to TRPC6. We also demonstrated that TRPC6 mediated increase in calcium influx resulted in apoptosis in both human mesangial cell and rat isolated glomeruli which can be attenuated by both TRPC6 and PDE1 inhibitor. This suggest that in the context of elevated intracellular calcium, inhibition of PDE1 rendered renal benefit by attenuating apoptosis.

Out of 11 family of phosphodiesterases, PDE1 is the only one that is activated by calcium. However, several Ca²⁺ entry pathways exist in cell and the specific source of calcium used for activation of PDE1 in the kidney is unknown. So far one report suggested that in cardiomyocyte PDE1 gets activated by TRPC3 mediated calcium influx[95] but no such data exist in kidney cell. Recently, studies have shown that disruption of calcium signaling in the kidney leads to kidney disease and using genetic or biochemical tools identified several channels that are important in renal disease [54]. Our analysis of gene expressions of the transcriptional dataset from European Renal cDNA Bank (ERCB) revealed TRPC6 as the most upregulated calcium channel in glomerular compartment of patients with different kinds of CKD, including DKD [150] . Interestingly, we did not see any change in the expression of major calcium channels in the tubular compartment. Dysregulation of calcium signaling has been implicated in the kidney disease and

evidence of several gain-of-function mutation in human TRPC6 channels has been implicated in FSGS, predominantly a glomerular disease that is characterized by massive proteinuria. The expression of TRPC6 in podocytes and as a component of the glomerular slit diaphragm has been confirmed by several studies [68, 151]. We also have found increased TRPC6 expression in the glomerular compartment of FSGS patients included in the ERCB dataset. Like FSGS, diabetic nephropathy is also characterized by loss of podocyte and proteinuria. TRPC6 has been shown to be increased in cultured podocyte in response to high glucose and in STZ-induced diabetic rats [76]. In our differential gene expression (DEG) analysis we also have found several fold increases of TRPC6 expression in DKD patients from ERCB cohort. Thus, our data also support that increased expression of TRPC6 may be involved in number of glomerular kidney diseases. Admittedly, one of the limitations of the study is based on the fact that we only focused on the channels that has been reported in literature to be involved in kidney diseases.

Based on gene expression data in CKD patients we postulated that TRPC6 is the major driver of calcium influx that is involved in PDE1 activation in the context of kidney disease. TRPC6 mediated increase in intracellular calcium have been shown to induce apoptosis in multiple cell type through different mechanism. Soni et al. have shown in neonatal pig glomerular mesangial cell that hyperforin, a selective TRPC6 activator, induced cellular apoptosis via calcineurin/NFAT and FasL/Fas signaling pathway [152]. Inhibition of TRPC6 has been reported to protect renal proximal tubule cell from oxidative stress mediated cellular apoptosis [95]. Here we have demonstrated for the first time that in primary human mesangial cell and in rat isolated glomeruli activation of TRPC6 induced apoptosis in PDE1-dependent manner. By using selective inhibitor of both TRPC6 and PDE1 we demonstrated the crosstalk of two major signaling pathway and its importance in maintaining cell viability. Our data corroborates similar findings in mouse cardiomyocytes where it has been shown that TRPC3 is involved in PDE1C-mediated cardiomyocyte death [95].

In summary, in this section we have demonstrated vasodilatory function upon PDE1 inhibition in vivo by adopting a novel technique using ear temperature as surrogate marker. Peripheral vasodilation resulted in lowering of blood pressure in both normotensive and hypertensive rats. We also demonstrated for the first time that PDE1 inhibition leads to the renal benefit using a

rodent model of DKD as evident by lowering of ACR, serum creatinine and several urinary biomarkers. The histopathological improvement due to PDE1 inhibition were associated with and likely driven by inhibition of inflammation and fibrosis pathways. Using gene expression analysis of CKD patients, we identified TRPC6 as major channel that is upregulated in the glomeruli and, using human primary mesangial cell and rat isolated glomeruli, we have shown that induction of TRPC6 leads to apoptosis in PDE1 dependent manner. In subsequent section we asked the question of how TRPC6 gets activated in the diabetic environment.

CHAPTER 3. ROLE OF TRPC6 AND PDE1 IN THE CROSSTALK OF CALCIUM AND CYCLIC NUCLEOTIDE SIGNALING

3.1 Introduction

In the previous chapter, we have demonstrated the role of PDE1 in DKD. That, on its own, laid out new ideas about pathogenesis of the disease and may provide novel approaches to its pharmaceutical treatment. However, both from the basic science and drug discovery perspectives, it is important to understand how PDE1 is activated. Therefore, the current chapter is focused on the upstream pathways that link extracellular risk factors of DKD and PDE1. Since PDE1 is activated by calcium, the first obvious question relates to the source of calcium leading to PDE1 activation. We have previously identified TRPC6 as a likely candidate. Here, going further upstream, we set out to link extracellular molecules/risk factors with TRPC6 and identify molecular mechanisms involved in opening/activation of this calcium channel.

Canonical transient receptor potential channel (TRPC) is one of the major ion channels that regulate calcium influx into the cell from the extracellular space. Among seven structurally related family members, the importance of TRPC6 has been emphasized by the discovery of gain of function mutation in FSGS clinically manifested by massive proteinuria [68]. Proteinuria is a clinical feature shared by FSGS and DKD. However, while a subset of FSGS patients exhibit a gain-of-function mutation of TRPC6, it is likely that in DKD, certain extracellular molecules associated with diabetes and serving as risk factors of DKD, directly activate TRPC6. Comprehensive review of these risk factors is beyond the scope of this study. Major risks of DKD stem from the hemodynamic and metabolic directions. Thus, we decided to focus on main representatives of these two groups, specifically, angiotensin II and endothelin 1 on the hemodynamic side, and glucose and insulin on the metabolic side. Any extracellular molecule can activate TRPC6 via generation of diacylglycerol (DAG) or reactive oxygen species (ROS). In this chapter, we developed or applied novel molecular tools to address two questions: (1) What hemodynamic and metabolic risk factors of DKD activated TRPC6 and (2) What was the molecular mechanism mediating this activation.

Intracellular DAG can be formed either via G-protein coupled (GPCR) receptor mediated hydrolysis of membrane phospholipids [153] or de novo synthesis using glycolytic intermediates as precursors or hydrolysis of triglycerides [70, 154]. In the extremely complex diabetic milieu, DAG is likely to be generated by all three sources [155]. Moreover, Gq receptors can be activated by multiple ligands: angiotensin II (Ang II), Endothelin-1(Et-1), thromboxane, prostaglandin E2 etc which are also abundant in diabetic milieu [72, 156, 157]. It is unknown if various Gq agonists lead to uniform generation of DAG and TRPC6 activation. Majority of publications used Ang II or a membrane-permeable DAG analog, 1-oleyl-2-acetyl-sn-glycerol (OAG) [153, 158]. While this generalized approach was fruitful in elucidating common signaling mechanisms, it is conceivable that individual Gq agonists may affect different facets of the pathway. Current literature strongly suggests differential pattern of activation of TRPC3, a close relative of TRPC6 [154]. Similar studies regarding TRPC6 are needed.

Reactive oxygen species (ROS) which are also abundant in diabetic milieu has also been implicated in the activation of TRPC6. Both angiotensin II and high glucose have been shown to activate TRPC6 via ROS generation [159, 160]. Kim et al, has demonstrated that ROS mobilized the TRPC6 channel in cultured podocytes [161, 162] and later on using pharmacological and genetic tools other investigators have shown that ROS dependent TRPC6 activation is the primary source of calcium influx in isolated glomeruli [159]. Later it was shown that the downstream signaling pathway involved Rac/Rho pathway and caused podocyte cytoskeleton derangement [163, 164]. Furthermore, in podocytes, Ang II induced apoptosis is associated with alteration of TRPC6 expression and Ca²⁺ influx [165].

Similarly, in monocytes it has been shown that high glucose induced ROS activates TRPC6 and increase calcium influx [160]. In cultured podocytes, it has also been demonstrated that glucose upregulated TRPC6 and increased calcium influx [165]. These indirectly suggest that high glucose might be activating TRPC6 via ROS generation. However, the possibility that high glucose can activate TRPC6 by generating DAG through de novo synthesis pathway has been overlooked.

Once activated TRPC6 allows influx of calcium ions into the cell which effects several downstream signaling pathways. For example, stimulation of TRPC6 channels has been shown to activate stimulus-responsive transcription factor activator protein-1 (AP-1) [166] which is at a

convergence point for multiple intracellular signaling pathways that operates in tissue-specific regulation of many biological functions [167]. TRPC6 mediated rise in calcium concentration has also been shown to activate calcium-dependent protein phosphatase calcineurin which dephosphorylates the cytoplasmic subunits of NFATc transcription factors resulting its nuclear translocation and upregulating many genes that are associated with neonatal glomerular mesangial cell apoptosis in kidney, whereas in cardiovascular biology it has been associated with myoblast transformation, and pathologic cardiac modeling [152, 168]. Moreover, overexpression of either wild type or of gain-of-function mutations of TRPC6 that is reported in human, triggered a constitutive activation of NFAT-regulated gene transcription involved with focal segmental glomerulosclerosis [78]. TRPC6 mediated intracellular increase in calcium also has been shown to activate Ca^{2+} /calmodulin-dependent protein kinase CaMKIV along with the MAP kinase extracellular signal-regulated protein kinase (ERK) [169].

Our data places PDE1 into the list of downstream mechanisms that link TRPC6 and DKD. In previous chapters we have demonstrated that TRPC6 might be another potential channel that might influence the intracellular calcium required to activate PDE1. Here using heterologous expression model, we showed how systemic risk factors in diabetic milieu activates TRPC6. We identified multiple clones that have several fold higher expressions of TRPC6 and selected one clone, C11 as functional clone based on the change in membrane potential in response to several known TRPC6 activator. Using small molecule, we demonstrated that this increase in membrane potential and corresponding calcium influx is TRPC6 specific. We also have demonstrated that several risk factors in diabetic milieu can increase intracellular calcium influx but differentially activate TRPC6. Finally, we have demonstrated that activation of TRPC6 leads to the depletion of intracellular cAMP. Although a large body of data exists pointing the importance of TRPC6 in the health of podocyte here we describe another mechanism where crosstalk between calcium and cyclic nucleotides that might play an important role in cellular physiology.

3.2 Methods and materials

3.2.1 Reagents

All chemicals and reagents were obtained from commercial sources. Hyperforin 9 (cat#H9791-25MG, Sigma Aldrich, St Louis, MO), Forskolin (cat#1099, TOCRIS Chemicals) were prepared as either 25 μ M or 10mM solution with DMSO. Both Angiotensin II (cat# A9525) and 1-Oleoyl-2-acetyl-sn-glycerol (OAG, cat# O6754) was purchased from Sigma Aldrich. The DAG sensor and cAMP sensor were purchased from Motana Molecular.

3.2.2 Cell Culture

TRPC6 overexpressed cell C11 (in the background of HEK293) cells were grown in mono layer culture at 37 °C in a humidified air atmosphere with 5% CO₂ using DMEM/F12 media with 250 μ g/ml HYGRO, 20mM Hepes, 1X NEAA, 1X NaPyruvate, 10% heat-inactivated fetal bovine serum, and 1% penicillin-streptomycin solution. All the experiments were performed between passage number 55-60.

3.2.3 Construction of recombinant plasmid and generation of TRPC6 stable cell line

Human TRPC6 gene was cloned using pcDNATM5/TO Mammalian Expression Vector system from Thermo Fisher (cat# V103320) using the manufacturer protocol. Briefly the human TRPC6 gene was first cloned between 1492 and 2870bp flanked by *ava* I and *Hind*III restriction sites. The whole construct was then chemically transformed in *E. coli* DH5 α TM-T1R strain and was propagated using the condition described by the manufacturer. Clones were selected on LB agar plates containing 50–100 μ g/mL ampicillin. Once the presence and orientation of the hTRPC6 was confirmed plasmid were isolated and stored in -800C. For making the stable cell line overexpressing hTRPC6, HEK293 cells were grown at approximately 60% confluent. Following day they were co-transfected with pcDNATM5/TO construct and pcDNATM6/TR at a ratio of 6:1 using lipofectamine 2000 (cat# 11668030). After transfection, fresh medium was added, and the cells were allowed to recover for 48 hours before induction. The final clones were selected based on a final concentration of 250 μ g/mL of hygromycin to the media. 10–20 clones were selected and analyzed for the presence and orientation of TRPC6 insert and plasmid vector.

3.2.4 Adenoviral construction of GCamp2 Ca sensor with hTRPC6

In order to monitor the calcium influx a hybrid construct was created by ligating GCamp2 sequence to the 5' end of the hTRPC6 under the CMV promoter. The hybrid construct was cloned into the pcDNA5/TO plasmid vector using the above protocol. Once the plasmid sequence and orientation confirmed the whole construct was commercially made by Vector Bio Labs. The titer was confirmed as 5×10^{13} gc.

3.2.5 Membrane potential assay

FLIPR assay development was performed following manufacturer's protocol (Molecular Devices, Sunnyvale, CA). Briefly, the day before the experiment TRPC6 overexpressed clones or HEK293 cells were seeded at 30K, 40K, 50K or 60K cells per well on Biocoat 96well plate (BE01770) for overnight incubation in cell culture incubator (5%CO₂, 37°C). Cell plates were loaded with 50ul of assay buffer containing 1× membrane-potential dye component A and incubated for 1hr. For making the stock solution of AngII and OAG, 1mM stock solution was prepared using the water and DMSO respectively. Either a single concentration was prepared, or a serial dilution was made to prepare the different doses of stimuli with their respective vehicle. For compound TRPC6 inhibitor a serial dilution was made using DMSO. The stimuli were prepared in 96 well plate and placed in the 'reservoir' section of the FLIPR system. The plate containing the cells and loading dye was placed in the on the platform of FLIPR384 (Molecular Devices), and the fluorescence signal was read with excitation/emission spectrum at 488/540 nm. The FLIPR tetra has a fully automated High-Speed Distributed Motion (HSDM) Thermo LAS microplate assay system which was used to conduct the HTS campaign. Measurements were made at 5s intervals. Basal fluorescence was measured for 15–30s, followed by addition of 5ul of the test stimuli and measurement of fluorescence for 300s. Raw fluorescence readings were first converted to response over baseline using the analysis tool of Screenworks 3.1.1.4 (Molecular Devices). The result was expressed relative to the maximum increase in fluorescence of control responses.

3.2.6 Measurement of Calcium influx in cell using FLIPR calcium assay kit

About 50K cells of TRPC6 stable cell line C11 were plated in each well of a black walled 96-well imaging plates and cultured for 24 h. The calcium dye used in the experiment was commercially available FLIPR Calcium 6 no-wash dye (Molecular Devices) that was prepared by dissolving the contents of one Component A vial by adding 10 ml of Component B or 1X HBSS Buffer plus 20 mM HEPES in physiological salt solution as per manufacturer's instructions. Before adding the appropriate stimuli growth media was completely removed and replaced with 100ul of the prepared reagent and incubated for 2hrs in the dark at 37°C. The plate was placed on the platform of FLIPR machine and the reagents were added using the automated injector system. The immediate change in fluorescence was measured using excitation 470–495 nm, and emission 515–575 nm every 5s after addition of test compounds. Raw fluorescence readings were first converted to response over baseline using the analysis tool of Screenworks 3.1.1.4 (Molecular Devices). The result was expressed relative to the maximum increase in fluorescence of control responses.

3.2.7 DAG measurement

C11 cells were plated at 20K per well in a 96-well black walled plate and transduced with either DAG sensing protein (cat#D0300G, BacMam; Montana Molecular, Bozeman, MT) or cADDi cAMP sensor (cat#during split and grown for 24hrs. Next day growth medium was removed and replaced with 100ul of PBS. Cells were mounted on a FLIPR station and stimulated with test compounds and fluorescent signal was captured at for 5 minutes at excitation 470–495 nm, emission 515–575 nm. Data was expressed as relative light units and the AUC was calculated using the Screenwork software.

3.2.8 cAMP measurement

A cAMP upward mNeon Green cADDi biosensor expressed under a CMV promoter was obtained from Montana Molecular (U0200G), and delivered by transduction with BacMam, a baculovirus modified to infect C11 cells. The cells were incubated in the presence of 2 mM sodium butyrate for 48 hours after transduction according to manufacturer's specifications before imaging. After

confirming the expression of the cAMP sensor cells were treated with test compounds. In case compound treatment, cells were pre-incubated with compounds for 1hr before the experiment. Some cultures were supplemented with 10 μ M forskolin for 30 minutes as positive control. Following the treatment with either test compounds or the positive control cells were fixed with 4% formaldehyde and stained with Hoechst dye. Cell images were captured using a Cellomics Arrayscan VTI and analyzed with the Target Activation BioApplication reading in two channels at a magnification of $\times 10$. An algorithm was used to identify objects by nuclear staining with Hoescht dye at 365nm, and cAMP was determined using 475nm wavelength. All fluorescent intensities are displayed as relative fluorescent units.

3.3 Results

3.3.1 Generation and selection of TRPC6-overexpressing stable cell line

As a first step towards the generation of stable TRPC6 overexpressing cell line, human embryonic kidney 293T cells (HEK293T) were transiently transfected with plasmid containing human TRPC6. Clones were selected based on their hygromycin resistance and expression of TRPC6 was measured using standard RT-PCR as shown in Fig 3.1. Based on relative expression of TRPC6, C1, C11, and C6 clones were selected to further evaluate their function. Membrane potential assay is a fluorescence-based method that does not directly measure ionic current, rather it measures the membrane potential-dependent changes of fluorescence signals as a result of ionic flux. As described in the Methods and Materials, the selected clones, including non-transfected HEK293T cells, were treated with either water or angiotensin II. Following the incubation with the dye, the fluorescent signal was captured by the FLIPR tetra high throughput imaging system. No changes in fluorescence was detected in HEK293 cell in response to 1 μ M of Ang II. However, C11 clone demonstrated a steep increase in fluorescent signal in response to Ang II-mediated depolarization, and the signal remained elevated during the time of the recording. The other two clones, C1 and C6, did not show any changes in the fluorescence signal (Fig 3.2A). Interestingly, even C1 had higher fold of TRPC6 expression compare to C11 but did not elicit any change in depolarization in response to angiotensin II. We further confirm this observation by treating the C11 along with C6 and naïve HEK293 cells with different doses of angiotensin II. As we have seen before, neither

naïve HEK293 nor C6 showed any change in the fluorescent signal. However, C11 demonstrated dose-dependent membrane depolarization (Fig 3.3). To confirm that AngII-mediated response is TRPC6 dependent, the cells were preincubated with a TRPC6-selective small molecule inhibitor and then treated with AngII. As shown in the Fig 4, TRPC6 inhibitor dose-

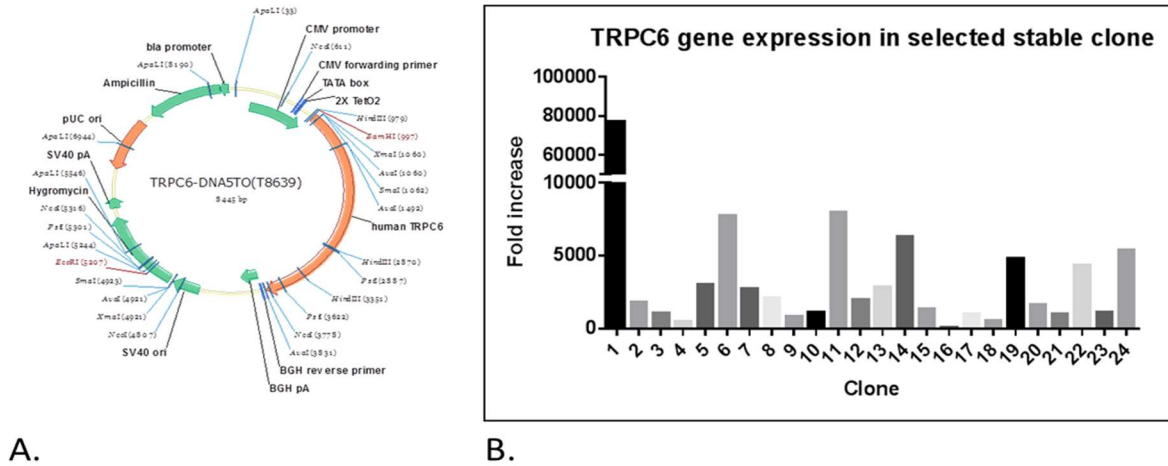


Figure 3.1. TRPC6 gene expression in the stable HEK293 cell line. Following transfection with hTRPC6 construct individual clones were selected in the presence of hygromycin . Twenty-four clones were selected, and RNA was isolated. Using human TRPC6/GAPDH taqman primer pair gene expression was analyzed. A) hTRPC6 plasmid map. B) Fold increase in TRPC6 expression.

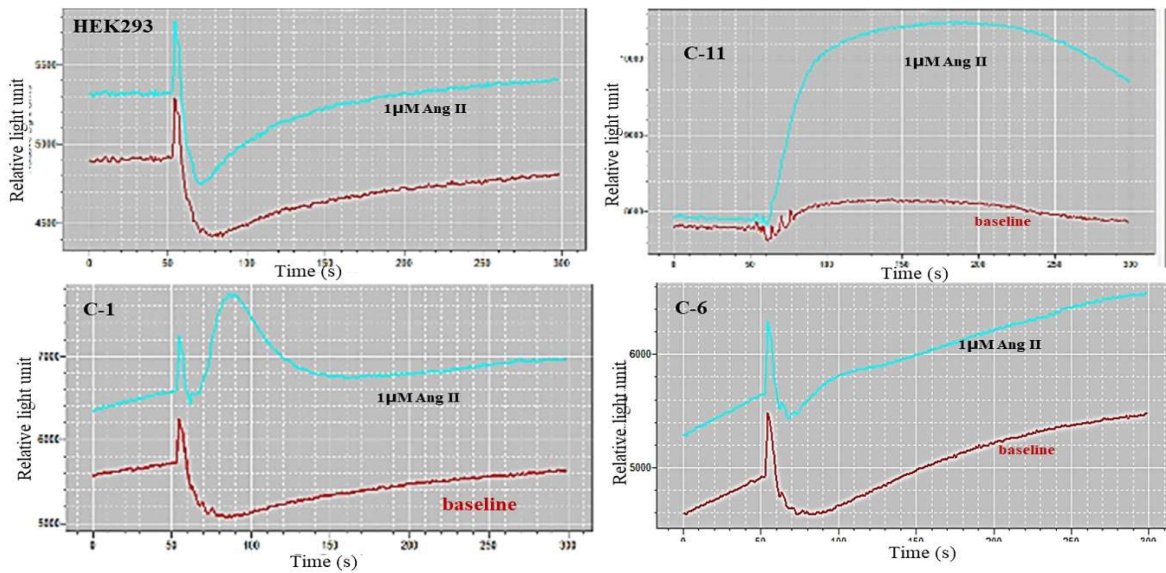


Figure 3.2. Comparison of fluorescent signal response of selected TRPC6 clones to membrane potential change during AngII stimulation. WT HEK293, clone 1(C-1), clone 11(C-11) and clone 6(C-6) were grown over night in poly-D-Lysine coated 96 well plate. After incubating with membrane potential dye for 30min cells were treated with 1uM angiotensin II and calcium signal was measured using FLIPR tetra high throughput screening system.

independently inhibits AngII-mediated membrane depolarization. Finally, we tested C11 against another well-known TRPC6 activator OAG and showed that C11 dose-dependently responded to OAG-induced change in membrane potential (Fig 3.5). The dose response study showed that, in C11 clone, OAG dose-dependently induced membrane depolarization at cell density between 30K-40K (Fig 3.5). Cell number higher than 40K did not show any response to Ang II stimulation.

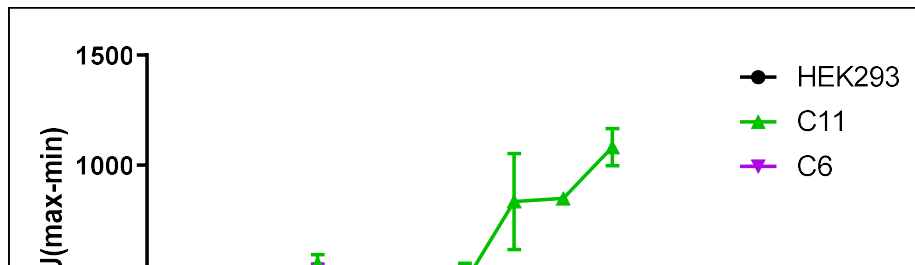


Figure 3.3. Membrane potential assay. About 30K cells of naïve HEK293 along with C6 and C11 clones were plated in a 96-well plate. After an overnight incubation the cells were incubated with membrane potential dye for 30 minutes. Cells were then treated with different concentration of AngII and the change in the fluorescent was captured in FLIPR. Relative fluorescence units (RFU) were calculated from the maximum fluorescence value (Max) after addition of AngII immediately before addition of AngII. Data shown represent the mean \pm S.E.M.

Taken together, these data suggested that the selected clone C11 is functionally active clone among others with similar level of TRPC6 gene expression.

3.3.2 Hyperforin 9 induced calcium flux in HEK293 cells in TRPC6-dependent manner

As a next step, we aimed to confirm that hyperforin 9, a widely used TRPC6 activator, induces calcium influx in a TRPC6-dependent manner. To achieve this goal, we constructed a plasmid whereby GCamp2, a calcium biosensor, was fused in the 3' end of human TRPC6 gene and cloned into pcDNA3.1 vector under CMV promoter (Fig 3.6 A). The whole construct was then packaged in an adenovirus for the ease of delivering to the cell. Following infection, HEK293 cells were treated

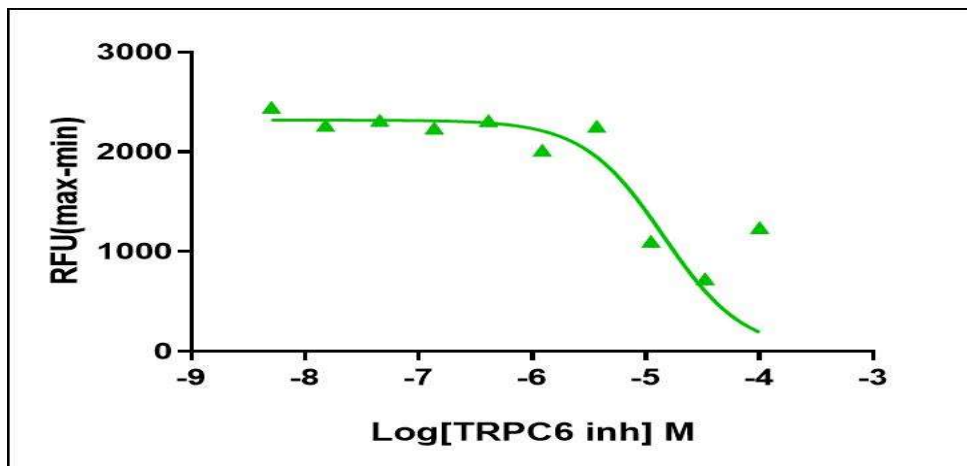


Figure 3.4. TRPC6 inhibitor inhibits AngII mediated change in membrane polarization.

About 30K cells of C11 clones were plated in a 96-well plate. After an overnight incubation the cells were pre-incubated with TRPC6 inhibitor for 1hr and with membrane potential dye for 30 minutes. Cells were then treated with 1 μ M of AngII and the change in the fluorescent was captured in FLIPR for 5minutes. Relative fluorescence units (RFU) were calculated from the maximum fluorescence value (Max) after addition of AngII and the minimum fluorescence value (Min) immediately before addition of AngII. Data shown represent the mean \pm S.E.M.

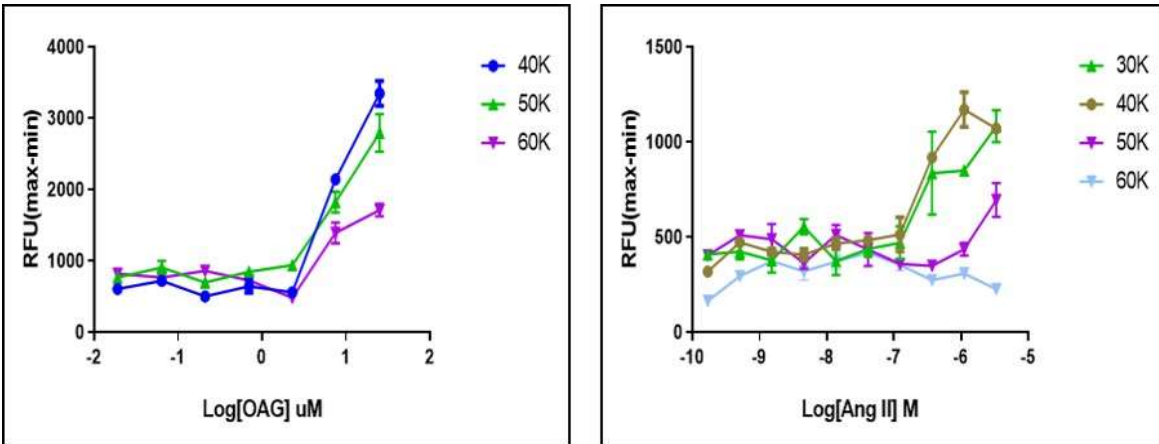


Figure 3.5. Effect of cell density on the fluorescence response of membrane potential dye in TRPC6 clone 11 against different stimuli. Different amount of clone 11 were plated in poly-D-lysine coated plate. Following loading with membrane potential dye for 30min cells were stimulated with different concentration of A) Angiotensin II (AngII) and B) 1-oleyl-2-acetyl-sn-glycerol (OAG). Fluorescent signal was captured in FLIPR for 5minutes. Relative fluorescence units (RFU) were calculated from the maximum fluorescence value (Max) after addition of AngII and the minimum fluorescence value (Min) immediately before addition of AngII. Data shown represent the mean \pm S.E.M.

with hyperforin 9, and the fluorescence signal was captured using a laser scanning confocal microscope. Hyperforin 9-treated cells have shown increased fluorescence signal within 30 sec of addition, and it reached its peak within 60s. To test if this signal is indeed mediated by TRPC6 activation, we pre-treated the cells for 2hr with TRPC6-specific small molecule inhibitor

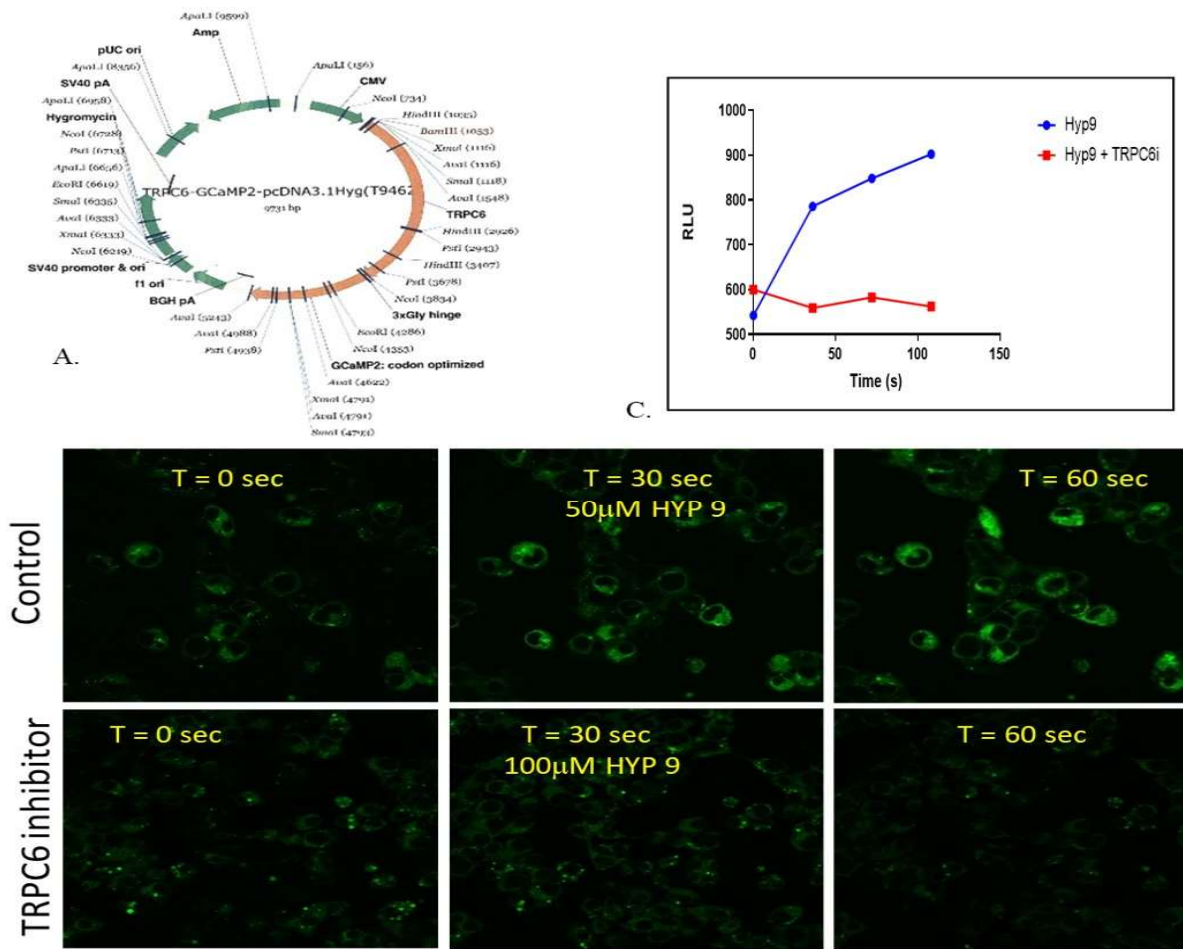


Figure 3.6. TRPC6 inhibitor inhibits hyperforin 9 induced calcium influx in C11. The hybrid construct to monitor the calcium signal was created by fusing GCaMP2 coding sequence to the human TRPC6 and cloned in adeno viral vector. HECK293 cells were infected with adenoviral TRPC6-Ca sensor hybrid. Following overnight infection, the cells were treated with 50uM Hyp9 in presence or absence of TRPC6 inhibitor. A. Genetic map for the hybrid construct B) upper panel: Time lapse fluorescent signal following Hyp9 stimulation. B) Lower panel: The fluorescence signal is inhibited by the pre-treatment of 10uM of TRPC6 inhibitor. C. Quantitative representation of the fluorescent signal.

and then treated the cells with hyperforin 9. As shown in the lower panel of figure 6B, TRPC6 inhibitor-treated cells showed complete attenuation of the fluorescent signal. Taken together, this suggests that hyperforin 9 induced calcium influx in TRPP6-dependent manner.

3.3.3 Several risk factors of DKD caused increased calcium influx in TRPC6-overexpressing cell line

Published studies have shown that several risk factors in diabetic milieu like AngII, endothelin 1, glucose can cause increased calcium influx in the cell. To evaluate the involvement of TRPC6, we treated C11 clone with several molecules representing these known risk factors and measured intracellular calcium release using high-throughput Fluorometric Imaging Plate Reader (FLIPR). About 50K cells were plated, and after overnight incubation with various “risk factor” molecules, cells were incubated with calcium 6 assay dye for 30 minutes, and fluorescence signal was captured with FLIPR. Representative fluorescence traces illustrating cellular response to different stimuli in C11 clone are shown in Fig 3.7. The corresponding solvent for each reagent was used as negative control. Carbachol and hyperforin 9 were used as positive controls. Incubation with water did not induce any change of fluorescence, whereas incubation with carbachol produced dose-dependent spikes in the fluorescent signal (fig 3.7). Out of the all stimuli tested, hyperforin 9 demonstrated the highest amplitude in the peak of calcium signal and an extended duration similar to glucose (Fig 3.7A). Among the hemodynamic risk factors, both Ang II and endothelin-1 demonstrated increased calcium influx (Fig 3.7B and 3.7C). Interestingly, even though they belong to the same class of vasoactive amines, endothelin-1 demonstrated a higher amplitude and instant increase in intracellular calcium whereas the response to Ang II was much delayed with much lower amplitude in the signal at the same concentration. Among the metabolic risk factors, glucose dose-dependently increased intracellular calcium and demonstrated extended response, whereas insulin did not induce any response (Fig 3.7D and Fig 3.7E). These data suggested that not all the risk factors in diabetic milieu induce similar response in intracellular calcium.

3.3.4 Diabetic risk factors differentially activate TRPC6

It has been demonstrated that both reactive oxygen species (ROS) and diacylglycerol (DAG) production are the key factors for activating TRPC6 [153, 170]. As we have demonstrated in the

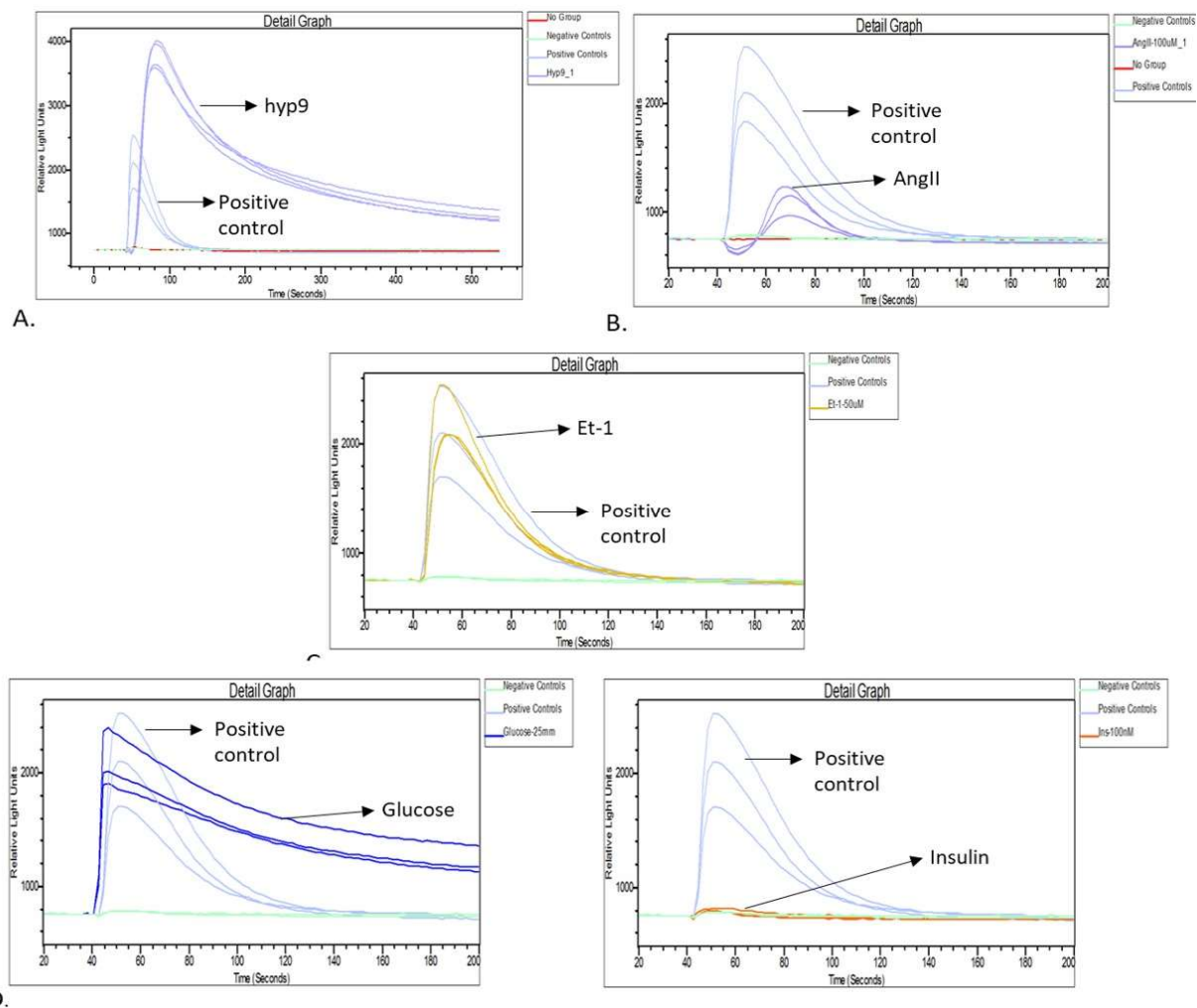


Figure 3.7. Representative FLIPR traces showing changes in calcium influx in C11 in response to diabetic risk factors. Cells were incubated with Calcium 6 dyes from Molecular Devices for 30 minutes before the treatment. Fluorescence measurements were taken for 30 seconds before addition of different stimuli. FLIPR traces showing change in fluorescence after addition of different doses of A. Hyperforin 9, B. Angiotensin II, C. Endothelin-1, D. Glucose and E. Insulin. In each cases water or DMSO were used as negative control and carbachol was used as positive control.

earlier section that systemic risk factors in diabetic milieu triggers TRPC6 mediated calcium influx, we next moved to evaluate if they differentially activate TRPC6. To evaluate the DAG-mediated activation of TRPC6, we employed a fluorescent downward DAG biosensor which is a fusion of a PKC-d fragment with circular permuted enhanced green fluorescent protein (GFP). Reactive oxygen species (ROS) were detected using cell-permeable dye, CELL ROX-Green, which is oxidized by O_2^- and $\bullet OH$ and the signal was captured by high throughput imaging platform called

Cellomics. Before proceeding with the actual risk factors, we tested detection assays using positive control. For DAG production, C11 cells were infected with mixture of Baculoviral construct of DAG sensor and muscarinic receptor M1 as described in the Methods. The change in fluorescence due to carbachol mediated DAG synthesis was captured by FLIPR. Carbachol demonstrated a rapid production of DAG soon after the compound injection. The calculated AUC of the fluorescent signal showed significantly higher DAG levels compared to water (Fig 3.8A). We then used hyperforin 9 to test if it induces any DAG production. Following infection with DAG sensor, plates were loaded to FLIPR chamber, and soon after adding hyperforin 9, dose dependent changes in the fluorescent signal was detected (Fig 3.8B). To measure ROS, C11 cells were treated with tert-Butyl hydroperoxide (TBHP) for 1hr. Before fixation with paraformaldehyde, cells were incubated with CELL ROX green dye and Hoechst stain for 30 minutes. The fluorescent signal was detected with Cellomics imaging system at 665nm. TBHP demonstrated dose-dependent production of ROS which was attenuated by treatment with a redox scavenger N-acetyl-L-cysteine (NAC), showing dose-dependent inhibition of fluorescence signal (Fig 3.9). After confirming that we have methods to detect DAG and ROS, we tested several diabetic risk factors in our system. To explore the risk factor-mediated DAG production, C11 cells were treated with different concentration of AngII, Et-1, glucose and insulin. As shown in Fig 11, glucose and Et-1 dose dependently induce DAG production whereas AngII did not. When tested for ROS production, hyperforin 9 did not induce any ROS generation. This would be the first time we demonstrated that hyperforin 9 activated TRPC6 via DAG production but not via ROS (Fig 11). When tested for differential activation of TRPC6 by the systemic risk factors, we found that Ang II activated TRPC6 via ROS generation but not via DAG production. In our experimental system, glucose demonstrated activation of TRPC6 via DAG production in dose-dependent manner but did not induce any ROS, whereas insulin induced neither DAG nor ROS (Fig 3.10 and Fig 3.11).

To confirm these findings in more complex system, we ran similar experiments in isolated rat glomeruli. Rat glomeruli were isolated as described in Methods and Materials. About 60-70 glomeruli were plated in a 96-well plate and, following overnight incubation in the media, they were treated with different agents to induce ROS, and the fluorescent signal was captured via Cellomics. As shown in Fig 12, TBHP dose-dependently produced ROS which can be inhibited

by NAC. AngII dose-dependently induced ROS within 1hr, and the signal remained elevated for 4hrs. Interestingly, THBP shown much higher level of ROS compare to AngII in one hour but the

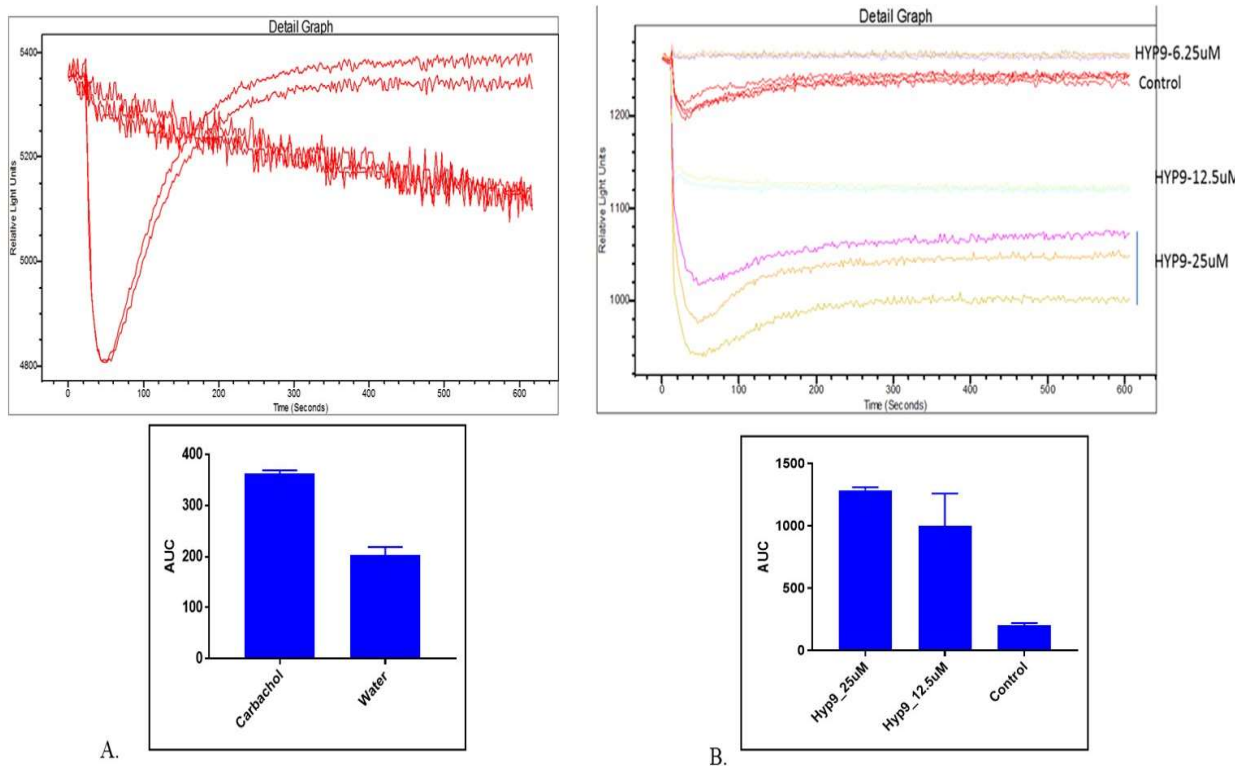


Figure 3.8. Hyperforin 9 induce transient intracellular diacylglycerol (DAG) in C11. Cells were plated overnight after infecting with baculoviral DAG construct. For testing carbachol the cells were also co-infected with muscarinic receptor M1. After overnight incubation cells were loaded in FLIPR chamber and treated with respective stimuli and the fluorescent signal was captured for 10 minutes. Baseline fluorescent signal was captured for 30s before the treatment. The traces show fluorescence changes following treatment with A. Carbachol and B. Hyperforin 9.

signal came down in 4hr. Like in C11 clone, glucose did not induced ROS even with longer incubation (Fig 3.12 B). We could not explore DAG production in isolated glomeruli using our existing DAG sensor as it failed to generate any signal with repeated effort.

3.3.5 Activation of TRPC6 caused depletion of cellular cAMP level

We used a genetically encoded single-color cAMP bio-sensor cADDIs, that has been validated previously [9] to evaluate the cellular cAMP level upon TRPC6 activation. To optimize the time,

TRPC6 overexpressed cells (C11 clone) were treated with 50uM of forskolin and incubated for 5, 10, 20 and 30 minutes. After incubation, cells were fixed with 4% paraformaldehyde and the

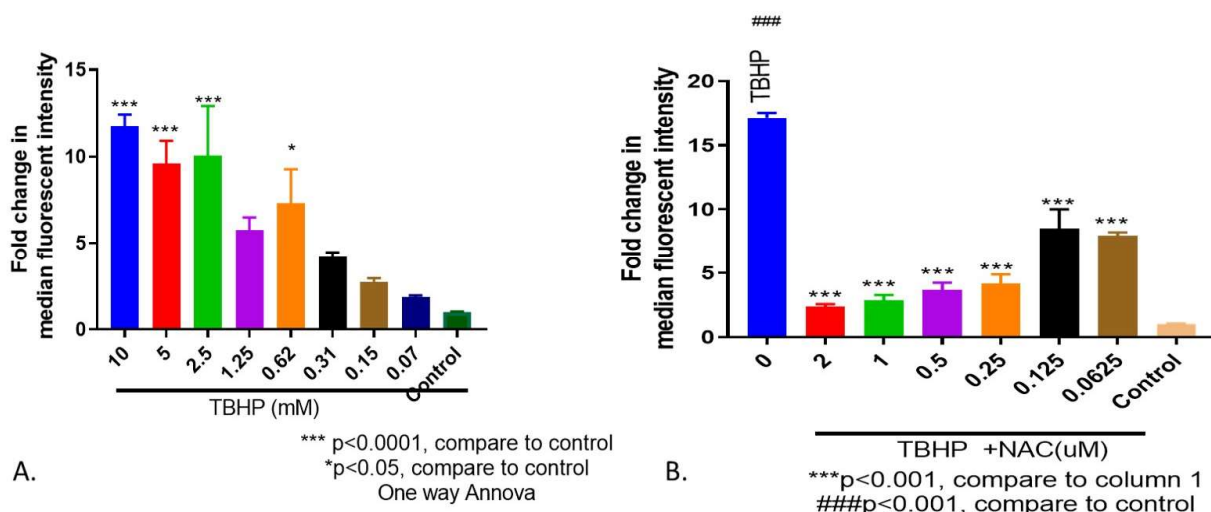


Figure 3.9. N-acetyl cysteine (NAC) attenuates tetra butyl hydrogen peroxide (TBHP) induced ROS in C11. Cells were treated with different doses of A) TBHP alone or with B) NAC for 1hr. Cells were fixed with 4% paraformaldehyde and ROS was detected using CELL ROX dye and the fluorescence signal was captured using cellomics. Qualitative analysis showing the fold induction as calculated by normalizing with respective control well. Data presented are the mean±s.e.m. p value calculated by one way ANOVA (N=4).

fluorescent signal was measured using Cellomic high throughput image analyzer. Forskolin showed a time-dependent increase in fluorescent signal that reached significance at 20 minutes, and the signal started to decrease at 30 minute (fig 3.13). To evaluate the effect of TRPC6 activation on cAMP level, clone C11 was treated with two different doses of hyperforin 9 in the presence or absence of forskolin. As shown in the Fig 13, forskolin significantly increased cAMP production in a dose-dependent manner. hyperforin9 caused reduction in the cAMP concentration. Hyperforin9 also significantly decreased cAMP in presence of forskolin (Fig 13). However, no obvious dose dependence was observed. Thus, it demonstrated that TRPC6-mediated increase in intracellular calcium resulted in the depletion of cellular cAMP (likely via activation of PDE1).

3.4 Discussion

In the previous chapter, we have identified TRPC6 as a likely source of calcium activating PDE1.

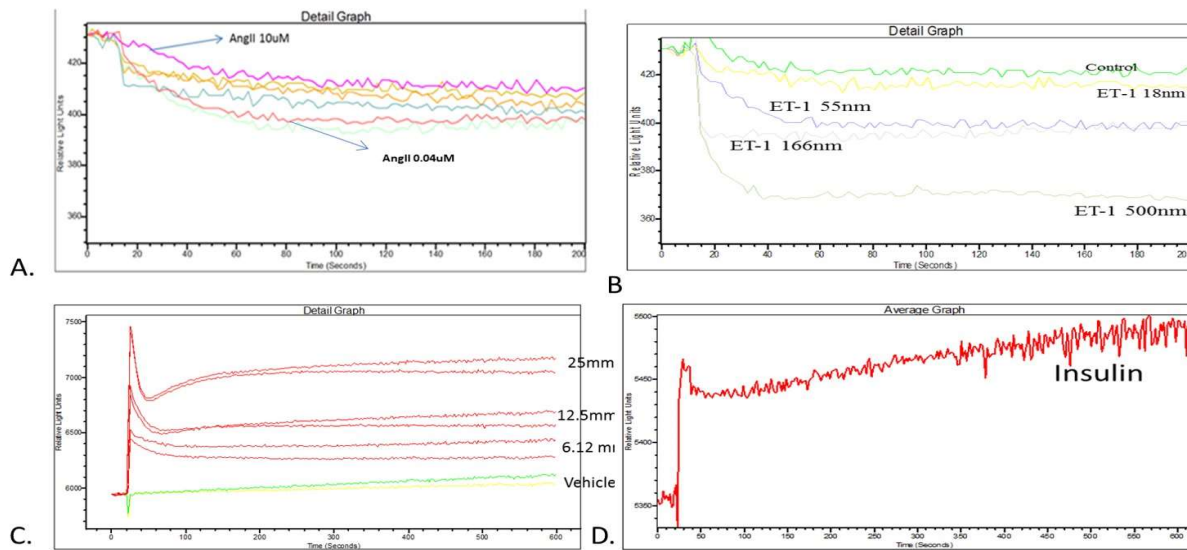


Figure 3.10. Differential response in DAG signal by diabetic risk factors in activation of TRPC6. Cells were plated overnight after infecting with baculoviral DAG construct. After overnight incubation cells were loaded in FLIPR chamber and treated with different doses of respective stimuli and the fluorescent signal was captured for 10 minutes. Baseline fluorescent signal was captured for 10s before the treatment. The traces show fluorescence changes following treatment with A. AngII and B. ET-1, C. Glucose and D. Insulin.

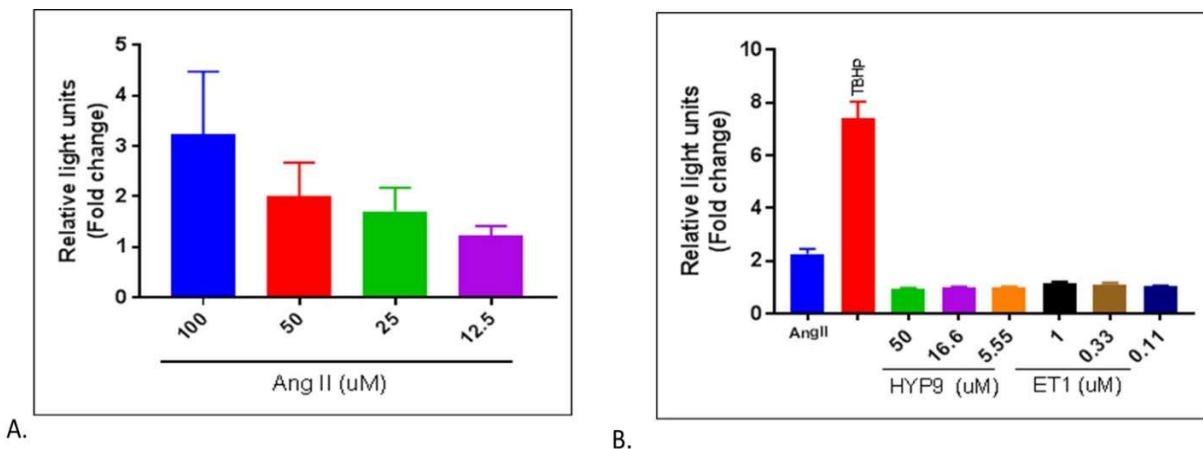


Figure 3.11. Differential response of TRPC6 activators in generating ROS in C11. Cells were treated with various doses of different TRPC6 activators for 1hr. Cells were fixed with 4% paraformaldehyde and ROS was detected using CELL ROX dye and the fluorescence signal was captured using cellomics. Qualitative analysis showing the fold change in fluorescent by A) AngII and B) Hyperforin 9 or endothelin 1 as calculated by normalizing with respective control well. Data presented are the mean \pm SEM. p value calculated by one way ANOVA (N=8).

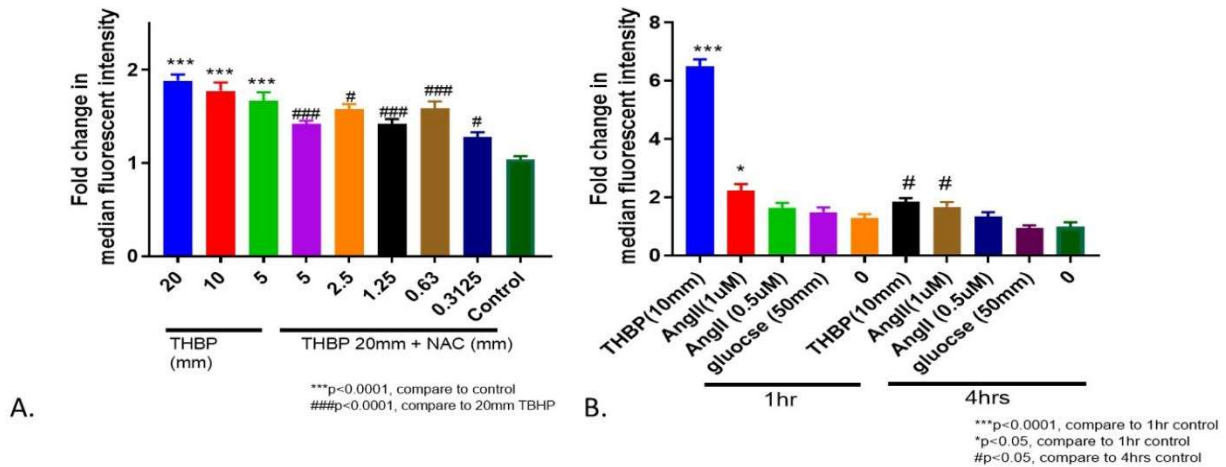


Figure 3.12. ROS signal in isolated glomeruli as assessed by CEL ROX dye. Equal number of glomeruli were plated in 96well plate and incubated with different ROS producing agent for 1hr. Following incubation and live Hoechst staining fluorescent signal was captured by Cellomics. Qualitative analysis showing the fold change in fluorescent signal as calculated by normalizing with respective control well following treatment with several doses of A) TBHP alone or with NAC., B) Isolated glomeruli was treated with different ROS producing agents and incubated for 1 and 4hrs. Following incubation and live Hoechst staining fluorescent signal was captured by Cellomics. Qualitative analysis showing the fold change in fluorescent signal as calculated by normalizing with respective control Data presented are the mean \pm s.e.m. p value calculated by one way ANOVA (N=8).

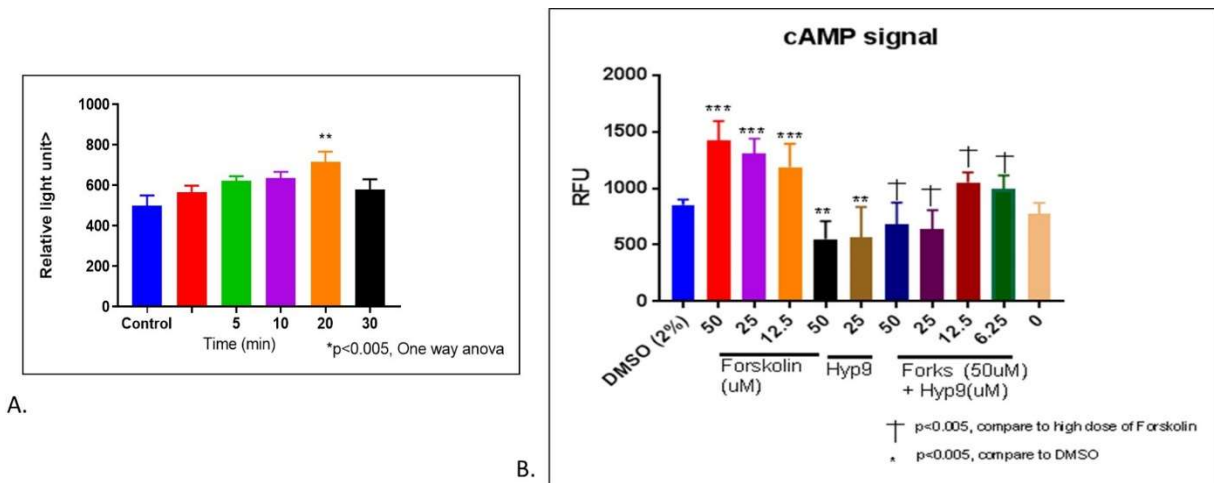


Figure 3.13. Detection of cAMP using green upward cAMP sensor. A) C11 cells were infected with baculoviral construct containing cAMP biosensor. Following overnight incubation cells were treated with 50uM forskolin and fluorescent signal was captured after 5, 10, 20 and 30 minutes incubation. B) C11 cells were incubated with forskolin or hyperforin9 or in combination with both. Fluorescent signal was captured using Cellomics after fixing the cells with 4% paraformaldehyde. Data presented are the mean \pm SEM. p value calculated by one way ANOVA (N=8).

In the present study, we investigated upstream mechanisms of TRPC6 activation. Specifically, using human embryonic kidney (HEK) cell expression model we investigated how/whether systemic risk factors of DKD interacted with TRPC6.

We identified multiple clones over-expressing TRPC6 and selected one clone, C11, based on the change in membrane potential in response to several known TRPC6 activators. Using small molecule TRPC6 inhibitor, we demonstrated that this increase in membrane potential and corresponding calcium influx were TRPC6-specific. We also have demonstrated that several risk factors of DKD can increase intracellular calcium influx but differentially activate TRPC6. Finally, we have demonstrated that activation of TRPC6 leads to the depletion of intracellular cAMP.

The role TRPC6 in chronic kidney disease has been of interest for many years since the discovery of gain-of-function mutation related to FSGS [68]. Using heterologous system and in vivo models, several reports have emphasized its role in regulating calcium influx and contribution in both cardiac hypertrophy and renal diseases [75, 171, 172]. Recent animal studies also demonstrated its involvement in the pathophysiology of DKD [77, 173, 174]. We also have reported in the previous chapter that TRPC6 expression is higher in the glomeruli of several form of CKDs including DKD in human. We also have demonstrated that activation of TRPC6 leads to renal cell apoptosis in PDE1 dependent manner. However, it is unclear what systemic risk factors activate TRPC6 and what are specific molecular mechanisms of TRPC6 activation. Here we set out to examine how these factors activate TRPC6 using biosensor technology in the cell-based systems.

Multiple researchers have shown enhanced calcium influx and associated increase in current as demonstrated by patch clamp using heterologous expression of TRPC6 in various cell lines including HEK293 [153, 175, 176]. Traditional patch-clamp has been the standard method for monitoring the ion channel activity. Several other techniques including radioligand binding, radio-active flux assay or optical recording are currently accepted methods for investigating the function of ion channels [177]. Fluorescent readouts are widely used both to monitor intracellular ion concentration and to measure membrane potential [177-179]. The principal behind the membrane potential assay is that any ionic flux across the membrane will result in the change in membrane potential which causes the redistribution of the dye and thus changes in the fluorescence.

They also have demonstrated a good correlation with the traditional patch clamping [177]. Here we generated similar heterologous system and used membrane potential as surrogate to calcium influx. Several stable cell lines were selected based on the gene expression. When tested for functional readout, only one clone, C11, showed positive response in membrane potential assay. Using this clone, we tested TRPC6-related activities of several DKD risk factors. For obvious reason, comprehensive investigation of multiple risk factors was not practical. Therefore, we decided to focus on two main groups of molecules: representing hemodynamic risk factors (angiotensin II and endothelin 1) and representing metabolic risk factors (glucose and insulin). In each case, we asked if a given extracellular molecule affected membrane potential and, if yes, what intracellular signaling molecule(s) mediated this effect. The former was assessed by changes in membrane potential, while the latter focused on DAG and/or ROS production as the main mechanisms of TRPC6 activation. As a positive control, we demonstrated that ROS, associated with several TRPC activators, and OAG, a DAG analog, modulated membrane potential dose-dependently in C11 corroborating published data [180].

Angiotensin II (AngII) has been shown to induce calcium influx in podocytes and in vascular smooth muscle cell of the small arteries and afferent arterioles [181]. It has also been shown that, at least in podocytes, AngII-mediated increase in calcium is TRPC6 dependent [170]. We also have demonstrated that AngII dose-dependently induced membrane depolarization in C11. Using a small molecule TRPC6 inhibitor and multiple known TRPC6 activators, we confirmed that both the calcium influx and membrane potential is indeed TRPC6 specific. Our data corroborated the fact that AngII, after binding to AT1R, a GPCR, activates TRPC6 by ROS generation[182].

Another mediator of hemodynamic stress, endothelin 1 (ET1), has been shown to increase calcium current and upregulate TRPC6 and induce hypertrophy in cardiomyocyte in calcineurin-NFAT dependent manner [183] but the mechanism of activation was not addressed. In our hands, ET-1 dose-dependently increased calcium influx and activated TRPC6 via DAG production but did not induce any ROS production. Interestingly we found that AngII activates TRPC6 via ROS generation, which corroborates others findings [159]. Unlike ET-1 it did not induce DAG production. Although both binds to the similar class of GPCRs and exert similar physiological effect, vasoconstriction, through elevation of calcium, the interim signaling pathways might be

different. Another observation we found in this study is that the amplitude of calcium signal is much higher in ET-1 compare to AngII. Further studies are needed to elucidate the detailed mechanism.

Among metabolic risk factors of DKD, plasma glucose and insulin are, arguably, playing the major role. While hyperglycemia is a broadly accepted cause of glucotoxicity, leading to the end-organ damage, insulin can play dual role as a factor reducing blood glucose levels thereby acting as a protective factor and, in the context of selective insulin resistance, also contributing to end-organ damage. Both glucose and insulin have been shown to activate TRPC6. High glucose has been shown to increase OAG-induced calcium current and upregulate TRPC6 in monocytes and platelets [80, 160]. We have found that glucose-induced, TRPC6-mediated increase in calcium influx is attributed to the DAG production but not ROS. This contradicts the data published by several authors that showed that glucose-mediated TRPC6 activation is ROS dependent [182]. This could be attributed to the use of two different cell types. Intracellular calcium influx did not change with insulin treatment nor it produces any DAG or ROS. Our data showed that although glucose and insulin are both risk factors for diabetic condition, glucose might be playing a role in TRPC6 mediated pathophysiology of DKD, while effects of insulin could be mediated by other mechanisms.

Thus, we have elucidated certain aspects of upstream activation of TRPC6 in a context of metabolic disturbances. What is happening downstream? Once activated, TRPC6 activates multiple signaling pathways. Calcium flux leads to activation of protein phosphatase calcineurin. Calcineurin, in turn, activates a transcription factor NFAT that upregulates several disease related genes. In addition to that, we identified PDE1 as another potential downstream effector of TRPC6, thereby connecting two second messenger systems, calcium and cyclic nucleotides. Among all the phosphodiesterase, PDE1 is the only one that is activated by calcium/calmodulin. Recently, Zhang et al showed that AngII mediated activation of PDE1 leads to the reduction of cAMP in cardiomyocyte and this requires TRPC3 [88]. We have shown in the previous chapter that TRPC6-mediated apoptosis can be attenuated by blocking PDE1. Thus, we confirmed that in renal cells, TRPC6 is associated with the PDE1-mediated apoptosis. Here, we provided some mechanistic connection that the cell death is associated with the depletion of cAMP. We showed that hyperforin

9-mediated TRPC6 activation resulted in depletion of cAMP implying that increased intracellular calcium activates PDE1 leading to depletion of cAMP. We also demonstrated that in human mesangial cells all three isoforms of PDE1 are upregulated by hyperforin 9.

Mechanisms of DKD are multifactorial. Elevated level of calcium, DAG and ROS are all thought to contribute to the pathogenesis of DKD. In our hands, glucose did not show any ROS generation, while other reports have shown it can induce ROS. We have demonstrated that glucose can activate TRPC6 by DAG production. Elevated levels of AngII and Et-1 in diabetic patients is known [72]. All these can contribute to the activation of TRPC6. Our studies for the first time connected the diabetic risk factors with activation of TRPC6. Our studies also have shown a crosstalk between two second messengers, calcium and cyclin nucleotides. Earlier we have shown pre-clinical evidence where inhibiting PDE1 exerted benefit in the animal mode of DKD. Here we provided mechanistic evidence of activation of PDE1 by the systemic risk factors that involves TRPC6. One of the limitations of this study is the lack of either pharmacological or genetic evidence of involvement of PDE1 in depletion of cAMP. Although we showed that hyperforin mediated increase in calcium is TRPC6 specific, but the depletion of cAMP could be due to potential non-specific action of hyperforin. Further studies are required to show the specificity. The lack of reliable cGMP biosensor also precluded us from investigation of potential mechanistic link between TRPC6, PDE1, and cGMP. More research is needed to interrogate this pathway. However, available data still provide sufficient evidence of a crosstalk between TRPC6 and PDE1 and their potential role in pathogenesis of DKD.

CHAPTER 4. TRANSLATING ANIMAL TO HUMAN; USE OF COMPUTATIONAL BIOLOGY IN UNDERSTANDING DIABETIC KIDNEY DISEASE

4.1 Introduction

In our earlier chapters we described a novel role of PDE1 in a mouse model of DKD and demonstrated that systemic risk factors of diabetes activate PDE1 in TRPC6 dependent manner. However, without conducting a clinical trial it is hard to predict whether this finding will translate to humans. This chapter describes the use of computational biology which was applied to renal gene expression, and histopathological data as well as clinical biomarkers from the DKD patients, in order to evaluate the pre-clinical to clinical translation.

DKD is the leading cause of chronic kidney disease and in the US its prevalence has progressively increased over the past few decades. Despite current treatment strategies for optimizing glycemic and blood pressure, DKD still contributes to almost one-half of all cases of end-stage renal disease and becoming a major medical burden in the United States. Development of new therapeutic interventions for DKD requires better understanding of the pathophysiology of the disease.

The use of genome wide Genome-wide transcriptome analysis kidney expression arrays recently advanced our understanding of DKD and provided insights into disease pathogenesis, and identification of biomarkers for progression or treatment response. Woroniecka et al, described a comprehensive catalog of gene-expression changes in human diabetic kidney biopsy samples using micro-dissected glomeruli and tubule samples and identified some novel pathways as well as confirmed some known pathways [82]. Several studies have been published based on the gene expression analysis from the European Renal cDNA Bank, a large collection of renal biopsies comprising of micro-dissected glomeruli and tubule segments from CKD patients They identified Janus kinase1/2/signal transduced and activator of transcription (STAT), nuclear factor NF κ B and Wnt/b catenin as major pathways altered in DKD [184-187]. But identification of a consensus sets of gene in multiple dataset is still lacking.

Deciphering the pathogenesis of DKD is not straightforward and has multiple challenges. The complexity stems from the interaction of hyperglycemia, hypertension and renal hemodynamics and later through the involvement of proinflammatory factors and immune cell infiltration, makes it difficult to identify a single causative mechanism [188]. Second, the complex architecture and heterogeneous cell populations of the kidney poses another challenge. The functional unit of the kidney, called the nephron, has a highly ordered structure, consisting of several specialized cell types. The important major components of the nephron are the glomeruli, which is functional barrier and the proximal and distal tubules that absorbs or excretes solutes. Specialized cells along the nephron include endothelium, mesangial cells, podocytes, and epithelial cells should be accompanied by corresponding regional variation in gene expression patterns [189]. In that context the gene expression analysis of the whole kidney often misinforms the role of specific cell types in the disease process. Third, DKD is clinically diagnosed by albuminuria but often the patients don't progress to ESRD which makes it challenging to associate the molecular changes to the disease progression. Moreover, the confirmatory diagnosis of DKD is still based on histopathology assessment which, most of the time, is not available thus making correlation of the clinical phenotype to renal structural changes difficult. Renal transcriptomic analysis of DKD patients sometimes does not provide relevant information as the alteration in a gene expression does not necessarily lead to proportionate changes in protein production.. To overcome some of these issues, the kidney molecular signature linked to histopathology constitutes a systems biology approach which is becoming the mainstream to understand the pathophysiology of DKD. For example, using cortical interstitial fractional volume (VvInt), an index of tubule-interstitial damage and compartment-specific gene expression profiling from CKD patients, Nair et al demonstrated the early molecular signature can be linked to long-term disease progression [76]. In a separate study Beckerman et al., identified key driver modules from kidney expression data which correlated with renal structural changes rather than functional GFR [77]. These data demonstrate that relating transcriptomic data with histological features, provides better understanding of DKD progression rather than relying on molecular data alone.

Finally, a severe limitation in finding a therapeutic intervention is the lack of animal models that accurately recapitulate human disease. Animal models often fail to reflect the diversity of the DKD population but also there is often a mismatch between endpoints measured in animals versus

humans. For example, any drug discovery process to evaluate an anti-fibrotic drug relies on the multiple histological, histochemical and biochemical parameters in animals whereas in clinic the more restrictive end points would be mortality, glomerular filtration or proteinuria. Also, most animal models demonstrate changes of early diabetic glomerulopathy, but they fail to capture later structural changes, including glomerulosclerosis, advanced tubulointerstitial fibrosis caused by chronic diabetes, and eventually renal function decline. These types of cross-species differences form barriers to translational research that ultimately hinder the success of clinical trials. Therefore, there is an urgent need to develop methodologies for reducing the gap between cross-species translational research.

We have used three publicly available gene expression datasets from DKD patients to find a consensus set of causal genes. The canonical pathway, disease and function analysis revealed the association of an inflammatory and immune response signature with DKD. Furthermore, we have analyzed the correlation coefficient density of the set of genes with individual clinical and histopathological features of DKD patients and used that data to develop a model for assessment of translatability of animal data to humans and provided two examples of this approach.

4.2 Methods and materials

4.2.1 Gene expression omnibus datasets.

The Gene Expression Omnibus (GEO) (<https://www.ncbi.nlm.nih.gov/gds>) hosted by the National Center of Biotechnology Information contains high-throughput gene expression datasets deposited by many authors. We selected potential GEO datasets according to the following inclusion criteria: 1) specimens had histological diagnosis; 2) micro-dissected human kidney tissues with clinically diagnosed diabetic kidney disease. 3) normal kidney tissues used as controls; 4) expression profiling by array OR RNA seq and raw data had the CEL format. Finally, 4 GEO datasets, GSE30528, GSE30529, GSE104954 and GSE50892 were included in our study. The gene expression data based from animal models was generated at Eli Lilly and Company disclosed in a previous publication [97]. All the data set that passed the initial QC inspection were imported and processed further by GeneSpring GX software, version 12.6 (Agilent Technologies). An R

language based function RMA () function available in Affy package was used to summarize raw expression levels. DEGs were identified with classical t test, statistically significant DEGs were defined with $p < 0.05$ and $[\log FC] > 1$ as the cut-off criterion.

4.2.2 Gene Ontology and Pathway Enrichment Analysis

Candidate DEGs functions and pathways enrichment were analyzed using multiple online and commercial software like Ingenuity pathway analysis (IPA) and Protein Analysis Through Evolutionary Relationships (PANTHER). Bonferroni corrected p values of < 0.05 were considered significant.

4.2.3 Statistical Analysis Software

Except where noted above, all statistical analyses were performed in R version 3.5.1. All the DEG analysis and correlation density analysis were used R packages from the bioconductor.org site. The following R code was used to create the correlation density between gene and histopathological score or clinical parameters.

```
# loading lib
library(aroma.light)
# set working dir
setwd('C:\\Projects\\DN\\Cell_Types')
# read in corr matrix from the dir
d = read.table("Susztak_RNA-vs-histopath_Corr.txt", header=1, sep='\t', row.names=1)
corr_type = 'Pearson_'
dcor = d[, grep(corr_type, names(d))]
dim(dcor)
names(dcor)
# read in genesets mapping
genesets = read.table("Genesets_Mapping.txt", header=1, sep='\t')
table(sort(genesets$Group))
cells = table(sort(genesets$Group))
cellnames = names(cells)
```

```

traits = sub('Pearson_', "", names(dcor))
# running parameters
K = median(as.vector(cells))
N=200
for (j in 1:length(traits)) {
  windows()
  #nf <- layout(matrix(c(1:6), 2, 3, byrow = TRUE), respect = TRUE)

  if (j==1||j==2||j==5||j==6||j==18||j==4) {
    plotDensity(dcor[, j], col='black', lwd=3, ylab='density', xlab=paste('Pearson
correlations w/ ', traits[j], sep="), ylim=c(0, 5))
  } else if (j==14||j==9||j==7||j==3||j==17) {
    plotDensity(dcor[, j], col='black', lwd=3, ylab='density', xlab=paste('Pearson
correlations w/ ', traits[j], sep="), ylim=c(0, 4))
  } else if (j==8||j==11||j==13||j==15||j==25||j==24||j==23) {
    plotDensity(dcor[, j], col='black', lwd=3, ylab='density', xlab=paste('Pearson
correlations w/ ', traits[j], sep="), ylim=c(0, 3))
  } else {
    plotDensity(dcor[, j], col='black', lwd=3, ylab='density', xlab=paste('Pearson
correlations w/ ', traits[j], sep="), ylim=c(0, 2))    }
  #      "DKD2000", "Renin+lisinopril", "renin+PDE1i", "Renin+Ucn2-16h", "Renin+Ucn2-
1wk", "reninAAV", "Spp1_interactome"
  cell.col = c('red', 'darkviolet', 'hotpink', 'aquamarine2', 'green', 'cyan', 'blue')
  cat("Median geneset size=", median(cells), "\n")
  ## simulating 100 times with min geneset_size
  for (k in 1:N) {
    plotDensity(dcor[sample(row.names(dcor), K), j], add=T, col='gainsboro') }
  for (i in 1:length(cells)) {
    x=names(cells[i])
    y=toupper(as.vector(genesets[genesets$Group==cellnames[i], 'Gene']))

```

```

        plotDensity(dcor[y, j], add=T, col=cell.col[i], lwd=3, ylab='density',
xlab=paste('Pearson correlations w/ ', traits[j], sep="))    }

    if (j==1||j==2||j==5||j==6||j==18||j==4) {
        plotDensity(dcor[, j], col='black', lwd=3, ylab='density', xlab=paste('Pearson
correlations w/ ', traits[j], sep="), ylim=c(0, 5), add=T)
    } else if (j==14||j==9||j==7||j==3||j==17) {
        plotDensity(dcor[, j], col='black', lwd=3, ylab='density', xlab=paste('Pearson
correlations w/ ', traits[j], sep="), ylim=c(0, 4), add=T)
    } else if (j==8||j==11||j==13||j==15||j==25||j==24||j==23) {
        plotDensity(dcor[, j], col='black', lwd=3, ylab='density', xlab=paste('Pearson
correlations w/ ', traits[j], sep="), ylim=c(0, 3), add=T)
    } else {
        plotDensity(dcor[, j], col='black', lwd=3, ylab='density', xlab=paste('Pearson
correlations w/ ', traits[j], sep="), ylim=c(0, 2), add=T)
    }

    legend("topleft", title='legend', c("all gene", cellnames), lwd=4, col=c('black', cell.col))
}

```

4.3 Results

4.3.1 Identification of common genes modulated in DKD patients

To identify a list of genes that are modulated in DKD patients we compared the expression profile using several public databases. European Renal cDNA Bank (ERCB) cohort with accession number GSE104954, had tubulointerstitial RNA-seq data from subjects with chronic kidney disease and from living donor biopsies. The dataset includes a broad range of CKD patients including DKD patients (N=12) and living donors. In all datasets the number of DEG was evaluated by filtering data using a false discovery rate (FDR) of >0.05, fold induction >1.5 and with a p value of <0.05. We found about 5564 tubular genes are differentially expressed in the

DKD patient in ERCB cohort when compared to the living donors. GSE50892 contained expression data from kidney biopsies of liver disease patients where the DEG was analyzed from 9 control and 8 CKD patients and a total of 4762 DEGs were found. GSE30529 dataset provided expression data of micro-dissected tubules from 12 control and 10 DKD patients and GSE30528 included RNA-seq data from glomeruli samples of 13 control and 9 DKD patients. We have found 3401 glomerular genes and 2996 tubular genes that are differentially expressed in DKD patients compare to controls. To increase the likelihood of identifying genes that are modulated in DKD, we performed concordance analysis which is defined by the percentage of DEGs shared by the two platforms with agreement in the direction of fold change. As shown in the Venn diagram in figure 2, 5564 genes detected in the tubule data of the ERCB cohort, 1129 overlapped with genes identified in the GSE30528 dataset. Only those genes showing the same direction of regulation whether up-regulated or down-regulated in both datasets, were further selected. This resulted in a set of 1081 (96%) genes with concordant expression out of 1129 total probes (Fig. 1). Similarly, comparing GSE30528 and GSE30529 we found 853 genes that are common in the two databases and 609 of them moved in same direction. Finally GSE104954 was compared to the GSE0892 dataset and 1513 genes overlapped with a concordance of 83% (1262 genes). To compile a set of consensus DEGs all the concordant genes among the three datasets were listed that resulted in 2040 genes identified, which would be referred as DKD2000 in the subsequent analysis. The intersection of these concordant genes showed that there are 207 genes common in all three concordant gene lists (Fig 4.1).

4.3.2 Gene Ontology analysis of DKD2000 genes

We used Ingenuity Pathway Analysis (IPA) to conduct a comprehensive analysis and identify the most significantly enriched molecular functions and discover any potential novel regulatory networks associated with our list of genes that are differentially regulated in DKD patients using a criterion of Benjamini-corrected p-value of less than 0.05. The top 10 canonical pathways based on the significance of the enrichment are shown in (Fig 4.2). Canonical pathways related to immune response was one of the most prevalent., specifically, iCOSL signaling in T helper cells with 27 molecules identified with a ratio of 0.407. About 63 molecules were found to be associated

with neuroinflammation signaling pathways with positive z score and a ratio of 0.22. Several of the genes pertained to the macrophage, fibroblast and endothelial cells in rheumatoid arthritis.

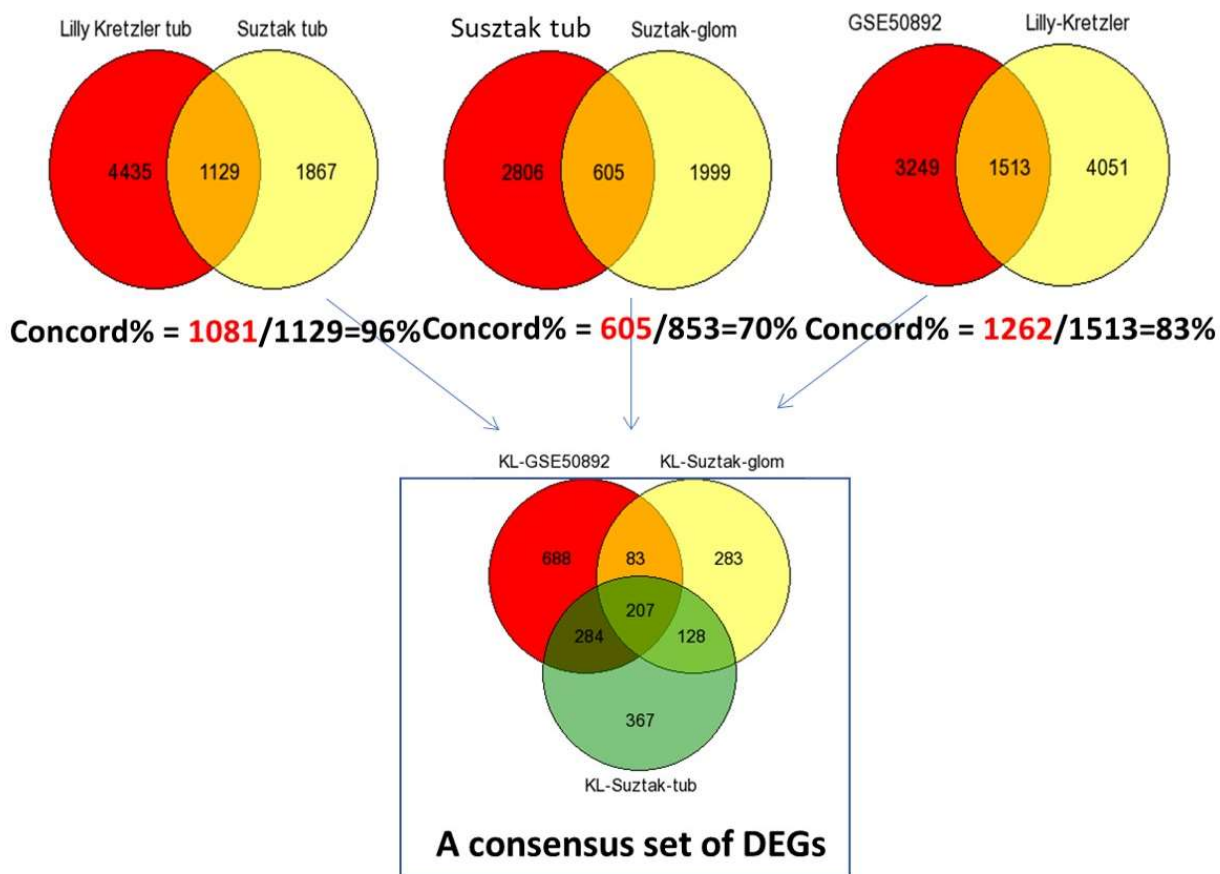


Figure 4.1. Identification of 2040 (DKD2000) commonly changed DEGs from the four cohort profile data sets (GSE30528, GSE30529, GSE104954 and GSE50892). Different datasets were represented using different color scheme. The cross areas meant the commonly changed DEGs. Statistically significant DEGs were defined with $p < 0.05$ and $[\log FC] > 1.5$ as the cut-off criterion and DEGs were identified with classical t-test.

Many genes were linked to the atherosclerotic signaling pathway with apparent to activity pattern but a ratio of 0.343. Some other pathways that are relevant to kidney diseases were the Endothelin-1 pathway, JAK1/JAK2/TYK2 pathway and the NFAT signaling pathway. The knowledge-based search for associations with disease and function revealed the association of the DKD2000 genes with cancer, immunological disease, metabolic disease, inflammatory disease, inflammatory response and cardiovascular disease (Fig 4.3). Further analysis for functional annotation in

immunological disease category revealed that the majority of the genes modulated belonged to the systemic autoimmune syndrome which are the diseases characterized by dysregulation of immune

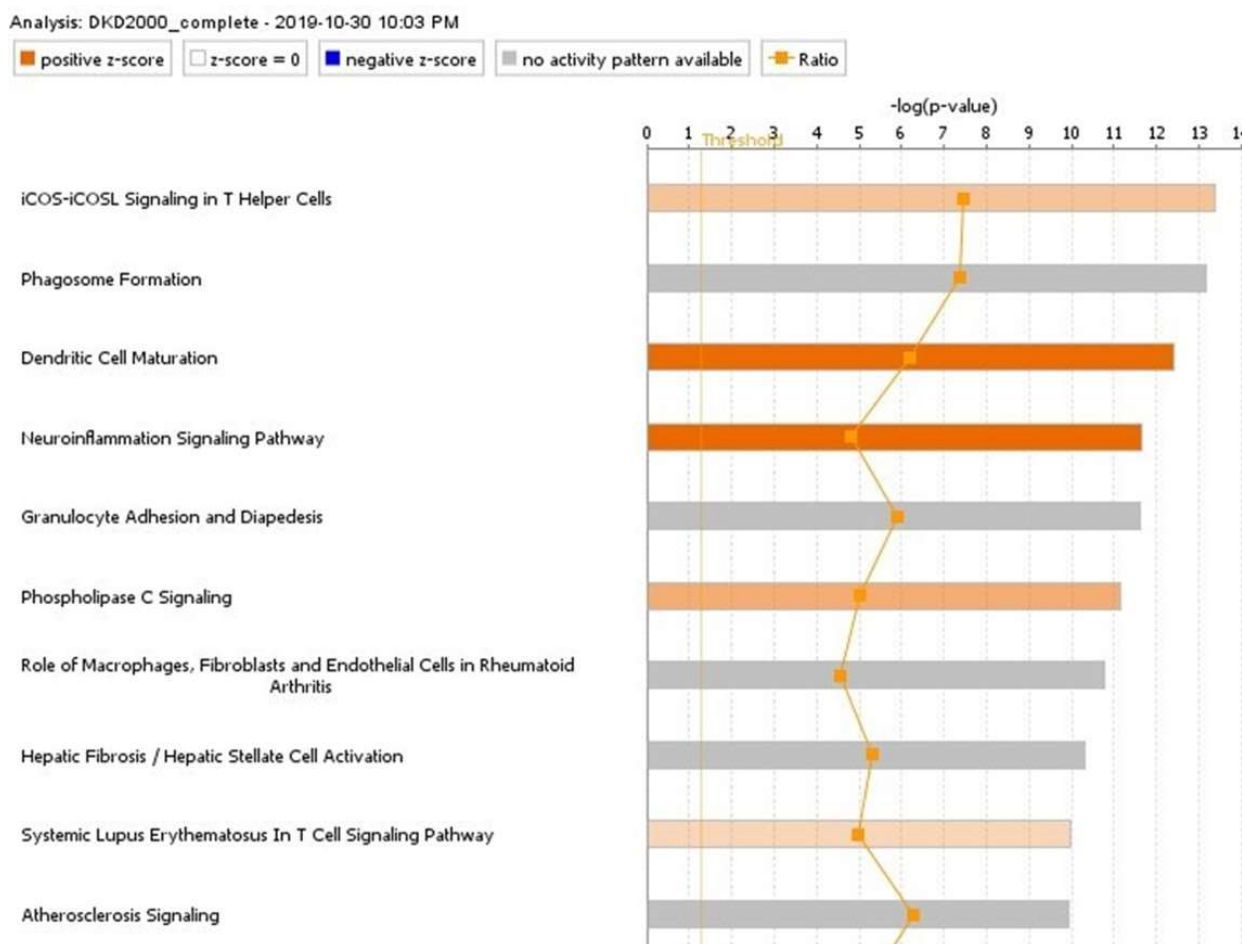


Figure 4.2. Ingenuity Pathway Analysis (IPA) top 10 canonical pathways for DKD 2000 DEG list. ($p < 0.001$). The canonical pathways identified that are most statistically significant are listed according to their p value ($-\log$; orange line). Blue bars represent negative z-score; orange bars represent positive z-score; gray bars represent no activity pattern available. The ratio of the number of differentially expressed genes found in each pathway over the total number of genes in that pathway were represented by the orange squares.

system. Although IPA analysis did not list metabolic dysregulation as one of the top disease functions a sub-analysis revealed several genes related to glucose metabolism disorder and involved in diabetic complications including DKD (Fig 4.3). A large number of genes were linked with the connective tissue disorder disease category and a sub-analysis revealed genes for rheumatoid arthritis or general arthritis are all significantly increased (Figure 4.3). We also

subjected the DKD2000 gene list to Protein Analysis Through Evolutionary Relationships (PANTHER) which revealed a significant number of genes associated with stress response and immune system process (Table 2). The molecular and cellular function analysis indicated numerous differentially expressed genes are involved in the cell movement, cell death and survival and cellular morphology.

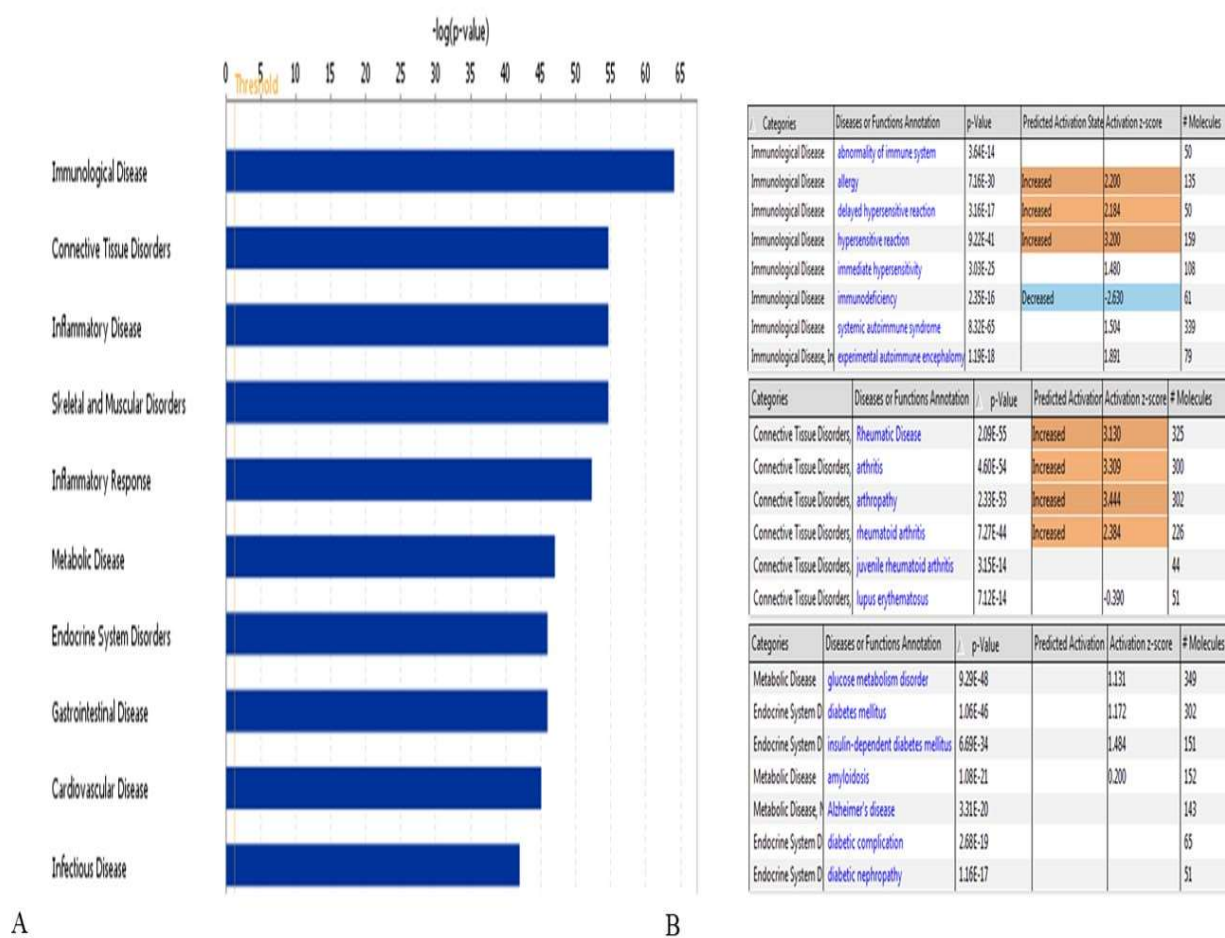


Figure 4.3. Significantly enriched A) disease and B) function pathway analysis of the DKD 2000 genes.

4.3.3 Correlations between clinical phenotype and expression data in diabetic nephropathy

To evaluate the shared contribution of differentially expressed genes towards the disease phenotype, we estimated the Pearson's correlation coefficient between each gene in DKD2000 list and the 25 different clinical and histopathological features reported in the DKD patients (N=146 data set as described in the methods and materials). A total of 17,000 genes were reported to be

present in kidney in that dataset and we measured the Pearson correlation coefficient between individual genes and each of the 25 different clinical and histopathological features of DKD patients (Fig 4.4). The correlation density curve showed a trend to zero meaning the neutral effect

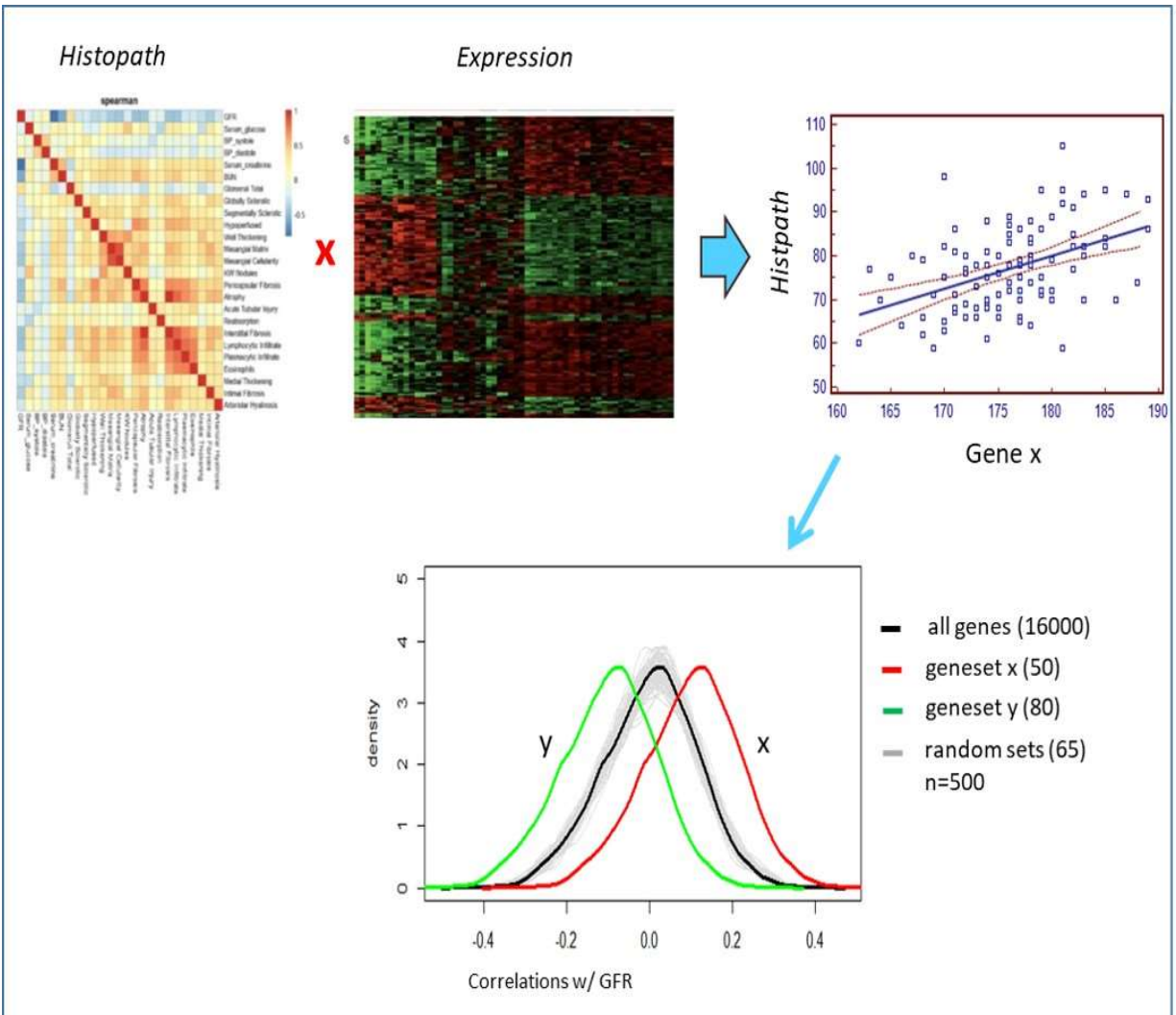


Figure 4.4. Schematic representation of the correlation density analysis of the DKD 2000 genes. The expression of all 17K genes reported in the kidney correlations with histopathology data across patients. Grey lines represented bootstrapping samples (500x) in order to establish significant boundaries.

of the genes on each of the clinical and histopathological traits. However, when similar analysis was done for the DKD2000 genes, the curve shifted towards left indicating a number of genes with

negative correlation with eGFR whereas it showed positive shift with serum creatinine and BUN (Fig 4.5). Comparatively less shift was observed with serum glucose and blood pressure indicating a weak correlation of the DKD2000 genes with these parameters. Similar analysis was done with the histopathological scores of the DKD patients. Positive correlations were observed with

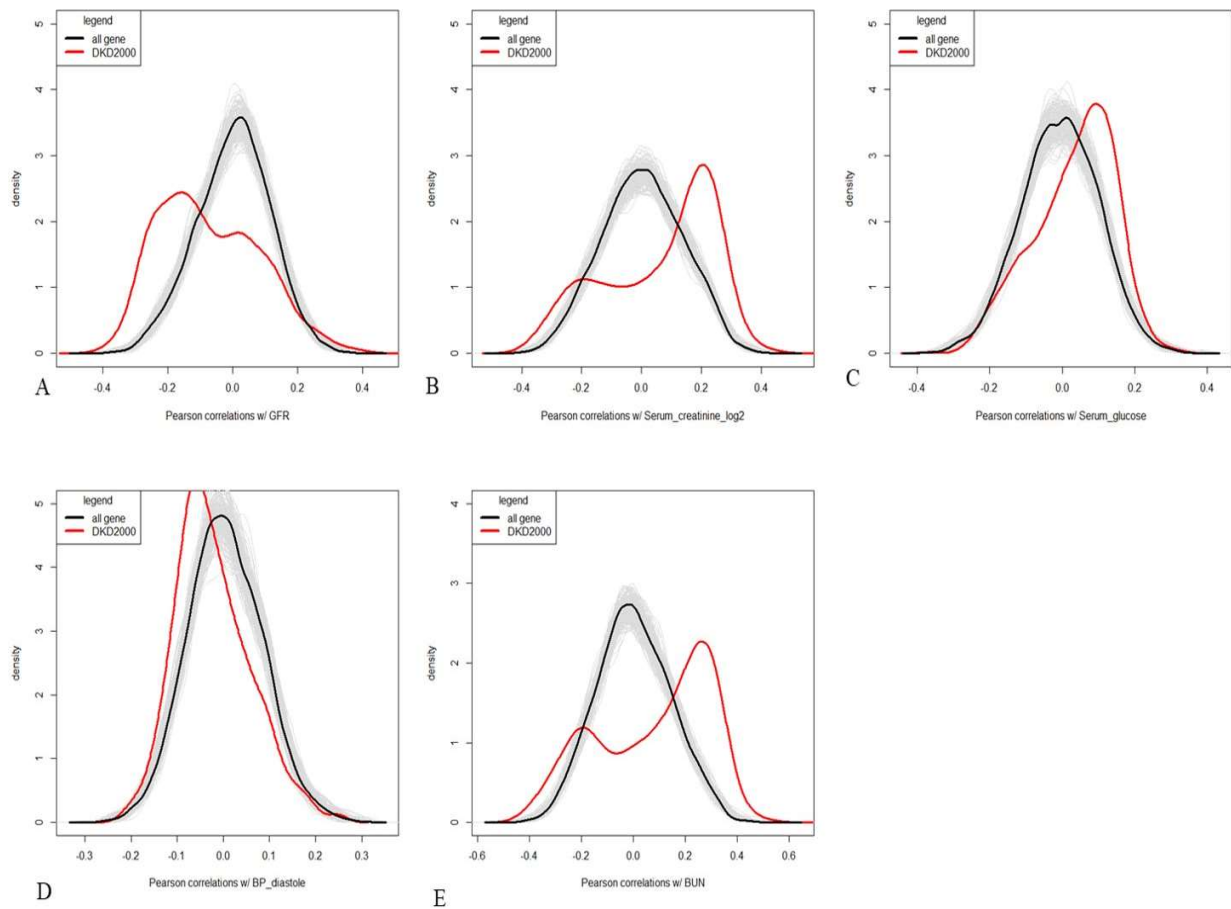


Figure 4.5. Density histograms of Pearson correlation coefficient between gene expression signature and clinical parameters of the DKD patients. Pearson correlation coefficient was measured for each of the DKD2000 genes against the clinical parameters and density histogram was created using R script. The black line showing normal human genes and the red line showing DKD2000 genes. Density correlation analysis of gene set and A) GFR, B) Serum creatinine, C) serum glucose D) diastole and E) serum BUN.

interstitial fibrosis, mesangial matrix formation, pericapsular fibrosis, arteriolar hyalinosis (Figure 4.6). The correlation analysis showed some genes were associated with renal Kimmel Wilson nodules, that is the pathology hallmark of DKD. Interestingly several genes were correlated with

a reduced number of glomeruli. Thus, the DKD2000 genes showed good correlations with the several clinical and histopathological traits in DKD patients.

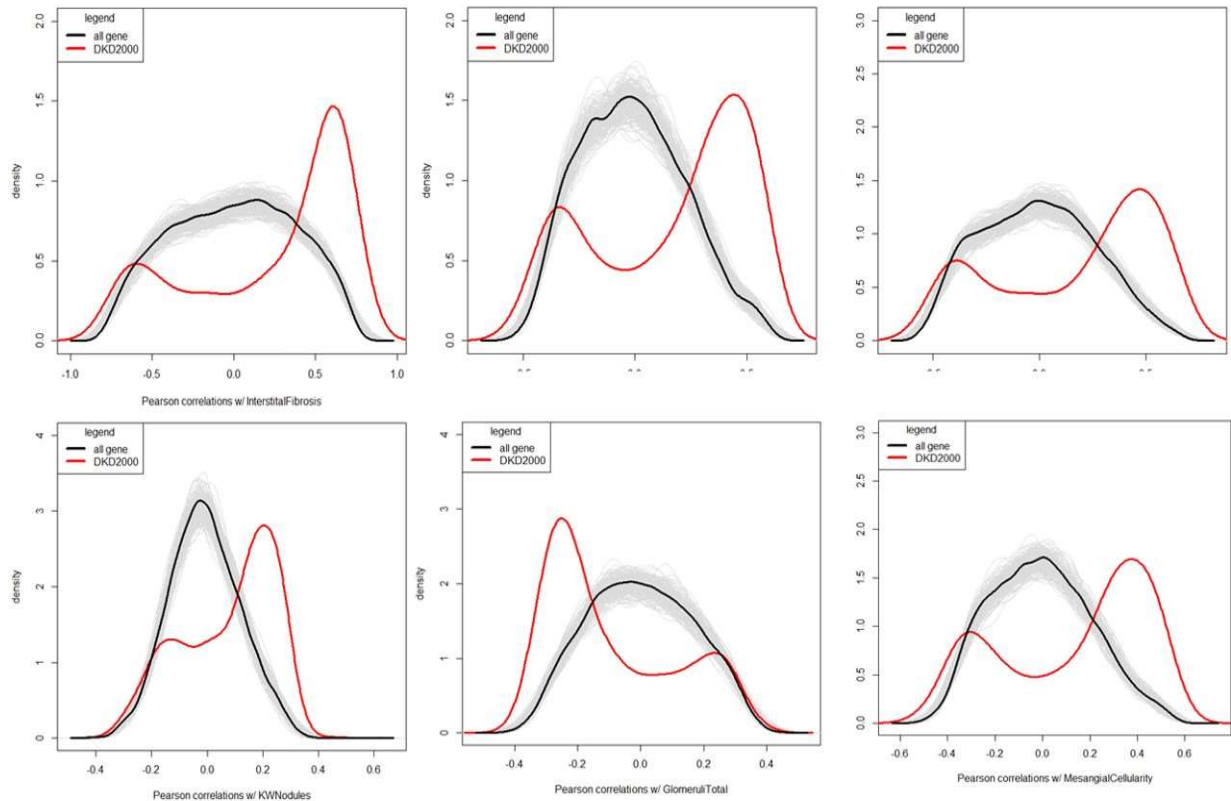


Figure 4.6. Density histograms of Pearson correlation coefficient between gene expression signature and histological parameters of the DKD patients. Pearson correlation coefficient was measured for each of the DKD2000 genes against the A) interstitial fibrosis, B) mesangial matrix, C) pericapsular fibrosis, D) KW Nodules, E) glomerular number and F) mesangial cellularity as reported in the clinical diagnosis of DKD patients.

4.3.4 Translatability assessment of animals to human DKD

Earlier we demonstrated that PDE1 inhibition resulted in renal protection in an animal model of DKD. To evaluate the translatability of this finding to humans we conducted a similar approach of associating transcriptomic data to human phenotype data. To build the model we first analyzed the microarray data as reported in the dbdb AAV renin DKD model [190]. We identified 800 genes that are differentially expressed using the same criteria as before (Fig 4.7). We also found that 300 genes were differentially expressed in the Lisinopril treated group compare to the vehicle group.

We identified the human orthologs of all the DEGs in both groups using the Ensembl database. Pearson correlation coefficient was calculated between each of the gene and 25 of the clinical and histopathological features of the DKD patients. As shown in figure 7 the cyan line showed that the density plot of the DEGs in dbdb AAV renin model shifted left like the DKD2000 genes the eGFR. Similarly, when correlation coefficient was calculated for some of the other clinical parameters like serum creatinine and BUN the correlation density plot mimicked human DKD2000 density plot and the lisinopril treated group demonstrated reversing those phenotype (Fig 4.7). We also measured the correlation of each of the genes in AAV renin animals with the histopathological traits of the DKD patients to further evaluate the relationship of the molecular signature to the clinical histopathology. We found the density curve for AAV renin model mimicked the DKD2000 profile for several histopathological traits of DKD. A positive correlation coefficient of greater than 0.5 was found for arteriolar hyalinosis, interstitial fibrosis, pericapsular fibrosis and global sclerosis (Fig 4.8). The DEG analysis of the microarray of PDE1 treated mice found about 836 genes that were modulated. After deriving the human orthologs we did the same correlation analysis and found that PDE1 treated animals demonstrated similar shift towards to the ‘zero’ as seen in the normal human (Fig 6) for GFR, mesangial matrix and interstitial fibrosis (Fig 4.9).

4.4 Discussion

By using computational biology, we identified a consensus group of DEGs that are common in two other sets of DKD gene expression data and we further confirmed the anatomical location of the genes using a whole kidney data set. We used IPA software suit to analyze the canonical ,disease and functional pathways to show that the molecular signature is predominantly associated with inflammation and the immune response. In the second stage we measured the correlation coefficient density of the consensus gene set to the 25 different histopathological features and some clinical parameters of DKD. Our data showed that these genes collectively shifted the curve that was otherwise would have remained neutral stage in normal human. We used two in vivo preclinical gene expression data sets and identified the human homologs. It was demonstrated that the gene expression changes occurring in a mouse DKD model recapitulated those of human DKD and standard ACE inhibitor therapy (lisinopril) or a novel PDE1 inhibitor shifted the Pearson’s correlation curve back to normal.

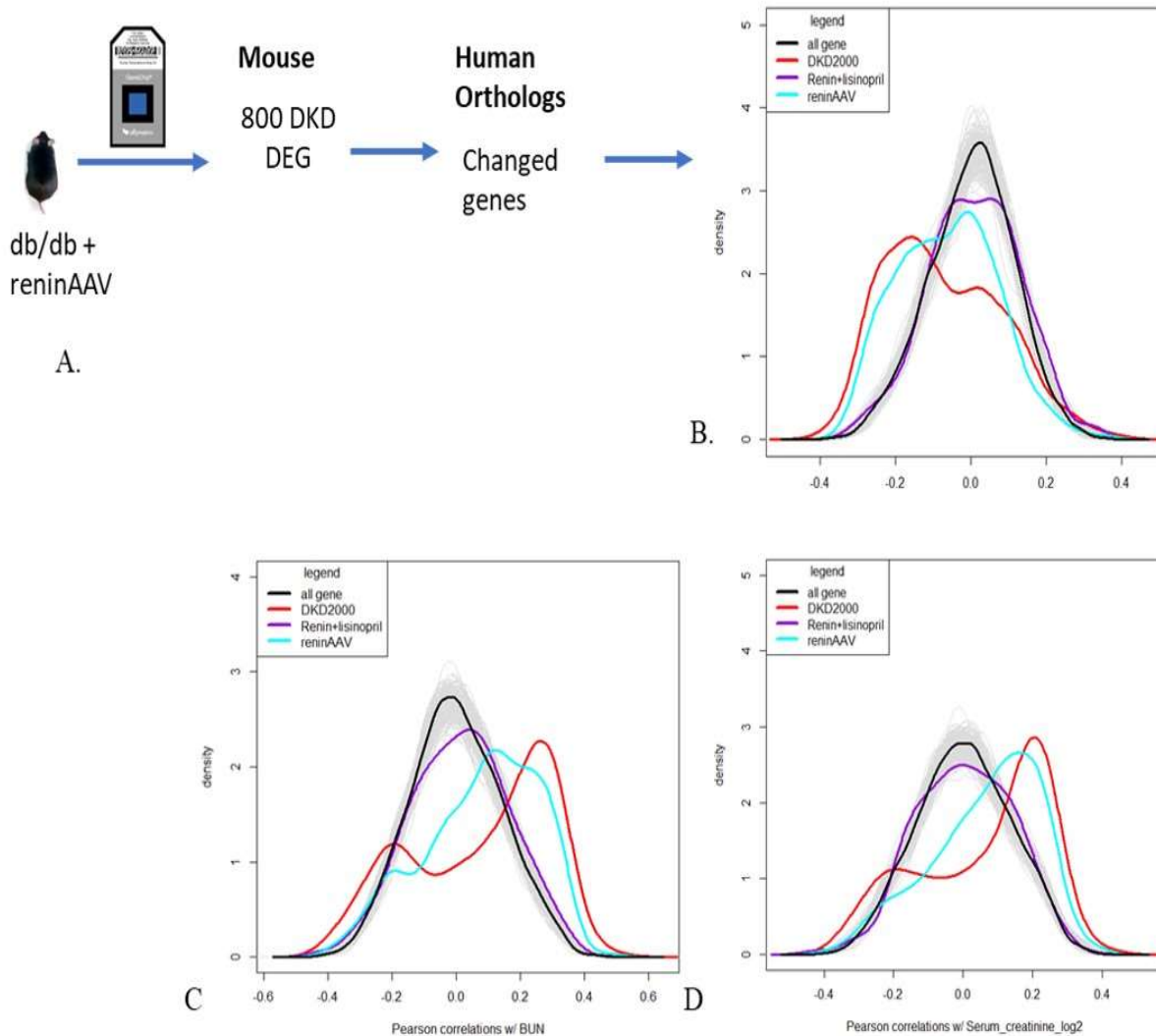


Figure 4.7. Model for cross species translation based on the correlation density analysis. **A) Schematic of the model.** Human orthologs of 800 mouse DEGs from AAV renin animal and 300 DEGs in lisinopril treated animals were derived from ensemble.org and correlation density as analyzed with the clinical parameters of DKD patients following the same method. The resulting density histogram showed the curve shifted left for B) GFR, but to the right for C) serum creatinine and D) serum BUN in disease state but shifted to towards to normal with lisinopril treatment. The black line represents normal human, 'red' line for DKD2000, 'blue' for renin AAV mice and 'cyan' for the lisinopril treated AAV renin animals.

DKD is emerging as a major public health burden in the US, as 1 in 4 patients with type 2 diabetes will develop nephropathy. Thus, the development of new therapies to treat the progression of DKD is a major unmet need. During the past few years, utilizing gene

expression profiling from renal biopsies of diabetic patients from has resulted in the identification of new therapeutic targets that enable the discovery of new drugs. In our present study we imported data from three publicly available GEO datasets and extract gene

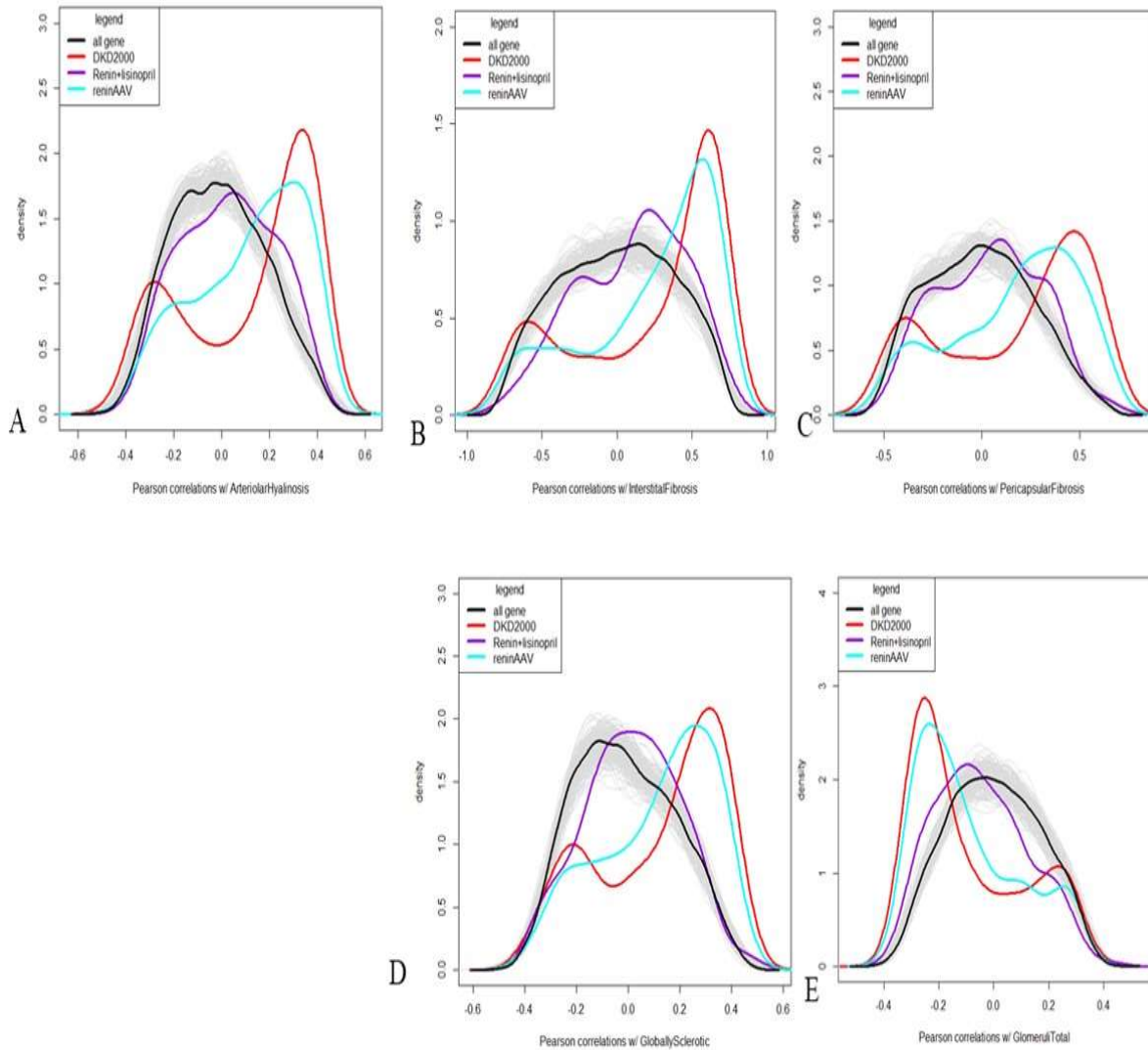


Figure 4.8. Density histograms of Pearson correlation coefficient between gene expression and histopathological parameters. Human orthologs of 800 mouse DEGs from AAV renin animal and 300 DEGs in lisinopril treated animals were derived from ensemble.org and correlation density as analyzed with the A)Arterial hyalinosis, B) Interstitial fibrosis, C) Pericapsular fibrosis, D) Global sclerosis, E) glomeruli number of DKD patients following the same method. The black line represents normal human, ‘red’ line for DKD2000, ‘blue’ for renin AAV mice and ‘cyan’ for the lisinopril treated AAV renin animals.

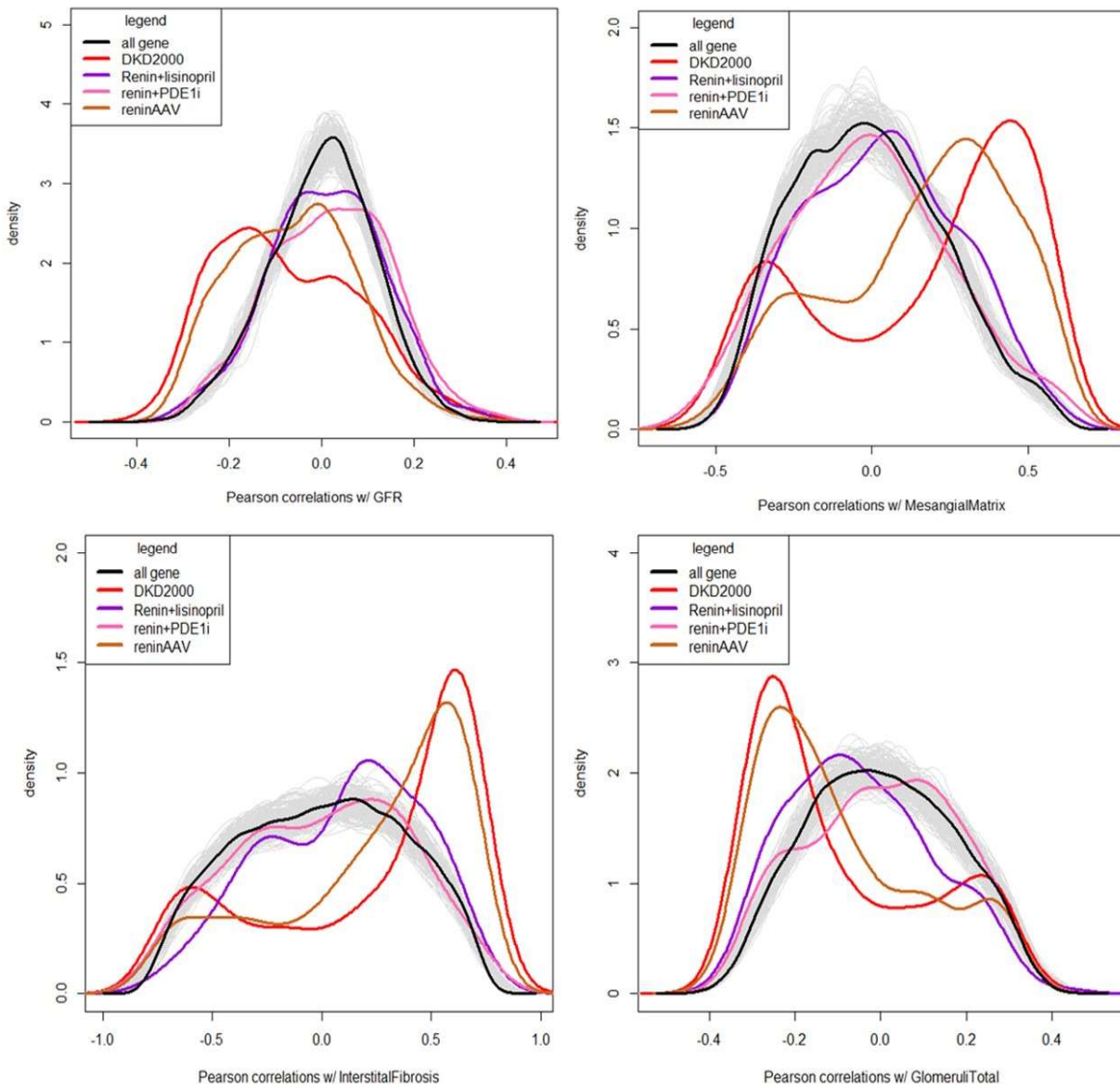


Figure 4.9. Density histograms of Pearson correlation coefficient between gene expression and histopathological parameters. Human orthologs of 800 mouse DEGs from AAV renin animal and 300 DEGs in lisinopril treated animals were derived from ensemble.org and correlation density as analyzed with the histopathological parameters of DKD patients following the same method. The black line represents normal human, ‘red’ line for DKD2000, ‘green’ for renin AAV mice and ‘blue’ for the lisinopril treated AAV renin animals and ‘pink’ for PDE1 treated animals.

expression dataset of DKD patients in order to compare the DEGs to the living donor samples. The kidney is has heterogenous structure and to identify compartment specific genes, we used gene

expression data from the micro dissected samples of the glomeruli and tubule. We found expression of some of the well-known glomerular genes were downregulated in our common gene list. For example, NPHS1 is downregulated by 7.3 fold and NPHS2 by almost 3 fold. NPHS1 gene code is for nephrin, a podocyte transmembrane protein that functions both as a structural and signaling protein and the loss of nephrin is a sensitive marker of podocyte injury. It has been reported that in DKD patients nephrin mRNA and protein is downregulated [191]. NPHS2 codes for podocin which is located on the cell surface in the area between two podocytes called the slit diaphragm. In a cross functional study of a few DKD patients found that both podocin and nephrin protein expression are downregulated in the kidney biopsies [192]. Moreover in a separate study urinary podocin level was higher in DKD patients with very low GFR [193]. Some other podocyte specific genes like WT1, SLIT2 and PODXL [189] were also found to be down regulated, overall indicating poor health of the podocytes in DKD. Several known tubular specific genes like SLC4A1, MME2, HNF1B and FBPI also were differentially expressed in the DKD patients [189]. Canonical pathway analysis indicated that the consensus genes in DKD2000 list mostly involved in the inflammation and immune response. We found the top five canonical pathways are associated with helper T cell, macrophage and dendritic cell biology. The top pathway based on the p value is iCOS/iCOSL signaling pathway, that involves inducible co-stimulatory molecule (ICOS) and ICOS ligand (ICOSL) which is critical in T cell activation and survival, particularly in T cell dependent humoral immunity [194]. Helper T cells are activated when exposed to antigens presented by such as dendritic cells, B cells, and macrophages which in turn orchestrates the adaptive immune response. Several studies have provided evidence that both Th1 and Th2 responses requires ICOS to preferentially stimulates the production of Th2 cytokines IL-4 and IL-10 [195]. In lupus nephritis both early and late blockade of ICOSL improved clinical signs [194]. Traditionally DKD is not considered “immune-mediated” form of kidney disease but recent data from both gene expression and experimental studies supports involvement of many immune system components during DKD progression. In an animal model of DKD, it has been demonstrated that the initial infiltration of T helper cells facilitates the later wave of macrophages and cytotoxic T cell, thereby suggesting a Th1-driven response [196]. We found a number of genes are linked to the signaling pathway of macrophages, fibroblast and endothelial cells in Rheumatoid arthritis. Baricitinib, a selective JAK1/2 inhibitor, demonstrated significant efficacy in the treatment of rheumatoid arthritis. In a phase 2 trial of DKD patients, this drug has demonstrated

significant reduction of albuminuria along with reduction of several inflammatory biomarkers in the plasma and urine. This supports our findings that the signaling pathway in rheumatoid arthritis plays a role in the pathophysiology of DKD. Our subsequent disease and function analysis along with upstream pathway analysis further support that the inflammation pathway is dominant in DKD. We found that injury and tissue abnormalities, and inflammatory response are among the top 10 disease categories and the major upstream regulators were INF- γ and TNF.

Analysis of transcriptional changes helps to understand disease progression, but a critical limitation is it cannot establish a causal relationship between the altered expression of genes and pathophysiological responses [197]. In an order to evaluate the functional significance of these DEG, an unbiased measurement of the association between the clinical and histopathological features of the clinically diagnosed DKD patients was undertaken. Our correlation density analysis with the clinical parameters demonstrated that the gene sets collectively shifted the Pearson's correlation curve left indicating a negative effect on eGFR. Some of the genes that showed strong correlation with eGFR included WFDC2, PAPP2, ADAM28 and RGS10 and they were previously associated with kidney disease. WFDC2 encodes a protein with a highly conserved whey acidic protein domain (WAP) – which is a known biomarker for ovarian carcinoma. and the WFDC2 protein was identified in tumor tissue, urine and serum. In a mouse model of acute kidney fibrosis, it has been shown that WFDC2 expression is high and correlated with tubulointerstitial fibrosis. High expression of WFDC2 has been reported in kidney biopsies of CKD patients [198]. We report for the first time reported its negative association with eGFR and also show a strong correlation with interstitial fibrosis in DKD patients. Similarly, macrophage gene MSR1 codes for a multifunctional scavenger receptor. Genetic deletion of MSR1 has been shown to be protective in streptozotocin induced mouse DKD by inhibiting the macrophage migration into the kidney [199]. Our analysis demonstrated MSR1 had a strong negative correlation with eGFR and positive correlation with interstitial fibrosis. In addition, we found both LCN2 and Sox9, two well-known markers for tubular injury strongly correlated with interstitial fibrosis. This type of corroborating evidence validates our method. Correlation analysis between structural features derived from whole slide images of tissue samples and gene expression data has been used to identify many biological pathways that are strongly associated with cancer [200, 201]. Our initial analysis also found some new as well as some known genes that strongly correlated with the DKD phenotype.

Using our gene expression to phenotype correlation model, we showed that the gene expression signature well correlated with some of the hallmark features of the DKD such as eGFR, interstitial fibrosis or mesangial matrix. Cancer gene signatures have been used to predict radiation response [201]. Similarly, mouse CKD studies have shown a unique molecular signature that recapitulates pathophysiological mechanisms of CKD and human orthologs of the mouse genes can be used to predict eGFR in humans at various stages of CKD [202]. We tried similar approach to predict the translatability of our PDE1 animal study to human DKD. We first validated our approach using gene expression database from untreated and lisinopril treated AAV renin overexpressed dbdb uninephrectomized mice [190]. DEG analysis of the microarray data showed 800 genes modulated in this disease model. When we analyze the data in our unbiased statistical model it demonstrated a similar pattern in the correlation density analysis as seen with human DEGs. For instance, the mouse molecular pattern showed a strong negative correlation with eGFR and positive correlation with interstitial fibrosis, mesangial matrix and some other features of human DKD histopathology. The lisinopril treated mice gene expression data shifted the curve more to the neutral position as seen in the normal humans. The dbdb AAV-renin model has been shown to have many physiological features of advanced human DKD like robust proteinuria, reduced GFR, and increased serum creatinine and lisinopril has been shown to be beneficial in this model [97, 190]. Moreover, lisinopril and related drugs are widely used as standard of care in the clinic for DKD patients. This analysis provides some validation of our model for translatability of mouse to human. Importantly, the DEGS from the PDE1 treated dbdb renin AAV DKD model similarly shifted of the disease molecular signature towards normal human, thus suggesting higher potential of renal protection translating to human DKD.

There are some limitations of this study. We have combined both microarray and RNA-seq data sets to do our analysis which might have resulted in loss of a few genes. RNA-Seq and microarray are the most commonly used high-throughput technologies for transcriptome profiling, each with their own inherent strengths and limitations. However Chen et al. reported that for most transcripts within the same tissue, the results obtained by RNAseq and microarrays were highly reproducible [203]. The other potential limitation is that we did not demonstrate the statistical significance of the relationship for our correlation density measurement. enough statistical power to demonstrate the confidence of the correlation density data. The patient cohort used in this study did not have large number of samples. Moreover, there was no simulation run with the correlation coefficient

to determine the significance of this relationship. More study is needed to determine the significance of this finding. At this stage our efforts should be deemed exploratory and require further refinement.

In summary we have found a consensus set of renal DEGS in multiple DKD patient cohorts and demonstrated that the expression signature is associated with inflammation and immune response. We also developed a molecular phenotype model to show that the renal gene expression signature strongly correlated with the histopathological and clinical features of DKD patients. The trend to normal human gene expression in in lisinopril treated DKD mice, suggested that this model has the potential to predict the progression of human kidney disease and thus estimate the likely the outcome for novel therapeutics.

CHAPTER 5. GENERAL CONCLUSION

By 2035 it has been estimated that the number of diabetic patients worldwide will reach about 593 million and with a $\frac{1}{4}$ of them progressing to the end stage renal disease and it is conceivable that a major medical and economic burden of DKD will occur in the future. In clinic, the treatment of diabetic kidney disease (DKD) is still mainly based on control of hyperglycemia and blood pressure, as there is no other validated and novel therapies able to halt the progression of renal failure. Several clinical trials controlling both blood pressure and/or hyperglycemia already established modest renal protection, however these approaches are not enough to stop the progression of DKD. The role of intensive glycemetic control in treating DKD is controversial. Two large observational trials, Diabetes Control and Complications Trial (DCCT) in T1DM and the United Kingdom Prospective Diabetes Study (UKPDS) could not provide a clear-cut HbA1c threshold in T2D patients, only further confirming that there is a strong relationship between glucose control and the risk of the development of diabetic microvascular complications. A more sophisticated designed trial called ADVANCE, included patients with a high HbA1C levels, but it also demonstrated no significant relationship between renal protection in T2D patients with HbA1C levels of 6.5% [204]. Moreover, the imprecision of HbA1C measurements and undesirable pharmacokinetics of some recent promising antidiabetic drugs, makes their use in glycemetic management in patients with DKD complicated. Despite the success with an SGLT2 inhibitor in slowing DKD, the trial indicates the limitations their use in renal impaired patients due to hypovolemia, ketoacidosis and hyperkalemia as issued by the FDA [205].

The mechanisms responsible for the development and progression of DKD remain incompletely understood. In the past several years there has been tremendous advancement in understanding several downstream signaling pathways that are triggered by the interplay of hemodynamic and metabolic factors of T2D. Chronic hemodynamic and metabolic changes as a result of prolonged exposure to systemic risk factors like high glucose or overactive RAAS can modulate various intracellular signaling pathways, transcription factors, cytokines, or growth factors that can ultimately promote structural abnormalities in the kidney, such as basement membrane thickening,

podocyte injury, and mesangial matrix expansion, glomerular sclerosis and tubulointerstitial fibrosis all of which associate with declining GFR [2, 10]. Despite some understanding of these signaling pathways causing DKD, it is less clear how risk factors activate of intracellular signaling pathways.

This thesis attempts to establish this connection. We provided a synopsis of how external stimuli activate cell surface receptors, generating secondary signals inside the cell to alter TRPC calcium channel function, calcium sensitive PDE1 and the downstream cyclic nucleotides that affect the progression of DKD. In our first chapter we used a potent and selective PDE1 inhibitor to address its hemodynamic properties and its potential to protect diabetic nephropathy. The vasodilatory properties of PDE1 inhibition has been featured in many publications but its effect on systemic hemodynamics has not been reported until very recently [50-52, 55, 101, 103]. Using a potent pan PDE1 inhibitor we have demonstrated vasodilation in vivo by adopting a novel technique using elevated ear temperature as surrogate marker for peripheral vasodilation which resulted in lowering of blood pressure in both normotensive and hypertensive rats. This prompted us to investigate PDE1 inhibitor's role in the context of renal disease as anti-hypertensive drugs have shown to be reno-protective. Moreover, PDE1 is highly expressed in both glomeruli and tubule [58] and preservation of cyclic nucleotide has been found beneficial for kidney [23, 43, 93], suggestion a direct renal protective role as well. Indeed, we demonstrated for the first time that PDE1 inhibition leads to the renal benefit using a rodent model of DKD as evident by lowering of ACR, serum creatinine and several urinary biomarkers of kidney injury. The histopathological improvements due to PDE1 inhibition were associated with and likely driven by inhibition of inflammation and fibrosis pathways. Using gene expression analysis of CKD patients, we identified TRPC6 as major calcium channel that is upregulated in the glomeruli and, using human primary mesangial cell and rat isolated glomeruli, we have shown that induction of TRPC6 activity leads to apoptosis in PDE1 dependent manner. In next section we asked the question of how TRPC6 gets activated in the diabetic environment, that is to focus on the upstream signaling pathway.

In the second chapter we have elucidated certain aspects of upstream activation of TRPC6 in a context of metabolic disturbances. Elevated level of calcium, DAG and ROS are all thought to

contribute to the pathogenesis of DKD. Elevated levels of angiotensin II and ET-1 in diabetic patients is known [[206]63]. Both can contribute to the activation of TRPC6. Our studies for the first time connected the diabetic risk factors with activation of TRPC6 and demonstrated a crosstalk between two second messengers, calcium and cyclic nucleotides. In connection to our earlier pre-clinical finding of renal benefit upon PDE1 inhibition, here we provided mechanistic evidence of activation of PDE1 by the systemic risk factors that involves TRPC6. One of the limitations of this study is the lack of either pharmacological or genetic evidence of involvement of PDE1 in the depletion of cAMP. Although we showed that hyperforin mediated increase in calcium is TRPC6 specific, the depletion of cAMP could be due to non-specific action of hyperforin. Further studies are required to show the specificity of hyperforin 9 with selective inhibitors of TRPC6. The lack of reliable cGMP biosensor also precluded us from investigation of potential mechanistic link between TRPC6, PDE1, and cGMP. More research is needed to interrogate this pathway. However, our data still provide sufficient evidence of a crosstalk between TRPC6 and PDE1 and their potential role in pathogenesis of DKD.

In this context of pathophysiology of DKD it is not surprising to see that the successful drugs in DKD are those that interfere with inflammation, fibrosis and hemodynamic pathways. Both canagliflozin (SGLT2 inhibitor) and atrasentan (ETA receptor antagonist) demonstrated their renoprotective effects in large clinical trials that were associated with lowering of systolic and diastolic blood pressures [13, 90]. Moreover, ET-1 has been linked with renal inflammation and ETA receptor blocker showed reduction of proteinuria by reducing inflammation. In this regard PDE1 inhibition seems to be an ideal candidate to treat DKD as it demonstrated its vasodilatory and anti-inflammatory and anti-apoptotic features in a pre-clinical model of DKD. The dbdb renin AAV model of diabetic nephropathy has been shown to demonstrate several human DKD features [97, 190], however translation of these results to human DKD remains to be determined. To tackle this translation problem, we utilized computational biology, analyzed gene expression data of DKD patients and correlated it with clinical parameters and renal histopathology of DKD patients to develop a predictive model.

Thus, the focus of the third chapter was to correlate human kidney gene expression to physiological and histopathology phenotypes and develop a statistical model to assess the preclinical DKD

treatments outcomes on gene expression with that observed in humans. While DKD is not regarded as a exclusive form of “immune-mediated” kidney disease, recent gene expression data from DKD patients and several preclinical data supports involvement of many immune system components in DKD progression. Our findings in DKD2000 gene pathway and disease analysis is in line with recent reports [207]. Our gene expression to phenotype model showed that the gene signature strongly correlates with the histopathological and clinical features of DKD patients. Using the gene expression data set from untreated and lisinopril treated mice with DKD, showed a high level of correlation with normal and diseased human DKD. This model could be used to predict the human outcome since the murine gene expression changes with the PDE1 inhibitor overlapped with the human data set.

Overall the contents of this thesis demonstrated a new unique biology connecting calcium and cyclic nucleotides, the two important intracellular messengers in the progression of DKD. In addition, an exploratory effort using bioinformatics provided some evidence of the clinical relevance of our findings.

REFERENCES

1. Thomas, M.C., et al., *Diabetic kidney disease*. Nat Rev Dis Primers, 2015. **1**: p. 15018.
2. Reidy, K., et al., *Molecular mechanisms of diabetic kidney disease*. The Journal of clinical investigation, 2014. **124**(6): p. 2333-2340.
3. Thomas, B., *The Global Burden of Diabetic Kidney Disease: Time Trends and Gender Gaps*. Curr Diab Rep, 2019. **19**(4): p. 18.
4. Duru, O.K., et al., *The Landscape of Diabetic Kidney Disease in the United States*. Curr Diab Rep, 2018. **18**(3): p. 14.
5. Kshirsagar, A.V., et al., *Effect of ACE inhibitors in diabetic and nondiabetic chronic renal disease: a systematic overview of randomized placebo-controlled trials*. Am J Kidney Dis, 2000. **35**(4): p. 695-707.
6. Zoungas, S., et al., *Combined effects of routine blood pressure lowering and intensive glucose control on macrovascular and microvascular outcomes in patients with type 2 diabetes: New results from the ADVANCE trial*. Diabetes Care, 2009. **32**(11): p. 2068-74.
7. Holman, R.R., et al., *10-year follow-up of intensive glucose control in type 2 diabetes*. N Engl J Med, 2008. **359**(15): p. 1577-89.
8. Holman, R.R., et al., *Long-term follow-up after tight control of blood pressure in type 2 diabetes*. N Engl J Med, 2008. **359**(15): p. 1565-76.
9. Tewson, P.H., et al., *New DAG and cAMP Sensors Optimized for Live-Cell Assays in Automated Laboratories*. Journal of biomolecular screening, 2016. **21**(3): p. 298-305.
10. Cooper, M.E., *Interaction of metabolic and haemodynamic factors in mediating experimental diabetic nephropathy*. Diabetologia, 2001. **44**(11): p. 1957-72.
11. Singh, R., et al., *Role of angiotensin II in glucose-induced inhibition of mesangial matrix degradation*. Diabetes, 1999. **48**(10): p. 2066-73.
12. Schrier, R.W. and H. Holzgreve, *Hemodynamic factors in the pathogenesis of diabetic nephropathy*. Klin Wochenschr, 1988. **66**(8): p. 325-31.
13. Heerspink, H.J.L., et al., *Atrasentan and renal events in patients with type 2 diabetes and chronic kidney disease (SONAR): a double-blind, randomised, placebo-controlled trial*. Lancet, 2019. **393**(10184): p. 1937-1947.
14. Judge, P., et al., *Neprilysin inhibition in chronic kidney disease*. Nephrology, dialysis, transplantation : official publication of the European Dialysis and Transplant Association - European Renal Association, 2015. **30**(5): p. 738-743.
15. Brownlee, M., *Biochemistry and molecular cell biology of diabetic complications*. Nature, 2001. **414**(6865): p. 813-20.
16. Hanssen, N.M.J., C.D.A. Stehouwer, and C.G. Schalkwijk, *Methylglyoxal stress, the glyoxalase system, and diabetic chronic kidney disease*. Curr Opin Nephrol Hypertens, 2019. **28**(1): p. 26-33.

17. Zhang, G., M. Darshi, and K. Sharma, *The Warburg Effect in Diabetic Kidney Disease*. Seminars in Nephrology, 2018. **38**(2): p. 111-120.
18. Toth-Manikowski, S. and M.G. Atta, *Diabetic Kidney Disease: Pathophysiology and Therapeutic Targets*. Journal of diabetes research, 2015. **2015**: p. 697010-697010.
19. Ruan, X. and W.J. Arendshorst, *Role of protein kinase C in angiotensin II-induced renal vasoconstriction in genetically hypertensive rats*. Am J Physiol, 1996. **270**(6 Pt 2): p. F945-52.
20. Ponchiardi, C., M. Mauer, and B. Najafian, *Temporal Profile of Diabetic Nephropathy Pathologic Changes*. Current Diabetes Reports, 2013. **13**(4): p. 592-599.
21. Nath, K.A., *Tubulointerstitial changes as a major determinant in the progression of renal damage*. Am J Kidney Dis, 1992. **20**(1): p. 1-17.
22. Newton, A.C., M.D. Bootman, and J.D. Scott, *Second Messengers*. Cold Spring Harbor perspectives in biology, 2016. **8**(8): p. a005926.
23. Dousa, T.P., *Cyclic-3',5'-nucleotide phosphodiesterase isozymes in cell biology and pathophysiology of the kidney*. Kidney Int, 1999. **55**(1): p. 29-62.
24. Schinner, E., V. Wetzl, and J. Schlossmann, *Cyclic nucleotide signalling in kidney fibrosis*. Int J Mol Sci, 2015. **16**(2): p. 2320-51.
25. Ott, I.M., et al., *Effects of Stimulation of Soluble Guanylate Cyclase on Diabetic Nephropathy in Diabetic eNOS Knockout Mice on Top of Angiotensin II Receptor Blockade*. PLOS ONE, 2012. **7**(8): p. e42623.
26. Geschka, S., et al., *Soluble Guanylate Cyclase Stimulation Prevents Fibrotic Tissue Remodeling and Improves Survival in Salt-Sensitive Dahl Rats*. PLOS ONE, 2011. **6**(7): p. e21853.
27. Kalk, P., et al., *NO-independent activation of soluble guanylate cyclase prevents disease progression in rats with 5/6 nephrectomy*. British Journal of Pharmacology, 2006. **148**(6): p. 853-859.
28. Cui, W., et al., *Increasing cGMP-dependent protein kinase activity attenuates unilateral ureteral obstruction-induced renal fibrosis*. American journal of physiology. Renal physiology, 2014. **306**(9): p. F996-F1007.
29. Rodraguez-Iturbe, B., et al., *Early treatment with cGMP phosphodiesterase inhibitor ameliorates progression of renal damage*. Kidney International, 2005. **68**(5): p. 2131-2142.
30. Guzeloglu, M., et al., *The beneficial effects of tadalafil on renal ischemia-reperfusion injury in rats*. Urol Int, 2011. **86**(2): p. 197-203.
31. Sohotnik, R., et al., *Phosphodiesterase-5 inhibition attenuates early renal ischemia-reperfusion-induced acute kidney injury: assessment by quantitative measurement of urinary NGAL and KIM-1*. Am J Physiol Renal Physiol, 2013. **304**(8): p. F1099-104.
32. Tikoo, K., et al., *Calorie restriction mimicking effects of roflumilast prevents diabetic nephropathy*. Biochem Biophys Res Commun, 2014. **450**(4): p. 1581-6.

33. He, T. and M.E. Cooper, *Renoprotective effects of pentoxifylline in the PREDIAN trial*. Nature Reviews Nephrology, 2014. **10**: p. 547.
34. Francis, S.H., I.V. Turko, and J.D. Corbin, *Cyclic nucleotide phosphodiesterases: relating structure and function*. Prog Nucleic Acid Res Mol Biol, 2001. **65**: p. 1-52.
35. Cheng, J. and J.P. Grande, *Cyclic nucleotide phosphodiesterase (PDE) inhibitors: novel therapeutic agents for progressive renal disease*. Exp Biol Med (Maywood), 2007. **232**(1): p. 38-51.
36. Kukovetz, W.R. and G. Poch, *Inhibition of cyclic-3',5'-nucleotide-phosphodiesterase as a possible mode of action of papaverine and similarly acting drugs*. Naunyn Schmiedebergs Arch Pharmacol, 1970. **267**(2): p. 189-94.
37. Lugnier, C., et al., *Selective inhibition of cyclic nucleotide phosphodiesterases of human, bovine and rat aorta*. Biochem Pharmacol, 1986. **35**(10): p. 1743-51.
38. Komasa, N., et al., *Characterisation of cyclic nucleotide phosphodiesterases from rat mesenteric artery*. Eur J Pharmacol, 1991. **208**(1): p. 85-7.
39. Jackson, E.K., et al., *Phosphodiesterases in the rat renal vasculature*. J Cardiovasc Pharmacol, 1997. **30**(6): p. 798-801.
40. Thomas, N.J., et al., *Chronic type IV phosphodiesterase inhibition protects glomerular filtration rate and renal and mesenteric blood flow in a zymosan-induced model of multiple organ dysfunction syndrome treated with norepinephrine*. J Pharmacol Exp Ther, 2001. **296**(1): p. 168-74.
41. Martin, W., et al., *Phosphodiesterase inhibitors induce endothelium-dependent relaxation of rat and rabbit aorta by potentiating the effects of spontaneously released endothelium-derived relaxing factor*. J Pharmacol Exp Ther, 1986. **237**(2): p. 539-47.
42. Sohotnik, R., et al., *Phosphodiesterase5 Inhibition Attenuates Early Renal Ischemia/Reperfusion-Induced Acute Kidney Injury: Assessment by measurement of urinary NGAL and KIM-1*. American journal of physiology. Renal physiology, 2013. **304**.
43. Afsar, B., et al., *Phosphodiesterase type 5 inhibitors and kidney disease*. Int Urol Nephrol, 2015. **47**(9): p. 1521-8.
44. Chini, C.C.S., et al., *Compartmentalization of cAMP Signaling in Mesangial Cells by Phosphodiesterase Isozymes PDE3 and PDE4 REGULATION OF SUPEROXIDATION AND MITOGENESIS*. Journal of Biological Chemistry, 1997. **272**(15): p. 9854-9859.
45. Schinner, E., V. Wetzl, and J. Schlossmann, *Cyclic Nucleotide Signalling in Kidney Fibrosis*. International Journal of Molecular Sciences, 2015. **16**: p. 2320-2351.
46. Tapia, E., et al., *Sildenafil Treatment Prevents Glomerular Hypertension and Hyperfiltration in Rats with Renal Ablation*. Kidney and Blood Pressure Research, 2012. **35**(4): p. 273-280.
47. Beavo, J.A., *Cyclic nucleotide phosphodiesterases: functional implications of multiple isoforms*. Physiol Rev, 1995. **75**(4): p. 725-48.

48. Sonnenburg, W.K., et al., *Identification, quantitation, and cellular localization of PDE1 calmodulin-stimulated cyclic nucleotide phosphodiesterases*. *Methods*, 1998. **14**(1): p. 3-19.
49. Giachini, F.R., et al., *Decreased cGMP level contributes to increased contraction in arteries from hypertensive rats: role of phosphodiesterase 1*. *Hypertension*, 2011. **57**(3): p. 655-63.
50. Goraya, T.A. and D.M. Cooper, *Ca²⁺-calmodulin-dependent phosphodiesterase (PDE1): current perspectives*. *Cell Signal*, 2005. **17**(7): p. 789-97.
51. Khammy, M.M., et al., *PDE1A inhibition elicits cGMP-dependent relaxation of rat mesenteric arteries*. *Br J Pharmacol*, 2017. **174**(22): p. 4186-4198.
52. Laursen, M., et al., *Novel selective PDE type 1 inhibitors cause vasodilatation and lower blood pressure in rats*. *Br J Pharmacol*, 2017. **174**(15): p. 2563-2575.
53. Miller, C.L., et al., *Cyclic nucleotide phosphodiesterase 1A: a key regulator of cardiac fibroblast activation and extracellular matrix remodeling in the heart*. *Basic research in cardiology*, 2011. **106**(6): p. 1023-1039.
54. Knight, W.E., et al., *PDE1C deficiency antagonizes pathological cardiac remodeling and dysfunction*. *Proc Natl Acad Sci U S A*, 2016. **113**(45): p. E7116-E7125.
55. Nagel, D.J., et al., *Role of nuclear Ca²⁺/calmodulin-stimulated phosphodiesterase 1A in vascular smooth muscle cell growth and survival*. *Circ Res*, 2006. **98**(6): p. 777-84.
56. Murray, F., et al., *Expression and activity of cAMP phosphodiesterase isoforms in pulmonary artery smooth muscle cells from patients with pulmonary hypertension: role for PDE1*. *Am J Physiol Lung Cell Mol Physiol*, 2007. **292**(1): p. L294-303.
57. Gretchen L. Snyder, S.D., Jennifer L. O'Brien, Stephanie Cruz, Yuan Tian, Joseph P. Hendrick, Lawrence P. Wennogle, Robert E. Davis, *SUPPRESSION OF CNS INFLAMMATION BY PHOSPHODIESTERASE-1 (PDE1) INHIBITORS: TOWARD NEW TREATMENTS FOR NEURODEGENERATIVE DISEASES*. Poster, 2018.
58. 18.1, H.P.A.v. 2018 July 7,2019]; Available from: www.proteinatlas.org.
59. Berridge, M.J., *Calcium signal transduction and cellular control mechanisms*. *Biochim Biophys Acta*, 2004. **1742**(1-3): p. 3-7.
60. Clapham, D.E., *Calcium signaling*. *Cell*, 2007. **131**(6): p. 1047-58.
61. Mears, D., *Regulation of insulin secretion in islets of Langerhans by Ca(2+)channels*. *J Membr Biol*, 2004. **200**(2): p. 57-66.
62. Draznin, B., *Cytosolic calcium: a new factor in insulin resistance?* *Diabetes Res Clin Pract*, 1991. **11**(3): p. 141-5.
63. Becerra-Tomás, N., et al., *Increased Serum Calcium Levels and Risk of Type 2 Diabetes in Individuals at High Cardiovascular Risk*. *Diabetes Care*, 2014. **37**(11): p. 3084-3091.
64. Levy, J., et al., *Plasma calcium and phosphate levels in an adult noninsulin-dependent diabetic population*. *Calcified Tissue International*, 1986. **39**(5): p. 316-318.

65. Sorva, A. and R.S. Tilvis, *Low Serum Ionized to Total Calcium Ratio: Association with Geriatric Diabetes mellitus and with Other Cardiovascular Risk Factors?* Gerontology, 1990. **36**(4): p. 212-216.
66. Zhou, Y. and A. Greka, *Calcium-permeable ion channels in the kidney.* American journal of physiology. Renal physiology, 2016. **310**(11): p. F1157-F1167.
67. Clapham, D.E., *TRP channels as cellular sensors.* Nature, 2003. **426**(6966): p. 517-24.
68. Winn, M.P., et al., *A mutation in the TRPC6 cation channel causes familial focal segmental glomerulosclerosis.* Science, 2005. **308**(5729): p. 1801-4.
69. Krall, P., et al., *Podocyte-specific overexpression of wild type or mutant trpc6 in mice is sufficient to cause glomerular disease.* PloS one, 2010. **5**(9): p. e12859-e12859.
70. Wang, L., et al., *Gq signaling causes glomerular injury by activating TRPC6.* J Clin Invest, 2015. **125**(5): p. 1913-26.
71. Kitada, M., et al., *Molecular mechanisms of diabetic vascular complications.* Journal of diabetes investigation, 2010. **1**(3): p. 77-89.
72. Schneider, J.G., et al., *Elevated plasma endothelin-1 levels in diabetes mellitus.* Am J Hypertens, 2002. **15**(11): p. 967-72.
73. Chawla, T., D. Sharma, and A. Singh, *Role of the renin angiotensin system in diabetic nephropathy.* World journal of diabetes, 2010. **1**(5): p. 141-145.
74. Schoenberger, S.D., et al., *Increased Prostaglandin E2 (PGE2) Levels in Proliferative Diabetic Retinopathy, and Correlation with VEGF and Inflammatory Cytokines.* Investigative Ophthalmology & Visual Science, 2012. **53**(9): p. 5906-5911.
75. Staruschenko, A., D. Spires, and O. Palygin, *Role of TRPC6 in Progression of Diabetic Kidney Disease.* Curr Hypertens Rep, 2019. **21**(7): p. 48.
76. Sonneveld, R., et al., *Glucose specifically regulates TRPC6 expression in the podocyte in an AngII-dependent manner.* Am J Pathol, 2014. **184**(6): p. 1715-26.
77. Wang, L., et al., *Knockout of TRPC6 promotes insulin resistance and exacerbates glomerular injury in Akita mice.* Kidney Int, 2019. **95**(2): p. 321-332.
78. Schlondorff, J., et al., *TRPC6 mutations associated with focal segmental glomerulosclerosis cause constitutive activation of NFAT-dependent transcription.* Am J Physiol Cell Physiol, 2009. **296**(3): p. C558-69.
79. Nijenhuis, T., et al., *Angiotensin II contributes to podocyte injury by increasing TRPC6 expression via an NFAT-mediated positive feedback signaling pathway.* Am J Pathol, 2011. **179**(4): p. 1719-32.
80. Liu, D., et al., *High glucose enhances transient receptor potential channel canonical type 6-dependent calcium influx in human platelets via phosphatidylinositol 3-kinase-dependent pathway.* Arterioscler Thromb Vasc Biol, 2008. **28**(4): p. 746-51.
81. Wang, L., et al., *Calcineurin (CN) activation promotes apoptosis of glomerular podocytes both in vitro and in vivo.* Mol Endocrinol, 2011. **25**(8): p. 1376-86.

82. Woroniecka, K.I., et al., *Transcriptome Analysis of Human Diabetic Kidney Disease*. *Diabetes*, 2011. **60**(9): p. 2354-2369.
83. Schmid, H., et al., *Modular activation of nuclear factor-kappaB transcriptional programs in human diabetic nephropathy*. *Diabetes*, 2006. **55**(11): p. 2993-3003.
84. Berthier, C.C., et al., *Enhanced expression of Janus kinase-signal transducer and activator of transcription pathway members in human diabetic nephropathy*. *Diabetes*, 2009. **58**(2): p. 469-77.
85. Nair, V., et al., *A molecular morphometric approach to diabetic kidney disease can link structure to function and outcome*. *Kidney Int*, 2018. **93**(2): p. 439-449.
86. Beckerman, P., et al., *Human Kidney Tubule-Specific Gene Expression Based Dissection of Chronic Kidney Disease Traits*. *EBioMedicine*, 2017. **24**: p. 267-276.
87. Dousa, T.P., *Cyclic Nucleotide Phosphodiesterases: New Role in the Pathogenesis of Glomerulonephritis?* *News Physiol Sci*, 1998. **13**: p. 51-52.
88. Zhang, Y., et al., *Multiprotein Complex With TRPC (Transient Receptor Potential-Canonical) Channel, PDE1C (Phosphodiesterase 1C), and A2R (Adenosine A2 Receptor) Plays a Critical Role in Regulating Cardiomyocyte cAMP and Survival*. *Circulation*, 2018. **138**(18): p. 1988-2002.
89. Soldatos, G. and M.E. Cooper, *Diabetic nephropathy: important pathophysiologic mechanisms*. *Diabetes Res Clin Pract*, 2008. **82 Suppl 1**: p. S75-9.
90. Minze, M.G., et al., *Benefits of SGLT2 Inhibitors Beyond Glycemic Control - A Focus on Metabolic, Cardiovascular and Renal Outcomes*. *Curr Diabetes Rev*, 2018. **14**(6): p. 509-517.
91. Cheng, J., et al., *Differential regulation of mesangial cell mitogenesis by cAMP phosphodiesterase isozymes 3 and 4*. *Am J Physiol Renal Physiol*, 2004. **287**(5): p. F940-53.
92. Cheng, J., et al., *TGF-beta1 stimulates monocyte chemoattractant protein-1 expression in mesangial cells through a phosphodiesterase isoenzyme 4-dependent process*. *Am J Physiol Cell Physiol*, 2005. **289**(4): p. C959-70.
93. Scheele, W., et al. *Phosphodiesterase Type 5 Inhibition Reduces Albuminuria in Subjects with Overt Diabetic Nephropathy*. *J Am Soc Nephrol* 2016 Nov [cited 27 11]; 2016/11/02:[3459-3468].
94. Tang, W.H., et al., *Cilostazol effectively attenuates deterioration of albuminuria in patients with type 2 diabetes: a randomized, placebo-controlled trial*. *Endocrine*, 2014. **45**(2): p. 293-301.
95. Hou, X., et al., *Transient receptor potential channel 6 knockdown prevents apoptosis of renal tubular epithelial cells upon oxidative stress via autophagy activation*. *Cell Death & Disease*, 2018. **9**(10): p. 1015.

96. Harlan, S., et al., *Viral transduction of renin rapidly establishes persistent hypertension in diverse murine strains*. American journal of physiology. Regulatory, integrative and comparative physiology, 2015. **309**: p. ajpregu.00106.2015.
97. Harlan, S.M., et al., *Progressive Renal Disease Established by Renin-Coding Adeno-Associated Virus-Driven Hypertension in Diverse Diabetic Models*. Journal of the American Society of Nephrology : JASN, 2018. **29**(2): p. 477-491.
98. Tragante, V., et al., *Gene-centric meta-analysis in 87,736 individuals of European ancestry identifies multiple blood-pressure-related loci*. Am J Hum Genet, 2014. **94**(3): p. 349-60.
99. Pollock, J.D. and A.N. Makaryus, *Physiology, Cardiovascular Hemodynamics*, in *StatPearls*. 2019: Treasure Island (FL).
100. Secomb, T.W., *Hemodynamics*. Compr Physiol, 2016. **6**(2): p. 975-1003.
101. Schermuly, R.T., et al., *Phosphodiesterase 1 upregulation in pulmonary arterial hypertension: target for reverse-remodeling therapy*. Circulation, 2007. **115**(17): p. 2331-9.
102. Bender, A.T. and J.A. Beavo, *Cyclic nucleotide phosphodiesterases: molecular regulation to clinical use*. Pharmacol Rev, 2006. **58**(3): p. 488-520.
103. Rybalkin, S.D., et al., *Cyclic nucleotide phosphodiesterase 1C promotes human arterial smooth muscle cell proliferation*. Circ Res, 2002. **90**(2): p. 151-7.
104. Cheng, K., et al., *Antagonism of the prostaglandin D2 receptor 1 suppresses nicotinic acid-induced vasodilation in mice and humans*. Proc Natl Acad Sci U S A, 2006. **103**(17): p. 6682-7.
105. Martyn-St James, M., et al., *Phosphodiesterase Type 5 Inhibitors for Premature Ejaculation: A Systematic Review and Meta-analysis*. European urology focus, 2017. **3**(1): p. 119-129.
106. Kamanna, V.S., S.H. Ganji, and M.L. Kashyap, *The mechanism and mitigation of niacin-induced flushing*. International journal of clinical practice, 2009. **63**(9): p. 1369-1377.
107. Stubbs, C., et al., *Do SSRIs and SNRIs reduce the frequency and/or severity of hot flashes in menopausal women*. The Journal of the Oklahoma State Medical Association, 2017. **110**(5): p. 272-274.
108. Johnson, J.M., C.T. Minson, and D.L. Kellogg, Jr., *Cutaneous vasodilator and vasoconstrictor mechanisms in temperature regulation*. Compr Physiol, 2014. **4**(1): p. 33-89.
109. Walløe, L., *Arterio-venous anastomoses in the human skin and their role in temperature control*. Temperature (Austin, Tex.), 2015. **3**(1): p. 92-103.
110. Gorgas, K., et al., *The fine structure of human digital arterio-venous anastomoses (Hoyer-Grosser's organs)*. Anatomy and Embryology, 1977. **150**(3): p. 269-289.
111. Gemmell, R.T. and J.R. Hales, *Cutaneous arteriovenous anastomoses present in the tail but absent from the ear of the rat*. Journal of anatomy, 1977. **124**(Pt 2): p. 355-358.

112. Alvarez, E., et al., *Testosterone and cholesterol vasodilation of rat aorta involves L-type calcium channel inhibition*. *Adv Pharmacol Sci*, 2010. **2010**: p. 534184.
113. Vincent, J.-L., *Understanding cardiac output*. *Critical care (London, England)*, 2008. **12**(4): p. 174-174.
114. Vemulapalli, S., et al., *Antiplatelet and antiproliferative effects of SCH 51866, a novel type 1 and type 5 phosphodiesterase inhibitor*. *J Cardiovasc Pharmacol*, 1996. **28**(6): p. 862-9.
115. Alexander, S.P., et al., *The Concise Guide to PHARMACOLOGY 2015/16: G protein-coupled receptors*. *Br J Pharmacol*, 2015. **172**(24): p. 5744-869.
116. Sasaki, T., J. Kotera, and K. Omori, *Transcriptional activation of phosphodiesterase 7B1 by dopamine D1 receptor stimulation through the cyclic AMP/cyclic AMP-dependent protein kinase/cyclic AMP-response element binding protein pathway in primary striatal neurons*. *J Neurochem*, 2004. **89**(2): p. 474-83.
117. Wu, S.N., H.F. Li, and H.T. Chiang, *Vincocetine-induced stimulation of calcium-activated potassium currents in rat pituitary GH3 cells*. *Biochem Pharmacol*, 2001. **61**(7): p. 877-92.
118. Jeon, K.I., et al., *Vincocetine inhibits NF-kappaB-dependent inflammation via an IKK-dependent but PDE-independent mechanism*. *Proc Natl Acad Sci U S A*, 2010. **107**(21): p. 9795-800.
119. Lukyanenko, Y.O., et al., *Ca(2+)/calmodulin-activated phosphodiesterase 1A is highly expressed in rabbit cardiac sinoatrial nodal cells and regulates pacemaker function*. *J Mol Cell Cardiol*, 2016. **98**: p. 73-82.
120. Maurice, D.H., et al., *Advances in targeting cyclic nucleotide phosphodiesterases*. *Nat Rev Drug Discov*, 2014. **13**(4): p. 290-314.
121. Pinterova, M., J. Kunes, and J. Zicha, *Altered neural and vascular mechanisms in hypertension*. *Physiol Res*, 2011. **60**(3): p. 381-402.
122. Hashimoto, T., et al., *Acute Enhancement of Cardiac Function by Phosphodiesterase Type 1 Inhibition*. *Circulation*, 2018. **138**(18): p. 1974-1987.
123. Lanfranchi, P.A. and V.K. Somers, *Arterial baroreflex function and cardiovascular variability: interactions and implications*. *Am J Physiol Regul Integr Comp Physiol*, 2002. **283**(4): p. R815-26.
124. Pettinger, W.A. and H.C. Mitchell, *Side effects of vasodilator therapy*. *Hypertension*, 1988. **11**(3 Pt 2): p. II34-6.
125. Shankar, A. and S. Teppala, *Relationship between serum cystatin C and hypertension among US adults without clinically recognized chronic kidney disease*. *J Am Soc Hypertens*, 2011. **5**(5): p. 378-84.
126. Vääräniemi, K., et al., *Lower Glomerular Filtration Rate Is Associated With Higher Systemic Vascular Resistance in Patients Without Prevalent Kidney Disease*. *The Journal of Clinical Hypertension*, 2014. **16**(10): p. 722-728.

127. Massry, S.G. and M. Smogorzewski, *Role of elevated cytosolic calcium in the pathogenesis of complications in diabetes mellitus*. Miner Electrolyte Metab, 1997. **23**(3-6): p. 253-60.
128. Lim, A., *Diabetic nephropathy - complications and treatment*. Int J Nephrol Renovasc Dis, 2014. **7**: p. 361-81.
129. Huang, W., et al., *Genetically increased angiotensin I-converting enzyme level and renal complications in the diabetic mouse*. Proc Natl Acad Sci U S A, 2001. **98**(23): p. 13330-4.
130. Lewis, E.J., et al., *The effect of angiotensin-converting-enzyme inhibition on diabetic nephropathy. The Collaborative Study Group*. N Engl J Med, 1993. **329**(20): p. 1456-62.
131. Lewis, E.J., et al., *Renoprotective effect of the angiotensin-receptor antagonist irbesartan in patients with nephropathy due to type 2 diabetes*. N Engl J Med, 2001. **345**(12): p. 851-60.
132. Brenner, B.M., et al., *Effects of losartan on renal and cardiovascular outcomes in patients with type 2 diabetes and nephropathy*. N Engl J Med, 2001. **345**(12): p. 861-9.
133. Wilmer, W.A., et al., *Remission of nephrotic syndrome in type 1 diabetes: long-term follow-up of patients in the Captopril Study*. Am J Kidney Dis, 1999. **34**(2): p. 308-14.
134. Eijkelkamp, W.B., et al., *Albuminuria is a target for renoprotective therapy independent from blood pressure in patients with type 2 diabetic nephropathy: post hoc analysis from the Reduction of Endpoints in NIDDM with the Angiotensin II Antagonist Losartan (RENAAL) trial*. J Am Soc Nephrol, 2007. **18**(5): p. 1540-6.
135. Ruggenenti, P., et al., *Proteinuria predicts end-stage renal failure in non-diabetic chronic nephropathies. The "Gruppo Italiano di Studi Epidemiologici in Nefrologia" (GISEN)*. Kidney Int Suppl, 1997. **63**: p. S54-7.
136. Wright, J.T., Jr., et al., *Effect of blood pressure lowering and antihypertensive drug class on progression of hypertensive kidney disease: results from the AASK trial*. Jama, 2002. **288**(19): p. 2421-31.
137. Nielsen, S.E., et al., *Neutrophil Gelatinase-Associated Lipocalin (NGAL) and Kidney Injury Molecule 1 (KIM1) in patients with diabetic nephropathy: a cross-sectional study and the effects of lisinopril*. Diabet Med, 2010. **27**(10): p. 1144-50.
138. Papadopoulou-Marketou, N., et al., *NGAL as an Early Predictive Marker of Diabetic Nephropathy in Children and Young Adults with Type 1 Diabetes Mellitus*. Journal of Diabetes Research, 2017. **2017**: p. 7.
139. Velho, G., et al., *Plasma Copeptin, Kidney Outcomes, Ischemic Heart Disease, and All-Cause Mortality in People With Long-standing Type 1 Diabetes*. Diabetes Care, 2016. **39**(12): p. 2288-2295.
140. Nielsen, S.E., et al., *Tubular markers are associated with decline in kidney function in proteinuric type 2 diabetic patients*. Diabetes Res Clin Pract, 2012. **97**(1): p. 71-6.
141. Bolignano, D., et al., *Neutrophil gelatinase-associated lipocalin (NGAL) and progression of chronic kidney disease*. Clin J Am Soc Nephrol, 2009. **4**(2): p. 337-44.

142. Jain, S., et al., *Proteomic analysis of urinary protein markers for accurate prediction of diabetic kidney disorder*. J Assoc Physicians India, 2005. **53**: p. 513-20.
143. Otu, H.H., et al., *Prediction of diabetic nephropathy using urine proteomic profiling 10 years prior to development of nephropathy*. Diabetes Care, 2007. **30**(3): p. 638-43.
144. Dekkers, C.C.J., et al., *Effects of the SGLT-2 inhibitor dapagliflozin on glomerular and tubular injury markers*. Diabetes, obesity & metabolism, 2018. **20**(8): p. 1988-1993.
145. Van Coillie, E., J. Van Damme, and G. Opdenakker, *The MCP/eotaxin subfamily of CC chemokines*. Cytokine Growth Factor Rev, 1999. **10**(1): p. 61-86.
146. Wada, T., et al., *Up-regulation of monocyte chemoattractant protein-1 in tubulointerstitial lesions of human diabetic nephropathy*. Kidney Int, 2000. **58**(4): p. 1492-9.
147. Adela, R. and S.K. Banerjee, *GDF-15 as a Target and Biomarker for Diabetes and Cardiovascular Diseases: A Translational Prospective*. J Diabetes Res, 2015. **2015**: p. 490842.
148. Simonson, M.S., et al., *The renal transcriptome of db/db mice identifies putative urinary biomarker proteins in patients with type 2 diabetes: a pilot study*. Am J Physiol Renal Physiol, 2012. **302**(7): p. F820-9.
149. Kim, M.J. and F.W. Tam, *Urinary monocyte chemoattractant protein-1 in renal disease*. Clin Chim Acta, 2011. **412**(23-24): p. 2022-30.
150. Ju, W., et al., *Tissue transcriptome-driven identification of epidermal growth factor as a chronic kidney disease biomarker*. Science Translational Medicine, 2015. **7**(316): p. 316ra193-316ra193.
151. Chiluita, D., et al., *Gain-of-function mutations in transient receptor potential C6 (TRPC6) activate extracellular signal-regulated kinases 1/2 (ERK1/2)*. J Biol Chem, 2013. **288**(25): p. 18407-20.
152. Soni, H. and A. Adebisi, *TRPC6 channel activation promotes neonatal glomerular mesangial cell apoptosis via calcineurin/NFAT and FasL/Fas signaling pathways*. Scientific reports, 2016. **6**: p. 29041-29041.
153. Hofmann, T., et al., *Direct activation of human TRPC6 and TRPC3 channels by diacylglycerol*. Nature, 1999. **397**(6716): p. 259-63.
154. Vazquez, G., J.Y. Tano, and K. Smedlund, *On the potential role of source and species of diacylglycerol in phospholipase-dependent regulation of TRPC3 channels*. Channels (Austin), 2010. **4**(3): p. 232-40.
155. Erion, D.M. and G.I. Shulman, *Diacylglycerol-mediated insulin resistance*. Nat Med, 2010. **16**(4): p. 400-2.
156. Lastra, G., et al., *Type 2 diabetes mellitus and hypertension: an update*. Endocrinol Metab Clin North Am, 2014. **43**(1): p. 103-22.
157. Fenske, R., et al., *Prostaglandin E2 (PGE2) Levels As a Predictor of Type 2 Diabetes Control in Human Subjects: A cross-sectional view of initial cohort study data*. The FASEB Journal, 2017. **31**(1_supplement): p. 675.6-675.6.

158. Soboloff, J., et al., *Role of endogenous TRPC6 channels in Ca²⁺ signal generation in A7r5 smooth muscle cells*. J Biol Chem, 2005. **280**(48): p. 39786-94.
159. Anderson, M., et al., *Angiotensin II activation of TRPC6 channels in rat podocytes requires generation of reactive oxygen species*. J Cell Physiol, 2014. **229**(4): p. 434-42.
160. Wuensch, T., et al., *High glucose-induced oxidative stress increases transient receptor potential channel expression in human monocytes*. Diabetes, 2010. **59**(4): p. 844-9.
161. Kim, E.Y., M. Anderson, and S.E. Dryer, *Insulin increases surface expression of TRPC6 channels in podocytes: role of NADPH oxidases and reactive oxygen species*. Am J Physiol Renal Physiol, 2012. **302**(3): p. F298-307.
162. Kim, E.Y., M. Anderson, and S.E. Dryer, *Sustained activation of N-methyl-D-aspartate receptors in podocytes leads to oxidative stress, mobilization of transient receptor potential canonical 6 channels, nuclear factor of activated T cells activation, and apoptotic cell death*. Mol Pharmacol, 2012. **82**(4): p. 728-37.
163. Tian, D., et al., *Antagonistic regulation of actin dynamics and cell motility by TRPC5 and TRPC6 channels*. Sci Signal, 2010. **3**(145): p. ra77.
164. Hsu, H.H., et al., *Mechanisms of angiotensin II signaling on cytoskeleton of podocytes*. J Mol Med (Berl), 2008. **86**(12): p. 1379-94.
165. Yang, H., et al., *High glucose-induced apoptosis in cultured podocytes involves TRPC6-dependent calcium entry via the RhoA/ROCK pathway*. Biochem Biophys Res Commun, 2013. **434**(2): p. 394-400.
166. Chiu, R., et al., *The c-Fos protein interacts with c-Jun/AP-1 to stimulate transcription of AP-1 responsive genes*. Cell, 1988. **54**(4): p. 541-52.
167. Shaulian, E. and M. Karin, *AP-1 as a regulator of cell life and death*. Nat Cell Biol, 2002. **4**(5): p. E131-6.
168. Kuwahara, K., et al., *TRPC6 fulfills a calcineurin signaling circuit during pathologic cardiac remodeling*. J Clin Invest, 2006. **116**(12): p. 3114-26.
169. Heiser, J.H., et al., *TRPC6 channel-mediated neurite outgrowth in PC12 cells and hippocampal neurons involves activation of RAS/MEK/ERK, PI3K, and CAMKIV signaling*. J Neurochem, 2013. **127**(3): p. 303-13.
170. Ilatovskaya, D.V., et al., *Angiotensin II has acute effects on TRPC6 channels in podocytes of freshly isolated glomeruli*. Kidney Int, 2014. **86**(3): p. 506-14.
171. Eder, P. and J.D. Molkentin, *TRPC Channels As Effectors of Cardiac Hypertrophy*. Circulation Research, 2011. **108**(2): p. 265-272.
172. Ilatovskaya, D.V. and A. Staruschenko, *TRPC6 channel as an emerging determinant of the podocyte injury susceptibility in kidney diseases*. Am J Physiol Renal Physiol, 2015. **309**(5): p. F393-7.
173. Spires, D., et al., *Protective role of Trpc6 knockout in the progression of diabetic kidney disease*. Am J Physiol Renal Physiol, 2018. **315**(4): p. F1091-f1097.

174. Slaughter, T.N., et al., *Characterization of the development of renal injury in Type-1 diabetic Dahl salt-sensitive rats*. Am J Physiol Regul Integr Comp Physiol, 2013. **305**(7): p. R727-34.
175. Boulay, G., et al., *Cloning and expression of a novel mammalian homolog of Drosophila transient receptor potential (Trp) involved in calcium entry secondary to activation of receptors coupled by the Gq class of G protein*. J Biol Chem, 1997. **272**(47): p. 29672-80.
176. Inoue, R., et al., *The transient receptor potential protein homologue TRP6 is the essential component of vascular alpha(1)-adrenoceptor-activated Ca(2+)-permeable cation channel*. Circ Res, 2001. **88**(3): p. 325-32.
177. Baxter, D.F., et al., *A novel membrane potential-sensitive fluorescent dye improves cell-based assays for ion channels*. J Biomol Screen, 2002. **7**(1): p. 79-85.
178. Gonzalez, J.E., et al., *Cell-based assays and instrumentation for screening ion-channel targets*. Drug Discov Today, 1999. **4**(9): p. 431-439.
179. Jane Denyer, J.W., Brian Cox, Gary Allenby, Martyn Banks, *HTS approaches to voltage-gated ion channel drug discovery*. Drug Discovery Today, 1998. **3**(7): p. 323-332.
180. Estacion, M., et al., *Activation of Human TRPC6 Channels by Receptor Stimulation*. Journal of Biological Chemistry, 2004. **279**(21): p. 22047-22056.
181. Loutzenhiser, K. and R. Loutzenhiser, *Angiotensin II-induced Ca(2+) influx in renal afferent and efferent arterioles: differing roles of voltage-gated and store-operated Ca(2+) entry*. Circ Res, 2000. **87**(7): p. 551-7.
182. Thilo, F., et al., *High glucose modifies transient receptor potential canonical type 6 channels via increased oxidative stress and syndecan-4 in human podocytes*. Biochem Biophys Res Commun, 2014. **450**(1): p. 312-7.
183. Seo, K., et al., *Combined TRPC3 and TRPC6 blockade by selective small-molecule or genetic deletion inhibits pathological cardiac hypertrophy*. Proceedings of the National Academy of Sciences, 2014. **111**(4): p. 1551-1556.
184. Schmid, H., et al., *Modular Activation of Nuclear Factor-κB Transcriptional Programs in Human Diabetic Nephropathy*. Diabetes, 2006. **55**(11): p. 2993-3003.
185. Walsh, D.W., et al., *Co-regulation of Gremlin and Notch signalling in diabetic nephropathy*. Biochim Biophys Acta, 2008. **1782**(1): p. 10-21.
186. Martini, S., et al., *Defining human diabetic nephropathy on the molecular level: integration of transcriptomic profiles with biological knowledge*. Rev Endocr Metab Disord, 2008. **9**(4): p. 267-74.
187. Baelde, H.J., et al., *Reduction of VEGF-A and CTGF expression in diabetic nephropathy is associated with podocyte loss*. Kidney Int, 2007. **71**(7): p. 637-45.
188. Pichler, R., et al., *Immunity and inflammation in diabetic kidney disease: translating mechanisms to biomarkers and treatment targets*. Am J Physiol Renal Physiol, 2017. **312**(4): p. F716-f731.

189. Higgins, J.P.T., et al., *Gene expression in the normal adult human kidney assessed by complementary DNA microarray*. *Molecular biology of the cell*, 2004. **15**(2): p. 649-656.
190. Harlan, S.M., et al., *Pathological and Transcriptome Changes in the ReninAAV db/db uNx Model of Advanced Diabetic Kidney Disease Exhibit Features of Human Disease*. *Toxicol Pathol*, 2018. **46**(8): p. 991-998.
191. Lin, J.S. and K. Susztak, *Podocytes: the Weakest Link in Diabetic Kidney Disease?* *Current diabetes reports*, 2016. **16**(5): p. 45-45.
192. Jim, B., et al., *Dysregulated Nephlin in Diabetic Nephropathy of Type 2 Diabetes: A Cross Sectional Study*. *PLOS ONE*, 2012. **7**(5): p. e36041.
193. Abdelsattar, H., *Urinary podocin level as a predictor of diabetic kidney disease*. *Journal of Nephropathology*, 2019. **8**: p. e26.
194. Odobasic, D., et al., *Inducible co-stimulatory molecule ligand is protective during the induction and effector phases of crescentic glomerulonephritis*. *J Am Soc Nephrol*, 2006. **17**(4): p. 1044-53.
195. Tafuri, A., et al., *ICOS is essential for effective T-helper-cell responses*. *Nature*, 2001. **409**(6816): p. 105-9.
196. Perez-Morales, R.E., et al., *Inflammation in Diabetic Kidney Disease*. *Nephron*, 2019. **143**(1): p. 12-16.
197. Emilsson, V., et al., *Genetics of gene expression and its effect on disease*. *Nature*, 2008. **452**(7186): p. 423-8.
198. Nakagawa, S., et al., *Molecular Markers of Tubulointerstitial Fibrosis and Tubular Cell Damage in Patients with Chronic Kidney Disease*. *PloS one*, 2015. **10**(8): p. e0136994-e0136994.
199. Usui, H., et al., *Macrophage Scavenger Receptor-A-Deficient Mice Are Resistant Against Diabetic Nephropathy Through Amelioration of Microinflammation*. *Diabetes*, 2007. **56**: p. 363-72.
200. Hanahan, D. and R.A. Weinberg, *Hallmarks of cancer: the next generation*. *Cell*, 2011. **144**(5): p. 646-74.
201. Zhan, X., et al., *Correlation Analysis of Histopathology and Proteogenomics Data for Breast Cancer*. *Mol Cell Proteomics*, 2019. **18**(8 suppl 1): p. S37-s51.
202. Ju, W., et al., *Renal gene and protein expression signatures for prediction of kidney disease progression*. *Am J Pathol*, 2009. **174**(6): p. 2073-85.
203. Chen, L., et al., *Correlation between RNA-Seq and microarrays results using TCGA data*. *Gene*, 2017. **628**: p. 200-204.
204. MacIsaac, R.J., G. Jerums, and E.I. Ekinci, *Effects of glycaemic management on diabetic kidney disease*. *World journal of diabetes*, 2017. **8**(5): p. 172-186.
205. Neumiller, J.J. and I.B. Hirsch, *Management of Hyperglycemia in Diabetic Kidney Disease*. *Diabetes Spectrum*, 2015. **28**(3): p. 214.

206. Migdalis, I.N., et al., *Elevated serum levels of angiotensin-converting enzyme in patients with diabetic retinopathy*. South Med J, 1990. **83**(4): p. 425-7.
207. Pichler, R., et al., *Immunity and inflammation in diabetic kidney disease: translating mechanisms to biomarkers and treatment targets*. American journal of physiology. Renal physiology, 2017. **312**(4): p. F716-F731.